中央大学博士論文

Development of a Variable Viscoelastic Handshake Manipulator Based on the Analysis of Viscoelastic Property of Human Elbow Joint in Handshake Movement

Kejia Dai
戴　可嘉

博士（工学）

中央大学大学院
理工学研究科
精密工学専攻

令和元年度
２０２０年3月

Contents

Chapter 1

Introduction

Chapter 1.
Introduction

1.1. Research background

In recent years, industrial robots are in an explosion, hundreds of thousands of robots in different shapes and sizes are working to replace human labor in manufactory lines. According to the statistics, the annual worldwide supply of industrial robots is growing over 14% on average [1]. The significant cost reduction of the mechanical parts used in robots and the development of microprocessors are the 2 main reasons why industrial robots suddenly started to boom about 3 years ago. As the microprocessors are growing smaller yet faster every year, the complicated calculations of kinetics and dynamics are made possible to be commercialized. Plus, the newly developed computer vision technology, robots begin to do some amazing work.

Conventional industrial robots are commonly shielded from humans. However, with the development of social robots [2] in recent years, robots are purposely put in contact with humans for interaction, such as rehabilitation or support for hard physical work. Therefore, social and physical interaction between robots and humans is foreseeably to extend in the future [3]. The cooperation between humans and robots calls for attention to an inevitable question about the safety of the robot and how to plan the movement so that the robot can move along with a human. Furthermore, since robots are expected to participate in our daily life in the future, the physical interaction between human and robots are gaining more attention every day. To this present day, social humanoids have already started working in public, some of the famous working robots include the front desk staff at a hotel, the saleswoman at the attire store and the guide at the information desk at the airport. The idea behind humanoids is that by giving robots the appearance of a human, customers feel more comfortable interacting with them other than a simple tablet. And also, it’s more natural for the humanoids to use body language during a conversation. Fig. 1.1 is a humanoid robot developed by G-Globot Co., Ltd. The mission of the humanoid is greeting customers, giving directions and answering questions at the front desk of a company or a store. The actuators used in this humanoid are all motors. But limited by the size of the humanoid, especially inside the arm, motors don’t have enough power to generate smooth movement. And motor also lacks back-drivability which make it vulnerable to external disturbance, so even though the robot can nod and bow,

it’s impossible for her to handshake with a customer.

Based on all the development tendencies in the robot industry this paper aimed at developing a manipulator for human-robot physical interaction research. Among all the possible ways to interact with robots, we have chosen handshake as a typical physical interaction for our research, because the handshake is a fundamental part of human physical interaction that is transversal to various cultural backgrounds. It is also a very challenging task in the field of physical human-robot interaction.

Fig. 1.1 Humanoid robot
(Project of G-Globot Co., Ltd. Under development)

1.2. Previous researches about handshakes

So far, lots of research has been done on handshakes covering all kinds of aspects. In order to get a better understanding of the existing handshake research, we categorized them into 3 areas, the social and psychological area, which studied the social function of the handshake as a non-verbal communication tool. The physical property of handshakes, which applied all kinds of sensors to analyze the kinetics and dynamics of handshakes. And the human-robot handshakes, which studies the controller for the robot arm and the physical interaction between humans and robots. Of course, the categories may not be exactly complete and mutually exclusive, many researches exist in between. This section introduces the history of handshake research and the position of our research.

The early research of handshakes can be dated back as early as the 1970s. However, at that time, handshake didn't exist as an independent research topic, rather it was mentioned in several papers about the human communication body language and non-verbal communication [4]. It was discussed as low intimacy interaction, and the differences were compared across age groups, personality and cultural backgrounds [5]. During that time, it was also when women started to leave home and enter into society, therefore, many social researchers focused on the gender differences in touching and social communication behaviors [6][7][8]. In the year 1992, David A. Wesson published his research of handshake as non-verbal communication in business, in which he pointed out that in the first several seconds you met someone you can tell that person who you think you are, who you think they are and what you think of the nature of your relationship is going to be all by communicating with a handshake, that is how powerful handshake can be in a business context [9]. This research also indicated that the handshake has started to become an independent research topic since then the social and psychological functions of handshake continue to be a very popular research area to this day [10][11].

After 2000's researchers started to apply different sensors such as the pressure sensor, accelerate meter, etc., on subjects' hands to analyze the physical property of handshakes, like the pressure variation and synchronization [12][13]. Research in this area usually overlaps with the other two areas. For example, in Orefice's research [14], multiple pressure sensors were attached to the subjects' fingers for pressure variation analysis and the correlations between pressure and mood and personality were examed. In Henaff's research, a sensor network was developed, a series of physical properties were measured and analyzed. The results are used for robot arm controller development.

The latest development of handshakes is the human-robot handshake area. So far, a lot of handshake robots have been developed, the majority of researches on human-robot handshakes focused on the planning of the shake motion [15] [16]

of the robotic arm. In order to achieve high precision of position and speed control of the movement, most of the handshake robots are driven by motors and reduction gears precisely mimic the up-and-down shaking move of a human arm. However, due to the lack of back-drivability in motor and the unpredictability of human movement, synchronization of human and robot movements is very difficult to achieve by accurate trajectory control. Therefore, more and more efforts have been put into developing pattern generator and motion controller in order to synchronize the movement in recent years [17] [18] [19].

The figure showing the development and categories of handshake research is presented below in Fig.1.2.

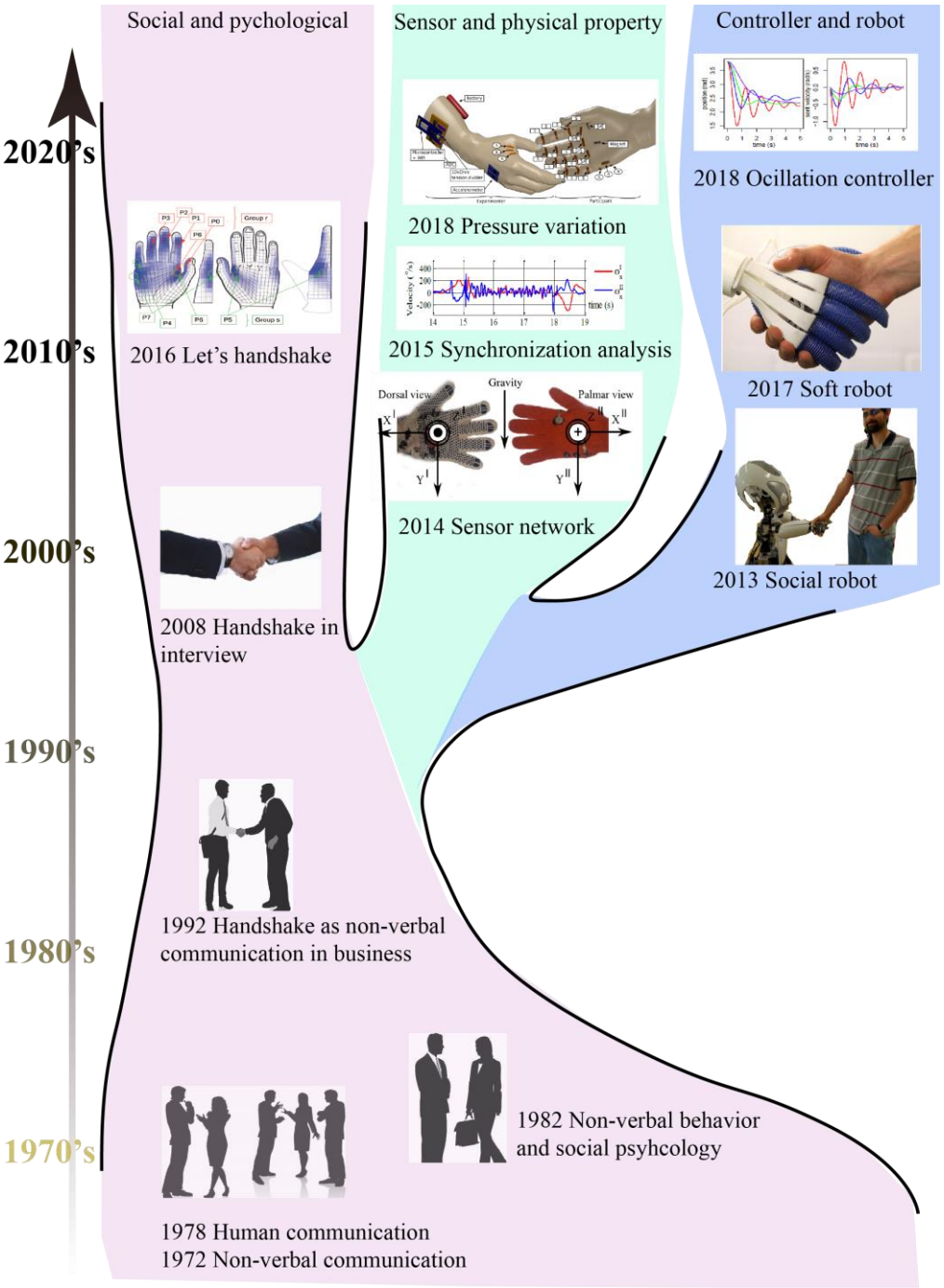

Fig. 1.2 The history and categories of handshake research

1.3. Introduction of human joint

Since the focus of this research is to study human handshakes, it is necessary to get a better understanding of the structure of human joints in arms first.

1.3.1. The structure of human joint

The main components of the human arm are bones and joints that connect the bones together. These joints allow a complex range of movements for the arm and without these joints, the human arm would not be able to carry out various moments such as: rotating, extending and retracting. The tolerances and strength of the materials that will be used in the elbow and shoulder require being significantly higher than the ones used for the wrist and fingers. The fundamental of the human elbow anatomy that the elbow joint will moves by three bones: humerus, ulna, and radius. The humerus is the longest bone of the upper extremity extended from the shoulder to the elbow. The forearm, connected from the humerus, which consists of the ulna and the radius. The upper end of the ulna is rounded with the end of the humerus to allow flexion and extension at the elbow. Fig.1.3 shows the anatomy of the elbow. The range of motion of the human elbow is about 150 degrees measured from the flexion and 0 degree in the extension. The relation movements between these bones look like a revolute hinge.

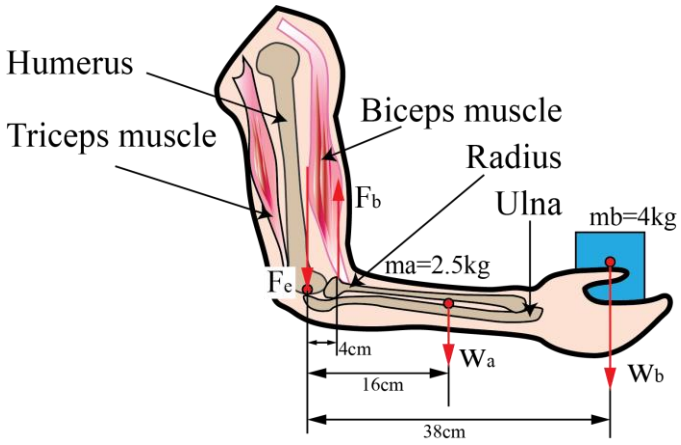

Fig. 1.3 Structure and force analysis of human elbow

1.3.2. Forces and torques in elbow joint

This section is a simple example of the statics of muscles, bones, and joints. There are some surprises. Muscles, for example, exert far greater forces than we might think. Fig. 1.3 shows a forearm holding an object and a schematic diagram of an analogous lever system was shown in Fig. 1.4. The schematic is a good approximation for the forearm, which looks more complicated than it is, and we can get some insight into the way typical muscle systems function by analyzing it. Muscles can only contract, so they occur in pairs. In the arm, the biceps muscle is a flexor—that is, it closes the limb. The triceps muscle is an extensor that opens the limb. This configuration is typical of skeletal muscles, bones, and joints in humans and other vertebrates. Most skeletal muscles exert much larger forces within the body than the limbs apply to the outside world. The reason is clear once we realize that most muscles are attached to bones via tendons close to joints, causing these systems to have mechanical advantages much less than one. Viewing them as simple machines, the input force is much greater than the output force.

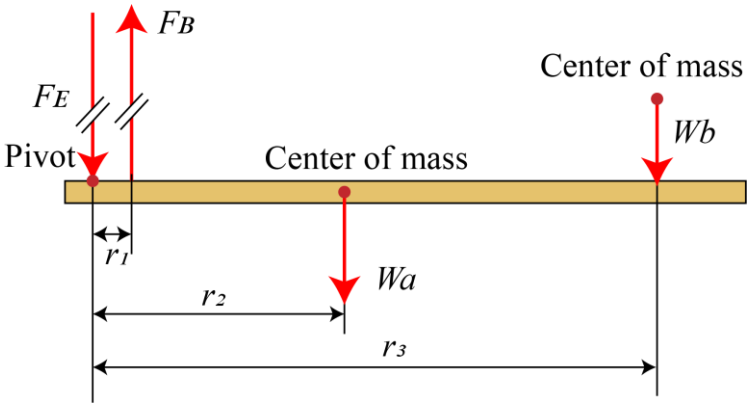

Fig. 1.4 Schematic diagram of an analogous lever system

In the above example of the biceps muscle, the angle between the forearm and upper arm is 90°. If this angle changes, the force exerted by the biceps muscle also changes. In addition, the length of the biceps muscle changes. The force the biceps muscle can exert depends upon its length; it is smaller when it is shorter than when it is stretched. There are four forces acting on the forearm and its load. The magnitude of the force of the biceps is F_B, that of the elbow joint is F_E, that of the weights of the forearm is W_a, and its load is W_b. The first condition for equilibrium is the force equilibrium shown in Eq.1.1. If we choose the pivot to be at the elbow, then the torques created by the weights are clockwise relative to the pivot, while the torque created by the biceps is counterclockwise; thus, the second condition for equilibrium, the torque equilibrium is shown in Eq.1.2. By solving the Eq.1.1 and 1.2, we can get F_B as in Eq.1.3. If we apply the real-life data of size and weight to the equations, it will be clear that the force exerted by

the bicep muscle is much higher than the external load.

$$F_B = F_E + W_a + W_b \tag{1.1}$$

$$r_2 W_a + r_1 W_b = r_1 F_B \tag{1.2}$$

$$F_B = (r_2 W_a + r_1 W_b) / r_1 \tag{1.3}$$

1.3.3. Different contractions of muscles

A concentric contraction is a type of muscle activation that causes tension on a muscle as it shortens. As the muscle shortens, it generates enough force to move an object. This is the most commonly used type of muscle contraction. Though effective, this type of contraction alone will not meet all the requirements of everyday movements. Therefore, there are three main types of muscle contractions:

- Concentric contraction
- Eccentric contraction
- Isometric contraction

Concentric contraction

Concentric muscle contractions involve movements that shorten the muscles as shown in Fig. 1.5(a). Most of the muscles utilize concentric movements to perform action. The heavier the object is you're trying to lift or move, the more strength that is generated. Common concentric movements include: lifting objects, standing up from a squat, etc.

Eccentric contraction

Eccentric contractions are lengthening movements of muscles as shown in Fig. 1.5(b). During this muscle movement, muscle fibers are stretched under tension from a force greater than the muscle generates. Unlike a concentric contraction, eccentric movements do not pull a joint in the direction of a muscle contraction. Instead, it decelerates a joint at the end of a movement. Some movements or exercises that display eccentric movement include: walking, lowering object, etc.

Isometric contraction

Isometric movements are muscle contractions that do not cause joints to move as shown in Fig. 1.5(c). The muscles are activated, but they are not required to lengthen or shorten. As a result, isometric contractions generate force and tension without any movement through joints. The best way to visualize this contraction is through the act of pushing up against a wall. When one performs any of these actions, the tension applied to the targeted muscle is consistent and does not

exceed the weight of the object one is applying force to. Common movements that demonstrate isometric contractions include: carrying an object in a steady position.

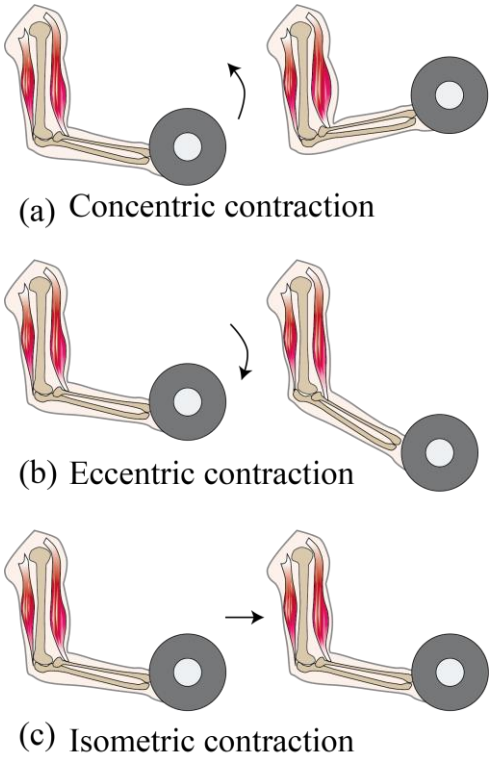

Fig. 1.5 Different types of muscle contractions

1.4. Viscoelasticity of human joints

This section introduces the general concept of the viscoelasticity of human joints. The more detailed definition of stiffness throughout history and its measurement will be covered in section 2.2 and the more detailed definition of joint viscosity throughout history and its measurement will be covered in section 2.3.

As described in the previous section muscles always work in pairs, and when both muscles in a pair contracts antagonistically, the joint output torque and stiffness at the same time. Because of the physical property of muscle tissue, when a muscle contracts or extends it is inevitable a part energy transfers into heat instead of output force, and this is considered to be the viscosity property of the human joint. Because of these particular characteristics of the muscles, humans can control not only the joint *torque* and *angle* but also the *stiffness* and *viscosity* of the joint, which is also known as the viscoelasticity property of joints. The viscoelasticity property provided a possible alternative explanation for motor control strategy of the human arm. There have been two different two controversial hypotheses in the field of motor control for human movements: whether the brain acquires internal models that generate accurate motor commands, or whether the brain avoids this by using the viscoelasticity of musculoskeletal system [21]. There have been proofs shown that short- and long-term motion learning may rely on different strategies of motor control. Even though the underlying control strategy of how the brain moves the muscles is not yet ascertained, by observing the movement development of babies it is safe to say viscoelasticity plays a very important role for a human to learn to interact with the environment. By adjusting the viscoelasticity of joints, human arm exhibits incredible compliance and softness when interacting environment or other people. That’s how human achieve physical interaction with each other naturally, and also the reason why human arm excels robot arms in the task of cooperation.

1.5. The purpose of this paper

As stated in the previous sections, the viscoelasticity property of human joint plays a very important role in motor control, however, according to the research background section, so far there has been no research of handshakes focused on the viscoelasticity properties.

Both to our common knowledge and the results of social studies, it is generally accepted that different handshakes convey different emotions. A firm and tight handshake usually represent enthusiasm, passion, and trustworthiness, whereas a weak and loose handshake usually makes people feel cold, indifferent and distant. But what is firm and tight or weak and loose exactly? How to translate the feeling into accurate physical characteristics? We made the

assumption that it is not only related to gripping force as suggested in the previous research but also affected by the stiffness of arm joints.

To sum it up, based on all aspects presented in the previous sections I have decided to focus my research on the following two areas.

1. Analysis of viscoelasticity properties of the human arm during handshakes.

   Since there has been no such research so far that focused on the viscoelasticity properties of handshakes, and because the stiffness and viscosity is not directly measurable dynamically, it is necessary to develop the measurement and analysis methods for studying the handshake movement. Several estimation methods were studied and carried out for the viscoelasticity properties estimation. The details are described in chapter II. At the end of chapter II, an attempt was made for classifying different handshakes.

2. Development of a variable viscoelastic handshake manipulator that can present different viscoelasticity properties that resemble real human movement.

   After the viscoelasticity properties of human handshakes were analyzed, a variable viscoelastic handshake manipulator driven by artificial muscles and MR-brakes was proposed and the prototype was developed. The details of the prototype and its effectiveness verification experiments were explained in chapter III. In chapter IV, the manipulator was optimized, and human-robot handshake experiments were performed under several stiffness and viscosity conditions. In the Conclusions part of chapter IV, the performance was compared when the subjects shook hands with the human experimenter and with the handshake manipulator. The results of the comparison experiments confirmed the effect of the viscoelastic properties on the subjective feelings of handshakes.

In conclusion, this research proposed a new aspect for analyzing human handshakes and provided a classification method for differentiating handshakes by measurable physical properties. And a variable viscoelastic handshake manipulator was developed for the purpose of human-robot physical interaction researches and provided a possible control strategy for human-robot cooperating smoothly.

1.6. The structure of this paper

For the purpose of studying human-robot physical interaction, we have chosen handshake as the topic for this research, in order to build a handshake manipulator that can generate realistic human-like movement we first studied the human handshake movements thoroughly and applied the characteristics on the handshake manipulator. The detailed structure of this paper is explained as follows.

This paper consists of two consecutive research areas, the first area is the analysis of the viscoelasticity property of human arm in handshake movements. The details of this research are explained in chapter 2, including the definition of the viscoelasticity property, the measurement method proposed in previous studies, the measurement method we applied in this research and the experiment setups and methods. As the Conclusions of chapter 2, it is demonstrated that viscoelasticity is a time-varying property during handshake movements and also in different social settings, different viscoelasticity property was utilized for physical interaction.

The second research area is the research of human-robot handshake. In chapter 3, a prototype of a handshake manipulator is proposed and developed, the basic performance and effectiveness of the manipulator is verified and analyzed by experiments. The experiment results demonstrated that the handshake manipulator is capable of generating different feelings of handshakes. In chapter 4, human-robot handshake experiments are carried out, and the performance of the subject's handshaking with the robot is compared with the performance when handshaking with a human experimenter.

Chapter 5 stated the Conclusions of the complete research and possible future application of the research.

Chapter 2

Human handshake analysis

Chapter 2.
Human handshake analysis

In this chapter, the detailed concepts of stiffness and viscosity of human arms are explained with an introduction of how these concepts were developed throughout the history and the attempts made in previous researches to measure them. Then stiffness and viscosity of human arms are measured and analyzed under different handshake conditions.

2.1. The necessity of viscoelasticity analysis

In order to make robots work better with humans, a set of research methods are necessary to both further the understanding of normal motion as well as developing devices to create movements as close to real humans as possible. The proposed research method should be able to reflect the relationships between physical properties of joints and muscles, and movements of the body, but also have a limited amount of parameters which can be modeled into mechanical parts like links and actuators.

One of the major tasks of the human central nervous system (CNS) is to control body movement. The study of the CNS cannot be separated from understanding the inherent properties of the musculoskeletal system that it must control. The physical properties of the musculoskeletal system have to be seen as a part of the control system. Therefore, analyzing the mechanical properties of the musculoskeletal system plays a central role to gain a better understanding of the control of movement in its entirety. When accomplishing a task that requires both the following of a trajectory and the exertion of a force, humans need to modulate not only the generated muscle forces but also the corresponding limb stiffness and viscosity. Hence, complete models of the musculoskeletal mechanics must represent the dynamics of muscle force production, and the dynamics of movement in the skeletal system. An accepted parameter to describe the mechanics of human limbs is its viscoelasticity, which can be computed either in the joint space or at the point of contact with the environment. A few theoretical models have been proposed to characterize whole limb mechanics. A common finding is that the muscle-tendon stiffness and the corresponding joint stiffness play a central role in shaping human motion.

To better reproduce human behaviors using robots, the latter must be endowed with learning capabilities enabling them to acquire new knowledge from humans. For example, most works in the robotic literature have focused on developing learning algorithms to encode kinematic trajectories using vision or kinesthetic systems to capture a teacher demonstration[22]. On the other hand, the new

variable viscoelasticity capabilities of recent robotic devices demand to reformulate these methods in order to exploit their new control schemes in performing more complex tasks. Such new methods should allow for the description of the uncertainty related to the measurement of the human physiological parameters and account for those variables that cannot be measured in-vivo. These techniques must capture the basis of human features so that the robot can adapt to what has been learned to execute new tasks.

We are working on this research aiming to better understand the mechanisms of actuation provided by human muscles. We believe that understanding these mechanisms is not only relevant but an essential key point for human-robot interaction. Such understanding will allow the robotic community to engineer a new generation of compliant devices capable to better characterize the dynamic coupling between humans and robots. Moreover, understanding how human muscles are activated to actuate the body and how joint stiffness is regulated during movement will directly allow designing motion and balance controller to move humanoid robots in a more sophisticated way.

2.2. Human joint stiffness

In the motor control researches, human muscle is usually modeled into a variable spring paralleled with a variable damper, also known as a Kelvin-Viogt model, shown in Fig. 2.1 The variable spring is considered to be elastic element of the muscle and the damper the viscous element of the muscle. This type of model has been commonly accepted for a long time.

Spring-like behavior of muscles and joints has been known since the middle of the last century. The importance of muscle spring properties was emphasized by such classics of biomechanics and motor control[22]. In particular, spring-like properties of muscles and joints are believed to play an important role in maintaining human vertical posture, in storing and recoiling elastic energy over a stretch-shortening muscle cycle and in control of muscular activity[23]. In order to describe and study these properties, researchers in the fields of biomechanics and motor control frequently use the well established physical notion of stiffness. However, the applicability of this term for describing such complex objects as muscles and joints is not obvious. Its usage in many of the studies is likely to make a physicist nervous and the emergence of such expressions as ‘negative stiffness’ in serious scientific publications may even cause a nervous breakdown. The notion of stiffness has been introduced in physics to characterize properties of certain types of deformable bodies under an influence of external forces. In the absence of external forces, these bodies are supposed to maintain constant shape. Muscles are not such bodies, and joints can hardly be considered bodies at all. They are rather links between the bodies or conglomerates of bodies. In particular, Hasan and Enoka reported unstable angle ranges in the human elbow

when changes in the force arms led to a seemingly negative stiffness in the joint while both flexors and extensors behaved like classical springs with positive stiffness. In order to apply the notion of stiffness to muscles and joints, one needs to redefine this notion, clarify how it can be measured in an ideal mental experiment, and explicitly state the differences between this ideal experiment and real procedures that are frequently used for measuring muscle and joint stiffness.

2.2.1. The physical notion of stiffness

In physics, the notion of stiffness is introduced for objects that deform under the influence of an external force, generate force to oppose the external force, and can store elastic energy. For an ideal, unidimensional spring, according to Hooke's law, this force is proportional to spring deformation and is directed along the same coordinate:

$$F_x = -kx \tag{2.1}$$

where x is coordinate of the tip of the object. If one imposes a force vector directed along with the spring, waits until the spring comes to a new equilibrium state, and then measures changes in force and length, stiffness, k can be defined as:

$$k = -\Delta F / \Delta x \tag{2.2}$$

where ΔF is change in force and Δx is the change in length. If the spring does not have inertia but has an inertial component attached to its end, it can be described as:

$$md^2x / dt^2 = -kx \tag{2.3}$$

where m is inertia. If the system also involves a viscous element, acting in parallel to the spring, that develops force proportional to velocity and directed against the velocity vector, the equation will be:

$$md^2x / dt^2 + bdx / dt + kx = 0 \tag{2.3}$$

where b is the coefficient of viscosity. Eq.(2.3) depicts a term in mechanics, "mechanical impedance", which reflects properties of a system determined by its inertial, viscous, and elastic elements. However, this equation only applies to ideal mechanical systems, where all the coefficient is time-independent. For describing the time-dependent property of biological objects, instead of Eq.(2.3) the system should be described by:

$$F(t) = m(t)d^2x / dt^2 + b(t)dx / dt + k(t)x(t) \tag{2.4}$$

Accordingly, stiffness was defined by:

$$k(t) = dF / dx \qquad (2.5)$$

This definition of stiffness represents the ability of the system to resist externally imposed displacements disregarding the time course of the displacement. This ability is not necessarily related to the ability of the system to deform or to store elastic energy.

2.2.2. Stiffness of passive muscles and active muscles

When muscle tissue is at resting length or less, it is rather compliant. Actin and myosin filaments, which are the main proteins that cause the muscle movement, can move past each other with little resistance, and the connective tissue surrounding contractile elements is in a slack state with no tension. The stiffness of the relaxed muscle tissue is much lower than the tendon stiffness, and in many cases can be disregarded. In a relaxed passive movement, the muscle can deform easily. And when the length of a passive muscle exceeds the resting length, the resistance is provided by connective tissue.

Measurement of muscle stiffness when muscles are active is considerably harder than measuring the stiffness of passive elements. First, the length of an active muscle is not directly prescribed by the level of its activation. It is also a function of external resistance. Second, muscle reactions are time-dependent. At least three time characteristics are important: (a) time of mechanical disturbance with respect to an initial stimulus triggering muscle activity; (b) duration (velocity) of mechanical disturbance; and (c) time after the mechanical perturbation. Third, a muscle is composed of many elements that have different mechanical characteristics.

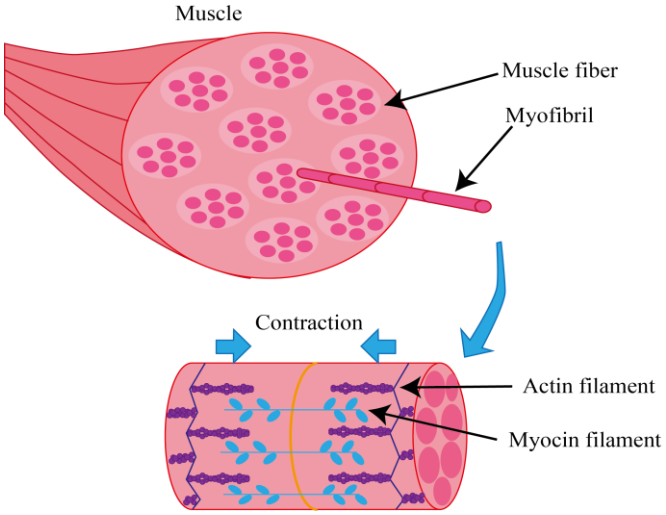

Fig. 2.1 Thick and thin filament in muscle fiber

In studies of muscle fibers, small stretches or releases are applied to one end of the fiber. A great amount of important scientific knowledge is collected with this method[23]. According to Woledge et al., ‘the stiffness of a muscle fiber can be measured by very rapidly changing its length while recording the tension’. This definition corresponds to mechanical stiffness as it has been defined earlier. When a muscle fiber is stimulated, its stiffness is proportional to the overlap between the thick and thin filaments and changes with time together with fiber tension. Muscle fiber stiffness is frequently assumed to reside in cross-bridge (shown in Fig. 2.1) and to lead to purely elastic storage of energy. It is assumed to increase with muscle force[24][25]. Based on a cross-bridge model, Morgan[25] predicted a linear relation between short-range muscle stiffness and muscle tension. He also experimentally observed such a relation by applying small fast stretches to an isometrically contracted cat soleus muscle. Short-range stiffness was found to be dependent upon force but not upon operating length.

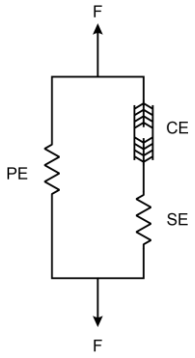

Fig. 2.2 Hill’s muscle model

According to the well-known classical Hill model [26][27](shown in Fig. 2.2), muscle stiffness is determined by its parallel elastic components (PE) as well as series elastic components (SE). PE is much more compliant than SE[28] and, in studies of active muscles, SE is typically the main object of interest. When contributions of parallel elasticity are ignored, muscle deformation is, at a first approximation, regarded as a combination of telescopic sliding of the thick and thin filaments past each other and, in addition, elastic length changes. The term ‘stiffness’ is used to characterize only the elastic component of deformation (where deformation energy is stored) but not the telescopic motion albeit this latter component changes the muscle force-length curve and its $\Delta F / \Delta x$ values.
Under this presumption, muscle stiffness is synonymous to SE stiffness, which can be determined when:

(a) values of $\boldsymbol{F}$ and x are measured at least at two points of the force-length curve, and
(b) length of contractile components (CE) is not changed during the entire measurement period.

At least two well-known methods are based on applying releases to one end of a

muscle: ‘quick release’[29] and ‘controlled release’ [30]. In the first case, a load applied to a muscle is decreased in a step-like manner, and in the second, a stimulated muscle is permitted to shorten over a preset small distance. Fast changes in muscle length (in the quick release method) or in muscle tension (during the controlled release procedure) are attributed to changes of SE only. The CE, by assumption, does not change its length and tension during and immediately after rapid releases. These methods have been broadly used to determine elastic characteristics of active human muscles[22][31]. However, all the methods for measuring series elastic properties of human muscle are indirect. Even though many models were made to estimate the interaction between muscle tissues and tendons, the biological structure of muscle is too complicated to be simplified into mechanical elements. It has been pointed out that these methods rely on a number of unproven assumptions and are not very accurate[32]. To this day, the most fundamental underlying mechanism of muscle fiber stiffness remains unclear, and an accurate physical model that can describe it is still undiscovered.

2.2.3. Joint stiffness

Most of the voluntary movements are controlled by a number of muscles and represent rotations in joints. Therefore, the analysis of single-joint movements becomes an important step towards the analysis of the control of natural movements. Unfortunately for the experimenters, most of the commonly studied joints of human limbs (e.g., shoulder, wrist, and ankle) have more than one degree-of-freedom and are controlled by more than two muscles. As a result, an absolute single-joint movement doesn't exist in real life. However, it is believed that the analysis of the single-joint is an important intermediate step in the analysis of more complex and more natural movements[33]. Therefore, the joint stiffness was defined on a simplified and idealized pin joint with only one DOF. The mechanical system described by Eq. (2.4) will be transformed into:

$$T(t) = m(t)d^2\alpha(t)/dt^2 + b(t)d\alpha(t)/dt + k(t)[\alpha(t) - \alpha_0(t)] \qquad (2.6)$$

where T is torque around the joint, a is joint angle, and a_0 is resting angle of the joint. This equation is analyzed with different degrees of simplifications in most of the mass-spring models of single-joint motor behavior. And many experimental methods have been proposed to measure the joint stiffness by this definition. And several of the methods will be introduced in the next section. Each method has its own focuses based on some arbitrary assumptions and can be applied to a certain situation. Because of the complexity of the nature of the biological element, no universally applicable definition of joint stiffness has been made.

The difficulties and ambiguities in trying to use the concept of stiffness for individual joints suggest that making another step up to the more complex multi-joint system is likely to make this concept even less applicable. Therefore,

this research will focus on the single-joint analysis of handshake movements.

2.2.4. Existing methods of estimating the joint stiffness

Based on the definition of joint stiffness discussed in the previous section, a great number of researches have been experimentally investigated joint stiffness in both static and dynamic paradigms. In limb postural experiments, system identification is accomplished using either stochastic perturbations [36][37][38] or regressive techniques [39][40][41]. Studies that quantify stiffness as a function of hand position along a reaching trajectory typically use regressive procedures [42][43]. Stochastic methods are based on ensemble techniques [44] and even though they identify the system non-parametrically they require hundreds of perturbed repetitions of the same movement to obtain a reliable estimate of stiffness. These repetitions can induce muscle co-contraction that leads to stiffening of the arm joints [45]. Regressive techniques allow for more natural (not continuously perturbed) movements, but still require many trials to produce reasonable stiffness time-profiles using a parametric approach.

Regressive techniques rely on the assumption that unperturbed arm movements are repeatable and that the mechanical characteristics of the arm do not change over a small set of repetitions, To obtain the estimation of the baseline trajectory and a set of perturbation responses with such techniques, a series of measures need to be taken using the same reproducible kinematic configuration; consequently, the data collection burden can be substantial. If a servo-commanded displacement is used, estimates of stiffness can be done independently of the values of damping and inertia when the perturbation reaches steady state [46][47]. As a consequence, the required characteristics of the robotic devices can be very demanding. In general, when using displacement perturbations, a very stiff environment must be rendered by the robot to keep the actual displacement of the hand as close as possible to the perturbation imposed and to break the feedback loop between joint torques and joint positions, effectively creating an open-loop system that it is possible to identify [48].

In Piovesan's study, a technique for measuring time-varying limb stiffness on a trial-by-trial basis was proposed. The technique is based on the time-frequency domain and modal analysis. It requires neither the assumption of stationarity nor the repeatability of the motor task. To show the utility of the proposed method it was compared with two well known regressive techniques, one using force perturbations, and the other displacement perturbations. It has been demonstrated that the proposed technique produces accurate estimates of time-variant stiffness on a single trial basis, under both static and dynamic conditions. Time-frequency techniques are relatively new to the field of motor control. They depend on evaluating the location of the maximal energy density of a signal in the time-frequency domain. Considering the non-repeatability of natural handshakes,

we applied this approach to estimate the variation of stiffness and damping across trials, thereby studying the relationship between stiffness modulation and different handshakes. In section 2.4, the details of how to implement the method will be explained and tested.

2.3. Human joint viscosity

The spring-like nature of muscles in isolation and under reflex control has long been recognized for its role in providing postural stability and permitting compliant interaction with the mechanical environment, damping properties of muscle are less frequently the primary focus of research although a number of studies have touched on them to greater or lesser extents. Without damping, it would not be possible to position a limb quickly and accurately, nor would it be possible to rapidly damp oscillations when the limb was subjected to an impulsive force. In the motor control literature, the expression ‘muscle/joint viscosity’ is often used to designate the force that is proportional to the magnitude of the velocity. The dimensionality of such viscosity is N/(m/s), the force per unit of velocity, or Nm/(rad/s), the force moment per unit of angular velocity. But same as the expression ‘stiffness’ as explained previously, a lot of ambiguity exists when attempts to apply mechanical terminology on biological tissues. This section designates in introducing the existing definition and estimation methods of viscosity.

2.3.1. The physical definition of viscosity

In the International System (SI) of metric units, viscosity is defined as the resistance that a gaseous or liquid system offers to flow when it is subjected to shear stress. The governing equation is:

$$f = \eta A dv / dx \tag{2.7}$$

where f is the force required to maintain a velocity gradient, dv/dx, between planes of fluid of area A, and η is the viscosity coefficient. The SI metric unit for viscosity is $(N/m^2)\cdot s = Pa\cdot s$. The viscosity unit is the force per unit area required to sustain a unit velocity gradient normal to the flow direction.

2.3.2. Human joint viscosity

Similar to the physical property of viscosity, human muscle also presents velocity-dependent damping characteristics. Unlike the spring-like nature of muscles which has long been recognized for its role in providing postural stability and permitting compliant interaction with the mechanical environment, damping properties of muscle are less frequently the primary focus of research. From a historical perspective, a specific interpretation of the term *viscosity* in the muscle physiology and motor control literature is easy to explain, “damping with

the energy dissipation and resistive force proportional to the velocity". The concept of muscle viscosity was introduced by A.V. Hill in the year 1922. Studying elbow flexion with maximal efforts against different inertial resistance, he discovered that the mechanical work decreased with increases in speed and explained this finding as a result of energy loss due to viscosity-resistance proportional to the velocity. The assumption was that the muscle, when stimulated, produced a given amount of energy which in part was used for the mechanical work and in part was degraded into heat.

In the later studies, it had been gradually unveiled that damping in the musculoskeletal system originates primarily from two sources, namely, intrinsic velocity-dependent properties of muscle and reflex muscle activation. The intrinsic damping derives, in large part, from the dependence of contractile force on the rate of change of muscle length[49]. Small-amplitude changes in muscle length, whether applied while a muscle fiber is held isometric or when it is undergoing a length change, suggest that attached cross-bridges are almost purely elastic. The damping must, therefore, derive from changes in the number of attached cross-bridges or some change in the cross-bridge strain as a function of velocity [50]. It is highly unlikely that the damping arises from the resistance of the myoplasm to cross-bridge movement since no velocity-dependent force is required to match the transient force response to rapid, small changes in muscle fiber length[50]. The damping coefficient of muscle has been shown to increase with muscle force under isometric conditions, suggesting further that it depends directly on the number of attached cross-bridges.

Without damping, it would not be possible to position a limb quickly and accurately, nor would it be possible to rapidly damp oscillations when the limb was subjected to an impulsive force. The term viscosity has frequently been used to refer to the velocity-dependent mechanical properties of joints. Without damping, a joint would tend to oscillate indefinitely following movement. Most studies that have estimated the damping coefficient of single joints such as the ankle, elbow, wrist, or finger articulations[51] have shown that these joints are underdamped. It is somewhat surprising then that humans are usually able to stop a rapid, voluntary limb movement without noticeable oscillation.

2.4. The approach of this paper to estimate the joint viscoelasticity

In this research, two different approaches of joint stiffness estimation were applied. The first on was using EMG signal as an indicator of muscle activations, and the second one was to used the calculated joint torque for estimating the joint stiffness. And for joint viscosity estimation, we modeled the joint as a harmonic oscillator and adopted the viscosity concept as the force moment per unit angular

velocity. The details of the calculation will be explained in the following sections.

2.4.1. Joint stiffness estimation by EMG signals

According to the result of previous research [52], the estimated joint stiffness has a linear relationship with the processed EMG signal. Therefore, we added the bicep and triceps EMG signal together to be used as the estimation of the joint stiffness. And considering the response time of the artificial muscles, we filtered the processed EMG signal one more time, with a low-pass filter of 2 Hz, and used the filtered signal as the target stiffness signal in the later experiments. And Fig. 2.3 showed the elbow angle measured by the motion capture device.

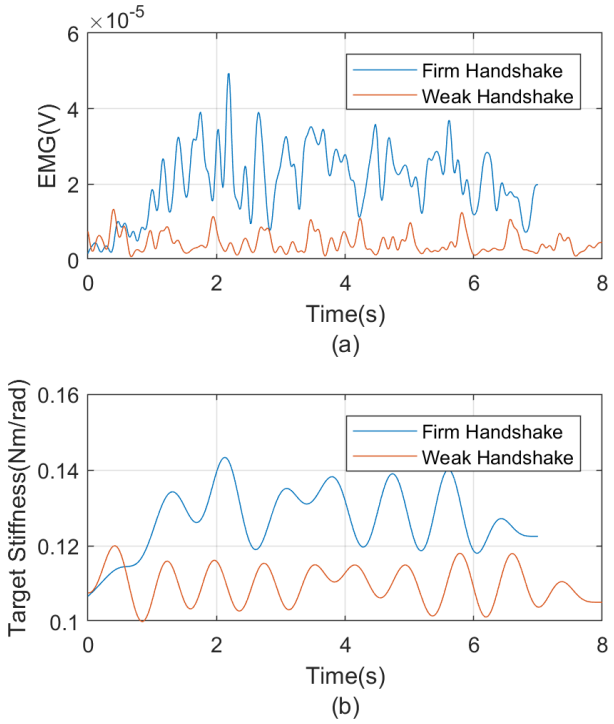

Fig. 2.3 EMG signal and the estimated joint stiffness

2.4.2. Quantitative joint stiffness estimation by joint torque

Since the direct measurement of the joint stiffness is impossible in a free movement, we used the simplified spring-damper model as introduced in Eq.2.6 as the quantitative estimation of the elbow stiffness. The estimated joint stiffness under different handshake conditions by two different methods as shown in Fig. 2.4. And the FFT analysis of the two signals was shown in Fig. 2.5. From the frequency domain of the signals, it can be seen that both estimation methods provided signals with the same main frequency.

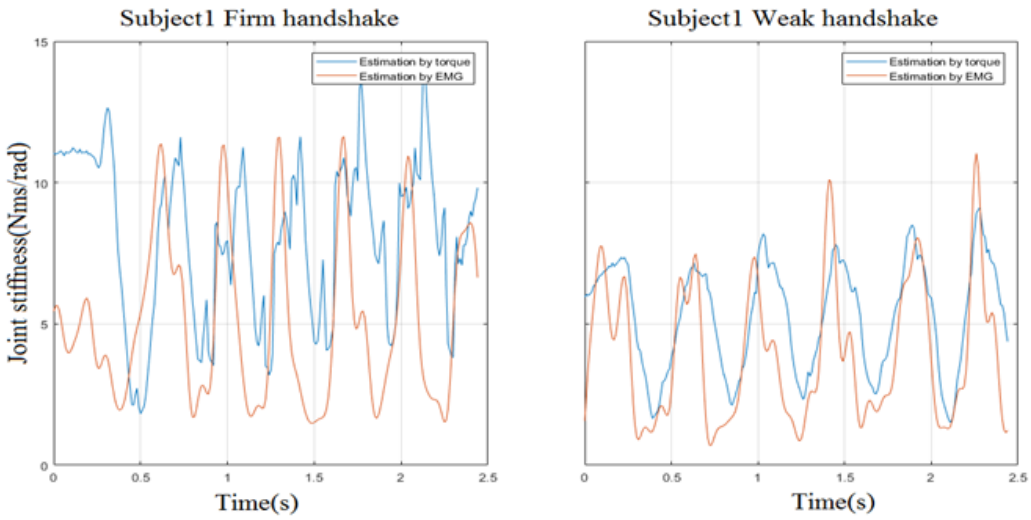

Fig. 2.4 Estimated joint stiffness from torque and EMG signal

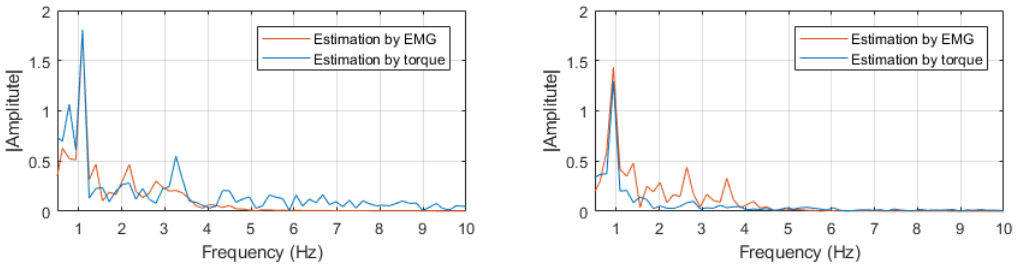

Fig. 2.5 FFT of the estimated joint stiffness from torque and EMG signal

2.4.3. Joint viscosity estimation

In the previous research [53], it had been verified that although the damping of a joint is tightly linked to its stiffness under isometric conditions where the damping ratio remains relatively constant, it's not the case during voluntary movement, because reflex torque contributes differentially to damping while stiffness depending on movement frequency. Also, that angular velocity of a joint has a significant effect on the damping coefficient. In this research, we modeled the elbow to be an underdamped mass-spring system. Mechanical parameters (damping coefficient, stiffness, and oscillation amplitude) were estimated by fitting oscillations occurring in the velocity record.

$$\dot{\theta} = -\frac{K(t)\theta_0}{I\omega} e^{-\beta t} \sin\omega t \tag{2.8}$$

$$\omega = \sqrt{\frac{K(t)}{I} - \beta^2} \tag{2.9}$$

$$\beta = \frac{D(t)}{2I} \tag{2.10}$$

Where represents the oscillation amplitude. I, the moment of inertia of the forearm. K(t), the stiffness of the wrist, and D(t) the viscosity coefficient.

2.5. Interaction force measure device

According to the detailed explanation of stiffness and viscosity in the previous section, it can be concluded that in order to analyze the viscoelasticity property of the human joint no matter what estimation method is used, it is inevitable to measure the output joint torque first. For that purpose, a measuring device was developed, and the details will be introduced in this section.

2.5.1. Problems with the existing research method

In the joint torque related research, it is common to apply a strain gauge on a link connect the joint to a load motor for estimating joint torque [54][55] or simply use the dynamic torque measurement method with a torque meter [56]. These methods all require a fixed frame to mount the measuring device so that the movement can only be limited to a 1-DOF movement. Whereas, in our experiment, we are trying to measure the joint torque as close as a natural state, so we don't want to fix the subjects' arms to a frame. In the research of the dynamic torque measurement for human arms, a handle with a loadcell is often used [57]. This method allows more freedom of the subject movements, therefore we considered to measure the interaction force between two parties of the handshake as an estimation for the joint torque.

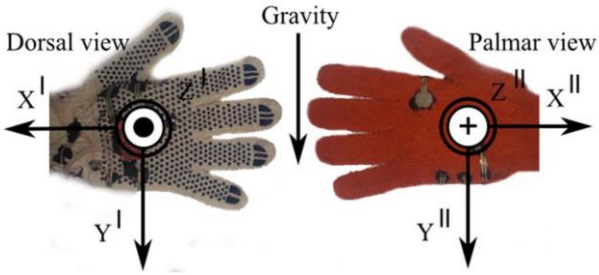

Fig. 2.6 Sensor network for handshake movement analysis

(Source: Artem A. Melnyk, Viacheslav Khomenko, "Sensor Network Architecture to Measure Characteristics of a Handshake Between Humans", *IEEE 34th International Scientific Conference on Electronics and Nanotechnology (ELNANO)*, 2014)

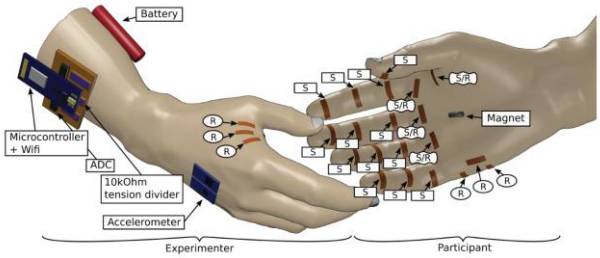

Fig. 2.7 Analysis of the pressure variation during a handshake

(Source: Pierre-Henri Orefice, Mehdi Ammi, "Pressure Variation Study in Human-Human and Human-Robot Handshakes: Impact of the Mood", Proceedings of the 27th IEEE International Symposium on Robot and Human Interactive Communication, Nanjing, China, August 27-31, 2018)

Several pieces of research have been done on measuring the contact area and contact pressure in human handshake interactions. Orefice et al. have analyzed the pressure variation of the hands in a handshake with an array of the pressure sensor (shown in Fig. 2.6), and attempted to establish the relationship of the pressure exerted by the participants in handshakes and their moods [58]. Melnyk et al. have developed a sensor network for measuring all the dynamics during a handshake (shown in Fig. 2.7) [59]. From a haptics perspective, physical interactions have a kinesthetic element (joint torques) and a cutaneous element of contact forces on the skin [60]. However, these two elements may not be independent in most situations. In the researches mentioned above, they measured the force on human hands directly during a handshake, but there is a defect to this approach which is the kinesthetic element and the cutaneous element of contact forces cannot be distinguished. Even though the grasping force of a handshake is mainly derived from 2 groups of muscles: the extrinsic and the intrinsic muscles of the forearm. During an up-and-down shaking movement, the joint torque can also affect the pressure distribution on hands. Therefore, we proposed a new device for the purpose of measuring the interaction force and the grasping force separately. The design of the device is shown in Fig. 2.8.

The following sections will explain in detail the structure of the measuring device and how it works. And we used the proposed measuring device to investigate two different types of handshakes and verified its effectiveness in doing research on analyzing the interaction forces of handshakes.

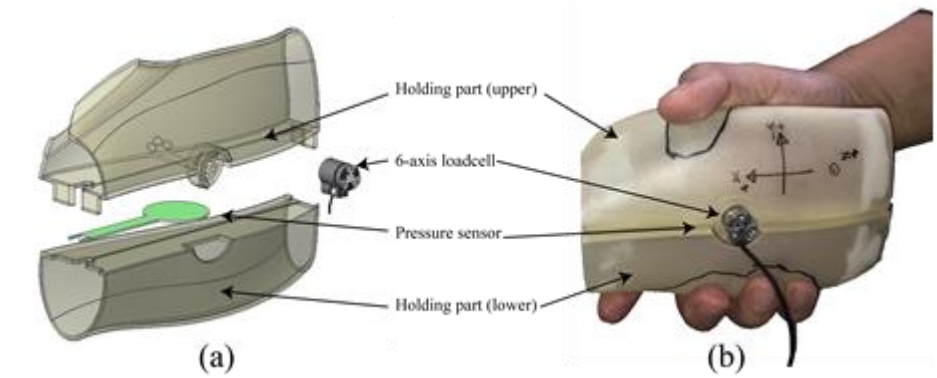

Fig. 2.8 Measuring device diagram. (a): Subject holding one side of the measuring device. (b) Exploded diagram of a single holding part

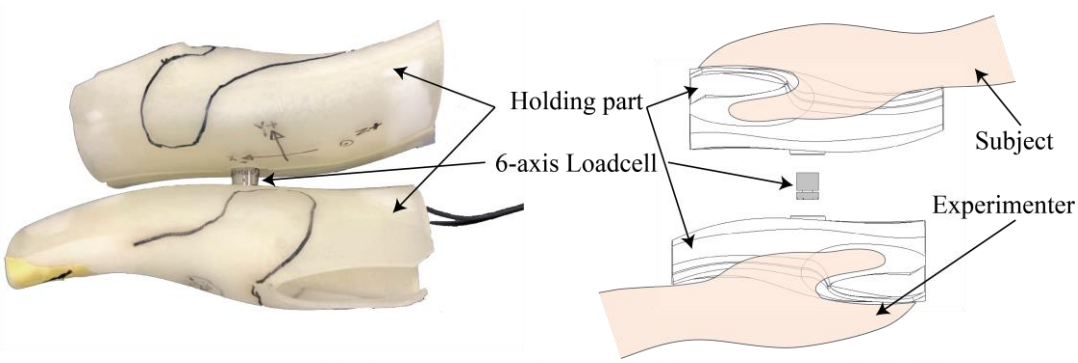

Fig. 2.9 Assembled measuring device and how two people hold it

2.5.2. Design of the interaction force measuring device

In order to measure the grasping force and the interaction force separately, we designed the measuring device shown in Fig. 2.8. The measuring device comprises two identical holding parts connected to each other with an angle of 180 degrees, which is the natural degree when two people hold hands in a handshake position. Each holding part is separated into two parts, a pressure sensor was installed between the upper and lower parts to measure the grasping force during a handshake. The exploded diagram of one holding part is shown in Fig. 2.8(a). Between the two holding parts a 6-axis load cell was installed to measure the interaction force and torque between two people when they shake hands. A diagram of two-person handshake holding the measuring device as shown in Fig. 2.9. The loadcell we used in this research is the production of Nippon Liniax Co., Ltd. The axis direction of the loadcell was shown in Fig. 2.10. The size of the holding part was designed according to the palm-size of an average Japanese adult male with the data published by AIST (National Institute of Advanced Industrial Science and Technology) in 1995 [61]. And the shape of holding part mimics the curving surface of a palm so that when subjects perform

handshake through the measuring device they can feel as natural as a real handshake. And the whole measuring device was made hollow inside to reduce the weight so that the device doesn't affect the movement of the handshake. The weight of the measuring device was 150g in total.

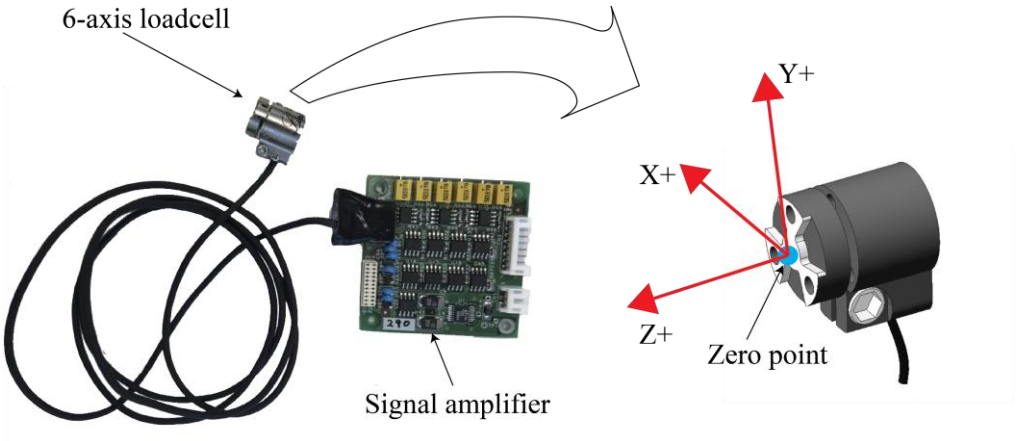

Fig. 2.10 6-axis load cell used in measuring device

2.5.3. Effectiveness test of the measuring device

The experimenter in this research is a healthy male Ph.D. student from our University. In order to acquire data of different types of handshakes, first, we studied the business manner of an official firm handshake and trained the experimenter accordingly. Then we asked the experimenter to loosen his arm and perform weak handshakes. The experimenter practiced the two different handshakes until he was able to perform both handshake movements steadily. Then we tested on 5 subjects who agreed universally that the two different types of handshakes can be clearly distinguished.

Then the experimenter shook hands with the subject through the measuring device, which is the experimenter and the subject both held one holding part as shown in Fig. 2.9, and they do not hold hands directly. The interaction force and torque and grasping force were measured by the measuring device. The movement of both the experimenter and the subject was recorded by the motion capture device, and the muscle activation of biceps and triceps of the experimenter was recorded by EMG sensors as an indicator of a firm handshake and weak handshake.

There was no specific instruction to the subject, except for asking him to handshake naturally with the experimenter through the measuring device. The experimenter shook hands with the subject 6 times in total, 3 times firm handshake and 3 times weak handshake. And the subject was not informed with the order of the handshakes.

EMG signal of the experimenter's bicep was recorded as an indicator to differentiate the firm handshake and the weak handshake. Fig. 2.11(a) showed the original EMG signal of the experimenter when performing firm and weak handshakes. The recorded signal was then processed in the following order: (1) DC offset was removed. (2) The signal was rectified. (3) The signal was filtered by a low-pass filter, with a cut-off frequency of 10Hz. (4) Linear Envelope of the signal was created. The processed signal was shown in Fig. 2.11(b). From the processed EMG signal it is easy to tell there is a difference in muscle activations when performing different handshakes. Root mean square (RMS) of the EMG signal was calculated with equation (1), during a firm handshake, the RMS of the bicep EMG signal is 0.0159 mV, while during a weak handshake the RMS of the bicep EMG signal is 0.0042 mV.

$$RMS[X] = \sqrt{\frac{1}{N}\sum_{i=1}^{N} X_i^2} \tag{2.11}$$

The measured interaction torques and forces of the handshakes are shown in Fig. 2.12. Fig. 2.12(a) showed the interaction torque of the handshakes, which indicated that during a firm handshake, the interaction torque is obviously larger than the interaction torque of a weak handshake. Fig. 2.12(b) showed the

resultant force (*Fr*) of *Fx* and *Fy* in different handshakes. It is unclear from the graph but the RMS value indicated that the interaction force of a firm handshake is larger than that of a weak handshake. The RMS value of each measured data was listed in Table 2-I. Fig. 2.12(c) showed the gripping force of the handshakes, which indicated that during a firm handshake, the gripping force of the experimenter is obviously larger than the gripping force of a weak handshake.

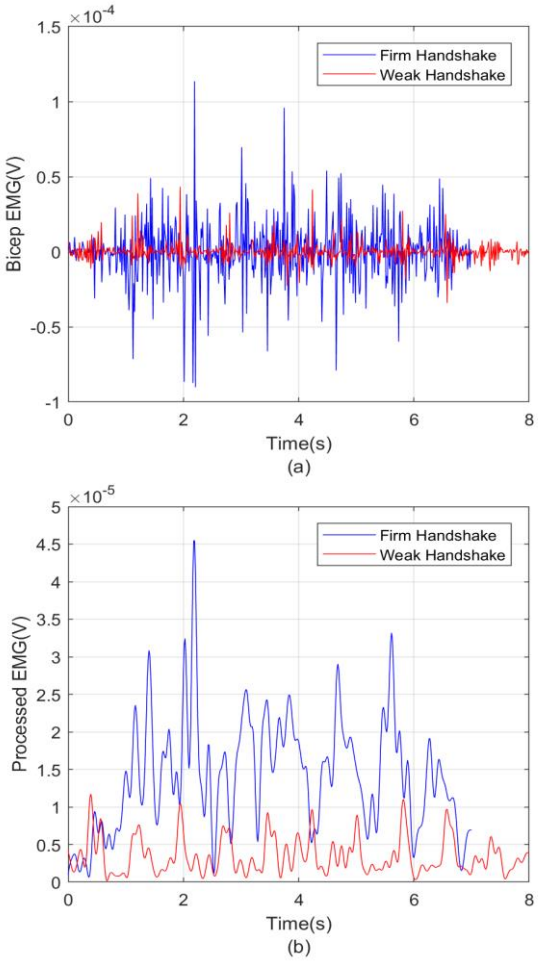

Fig. 2.11 Bicep EMG signals. (a): Original EMG signals. (b) Processed EMG signals

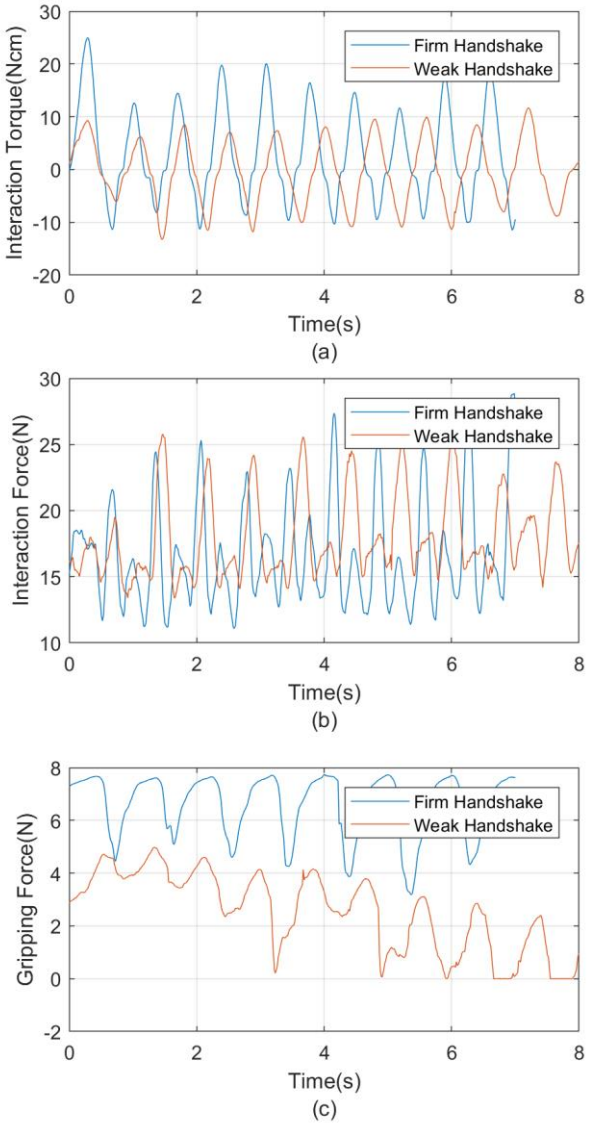

Fig. 2.12 Measured data of different handshakes. (a): Interaction torque of the handshakes. (b) Interaction force of the handshakes. (c) Gripping force of the handshakes.

Table 2-I: RMS of the measured data

Handshake Conditions	Interaction Torque(Ncm)	Interaction force(N)	Grasping Force(N)
Firm	9.1829	18.2595	6.6768
Weak	6.0399	17.2400	2.9449

In this research, we proposed a new device to investigate the interaction force of a two-person handshake and we measured different types of handshakes to demonstrate the effectiveness of the device. The results of the experiment indicated that there is a difference between firm handshake and weak handshake in term of interaction force and grasping force, therefore in order to regenerate different types of handshakes on a robotic arm, it is necessary to create both the grasping force and interaction force which is related to the muscle activation and joint stiffness of human arm.

2.6. Variable viscoelasticity estimation experiments

In this section, we measured the physical characteristics of 10 subjects in different social settings and analyzed the measured viscoelasticity properties to find the difference in different types of handshakes.

2.6.1. Experiment purpose

Based on the assumption that variation in joint viscoelasticity can create different handshake feelings, first we need to acquire the quantitative joint viscoelasticity property under different handshake situations for analyzing. However, because the joint viscoelasticity is not directly measurable in complete free motion[62], we used the estimation methods introduced in section 2.4 to estimate the joint viscoelasticity property. For that purpose, we need to measure the basic physical property during a handshake, i.e. length and weight of the arm, joint angle, angular speed, and interaction force, etc.

2.6.2. Experiment setup

9 male subjects (ages from 21 to 37) who were moderately active participated in the study. The subjects ranged in height from 168 to 180 cm and in body mass from 50 to 80 kg. All the subjects were in good physical condition, without injuries or muscular problems. The height and weight of each subject were recorded for the analysis of the dynamics in nMotion and in order to get a more accurate musculoskeletal model in nMtion, we measured the shoulder width of each subject. All the data of the subjects were shown in Table 2-II. For the details of how to create a musculoskeletal model in nMotion please refer to Appendix D. The study was approved by the Ethics Committee of Chuo University and was performed after each subject signed informed consent. The experimenter in this research is a healthy male research assistant from the same research lab.

Table 2-II Subject list of the experiment

Subject No.	Height (cm)	Weight (kg)	Age	Shoulder width (cm)
1	168	68	37	42.5
2	168	50	23	40.2
3	177	68	30	42.5
4	180	78	22	43.6
5	176	64	21	41.6
6	171	68	23	43.4
7	175	54	21	42.1
8	175	78	23	42.6
9	180	80	35	43.8

In order to measure the different handshakes, an instruction video was made to explain two different feelings of a handshake: an enthusiastic handshake (firm handshake) and an indifferent handshake (weak handshake) (shown in Fig. 2.13). Then we made a conversation with each subject to make sure that they had experienced the actual feelings of these 2 different handshakes and then they were asked to practice different handshakes until they were confident to perform both. During the experiments, the subjects were instructed to do the firm handshake and weak handshake 3 times each with the experimenter. One scene of the experiments is shown in Fig. 2.14.

Each trial of the experiment started by the staff saying “start!” and press a button to send the start signal to the motion capture device. And each subject was instructed to shake hands ten times in each trial. This handshake duration was around 1.5 times longer than a common business handshake. The start trigger was applied for the convenience of comparison in the analysis of the data, and the handshake duration was determined to make sure there is enough data for analysis and the ending cycle of the movement will be trimmed in when the data was processed.

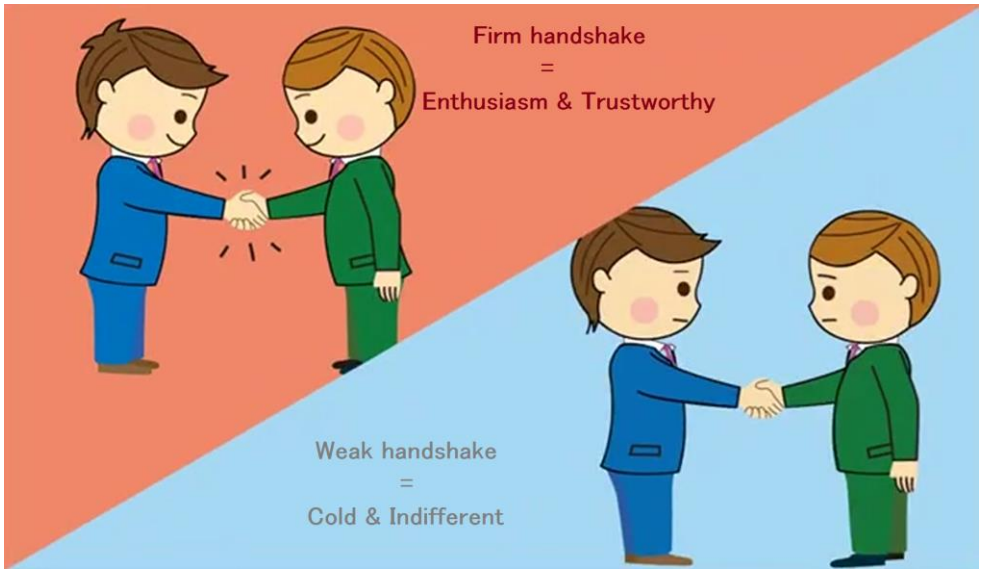

Fig. 2.13 Introduction of experiment conditions

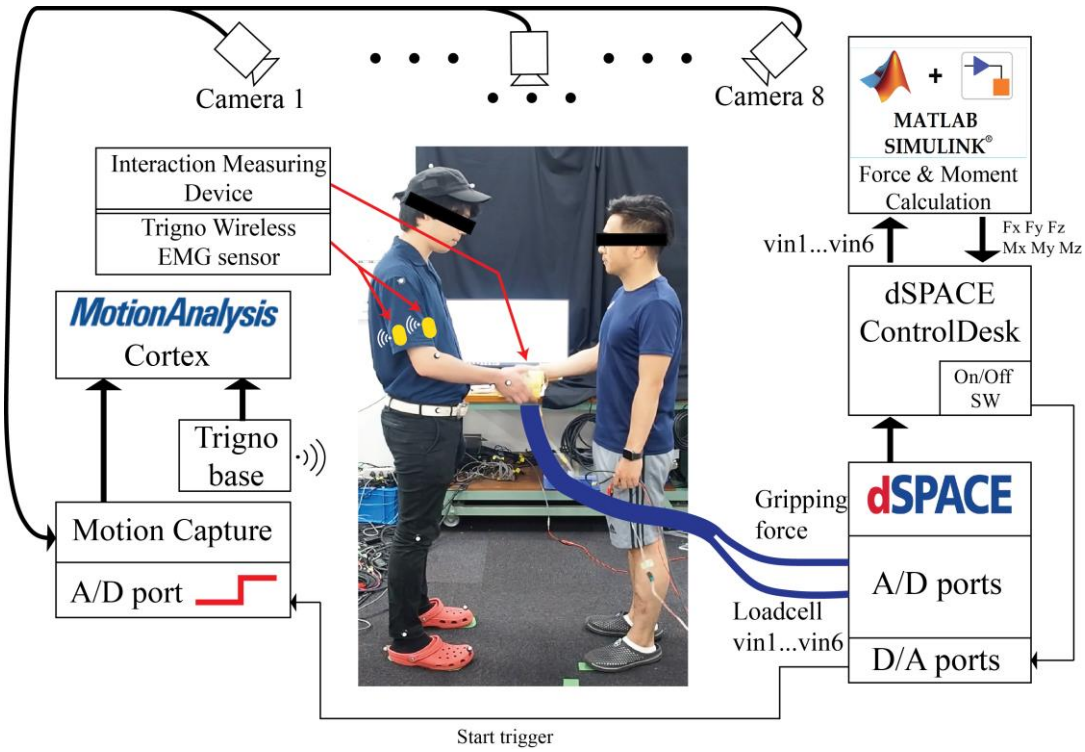

Fig. 2.14 The diagram of the complete handshake measurement system

2.6.3. Data acquisition and processing

In this experiment, the interaction forces and moments of 3 axes were measured by the measuring device proposed in section 2.5. The 6 output voltage signals of the loadcell were amplified by a special amplifier and sent into the AD ports of dSPACE. A mathematic model of the loadcell was built by Matlab and the forces and moments of 3 axes were calculated (refer to Appendix C for the details of the input and output of the loadcell used in this experiment).

The movement of the subject was recorded with the motion capture device (MAC3D System). 20 points Helen-hayes marker-set was applied (shown in Fig. 2.15) Then the captured motion data were processed in the motion capture analyzing software called Cortex. The recorded markers were first assigned to the Helen-hayes model, then the unnamed markers were deleted to make the model clean. Next, the trajectories of the marker with lost frames of each were connected with linear interpolation of cubic interpolation. Followed by, the trajectory of each marker was filtered with a low-pass filter (cut-off frequency 6Hz) to remove the high-frequency noise. (refer to Appendix B for details of the motion capture device). Finally, the whole capture data were trimmed. The starting point of the trimmed data was set at receiving the trigger signal sent by the staff of the experiment, and the ending point of the data was set at the end of the second last shaking cycle of the handshake.

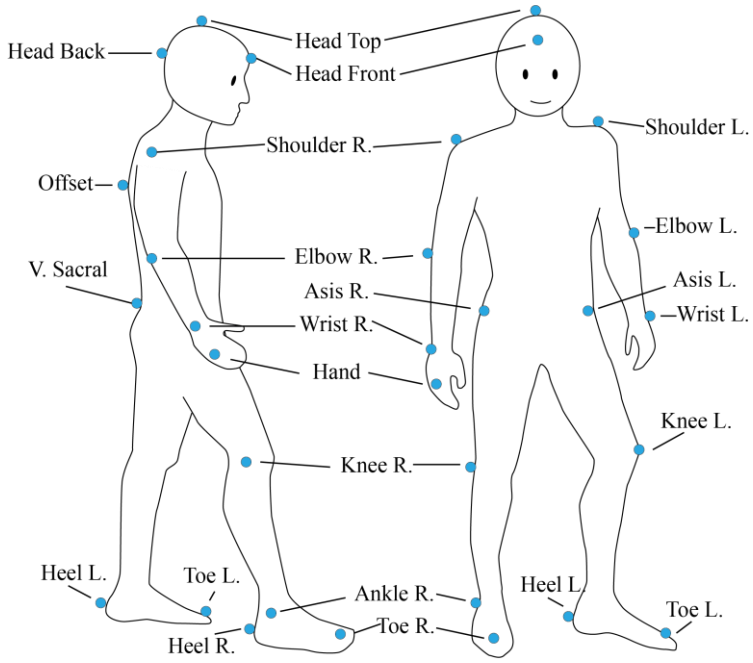

Fig. 2.15 Modified Helen-hayes markerset

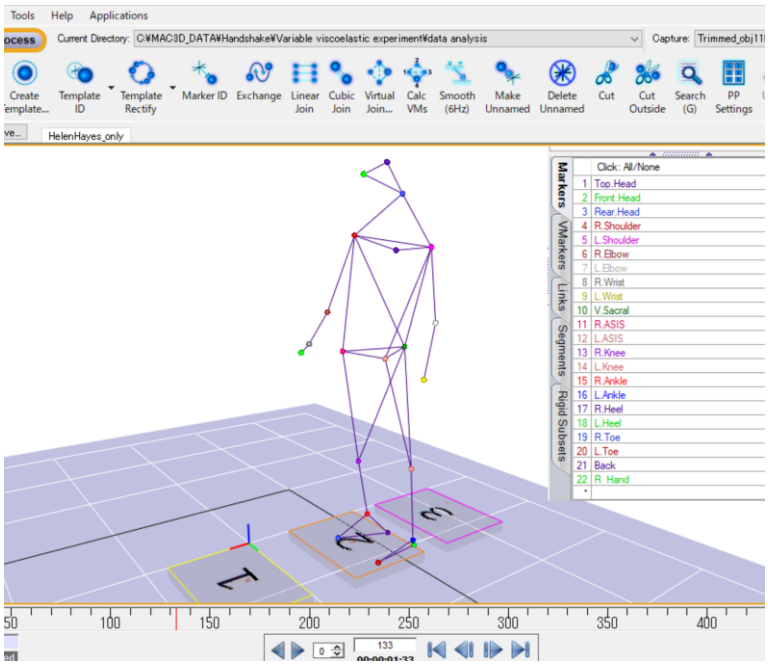

Fig. 2.16 Model in the motion capture analysis software

The processed motion capture data and the calculated interaction forces data were then applied to the musculoskeletal model motion analysis software nMotion for kinetics, i.e. joint angle and angular velocity, etc. The interaction forces and moments were then fed into the musculoskeletal model in nMotion as the external force for the calculation of joint torque (shown in Fig. 2.16) (refer to Appendix D for the processing steps of nMotion). Joint stiffness and viscosity are estimated form the kinetics and dynamics derived in nMotion using the methods introduced in section 2.4.

EMG signals of bicep and tricep of both the subject and the experimenter were recorded by Delsys wireless EMG sensor (refer to Appendix E for details of the sensor). EMG signal was sampled at 2 kHz with a 16-bit resolution. EMG signals were recorded together with the motion capture data in Cortex and were trimmed with the same starting point and ending point as the motion capture data, then exported for processing. First, the DC offset of the signal was removed then the signal digitally rectified, filtered with a second-order, low-pass filter with cut-off frequency at 10 Hz, and finally sampled at 100Hz. All the processing was done in Matlab.

After preprocessing the acquired data, we excluded the data of EMG and interaction force with too much noise and the motion capture data with invisible markers. Eventually, we obtained valid data of 51 trials in total, 24 trials of firm handshake and 27 trials of weak handshake. The details of the analyzed data are presented in the next section.

2.6.4. Experiment results

Interaction force

The graph of forces and moments of one subject in the same trial were shown in Fig. 2.17. As the graph indicated, the moments are relatively small compared to the forces (average moment/force is around 10^{-2}), and it has been verified in the later analysis in nMotion that the moments' have little effect on the joint torque calculation. Therefore, we only analyzed the forces in this section.

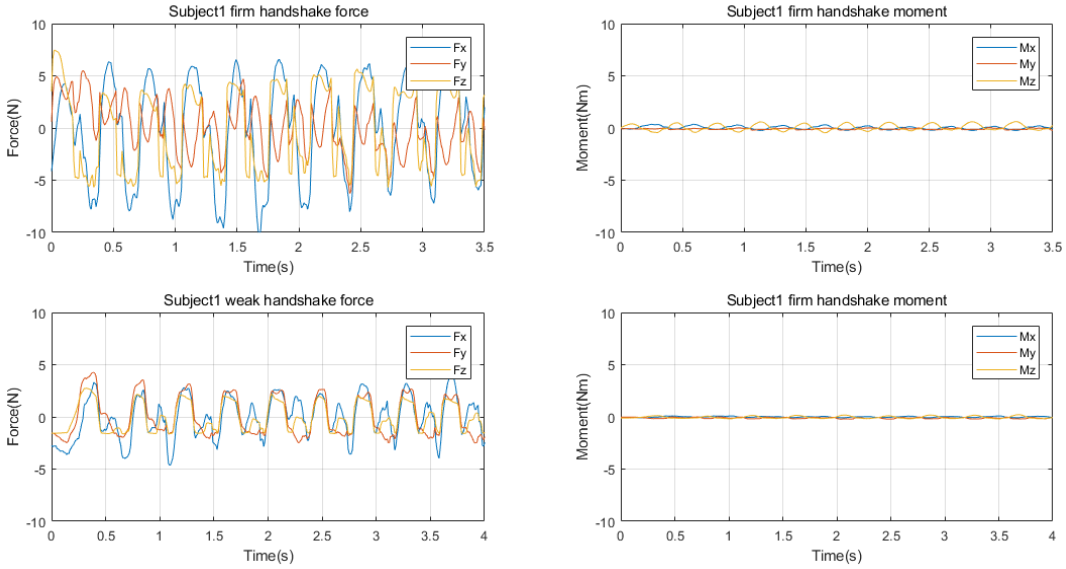

Fig. 2.17 The interaction forces and moments in different handshake conditions

The graph of the forces of the first 5 subjects was shown in Fig. 2.18. The graph indicated that the interaction forces are distinctively higher in firm handshake conditions than in weak handshake conditions and that even though the all the forces showed the similar cycle as the elbow angle every subject presented a distinctive pattern, which is an indication that different people regulates the stiffness of the arm in a different way. This is also part of the reason that caused different feelings of handshakes. Because the characteristics of the interaction force is difficult to see in a periodic signal, we rectified the signal and calculated the average. Data of all trials are shown in Fig. 2.19. The x and y coordinates of each marker represented the forces on x- and y-axis, while the force on the z-axis was represented by the size of the marker. The red markers are the interaction forces measured under a firm handshake condition, while the blue markers are the forces measured under a weak handshake condition. It was demonstrated in the graph that the distribution of the interaction forces in the x-y plane in a weak handshake condition forms a relatively clear cluster, while the markers for the firm handshakes were scattered more widely, which may indicate that different subjects have different standards of firm handshakes.

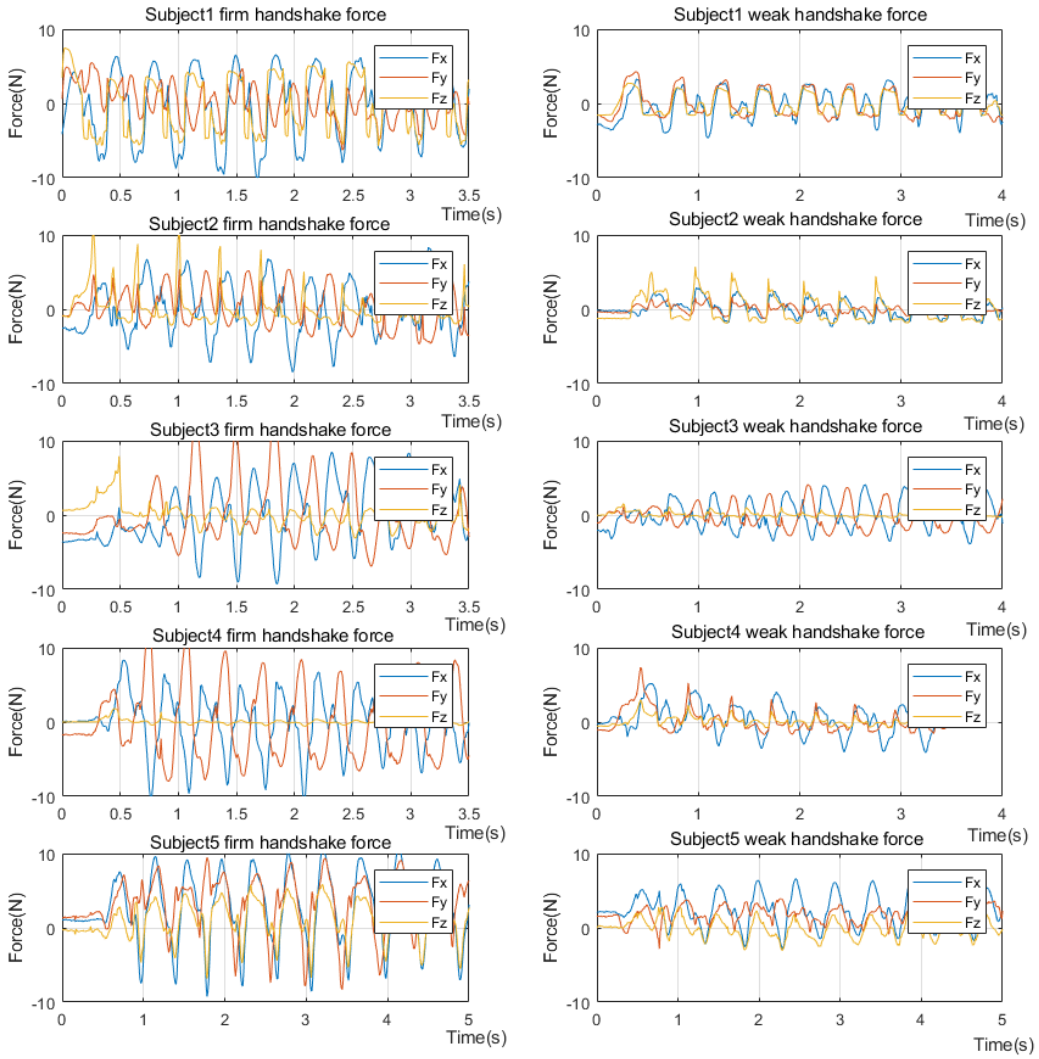

Fig. 2.18 Interaction forces of 5 subjects in firm and weak handshakes

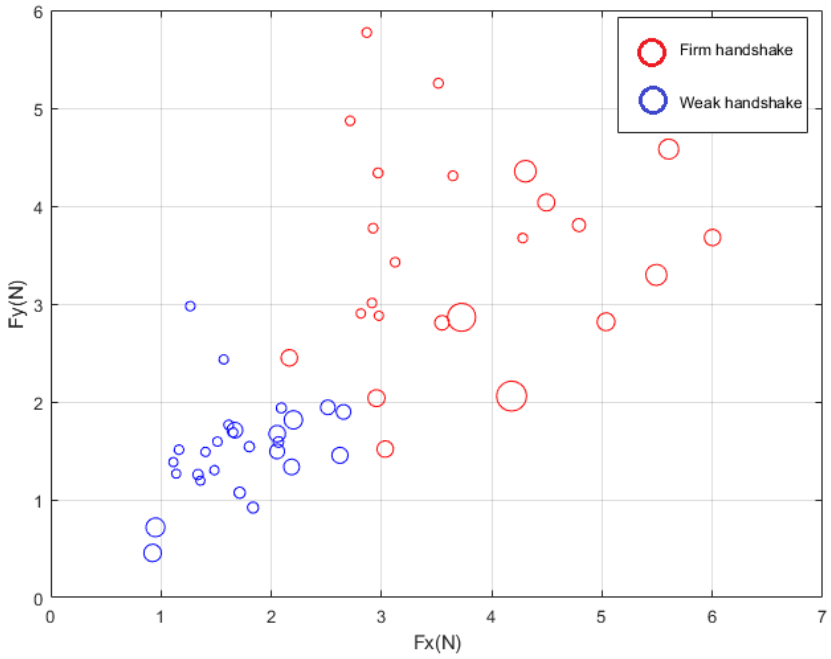

Fig. 2.19 Interaction forces mapped in a two-dimensional plane

Since the musculoskeletal model in nMotion utilizes different sets of coordinations as the loadcell, it is necessary to do a coordination transfer before the measured interaction force can be used in nMotion for dynamics analysis. The transfer function is given by Eq.(2.12), and the different coordinations are shown in Fig. 2.20.

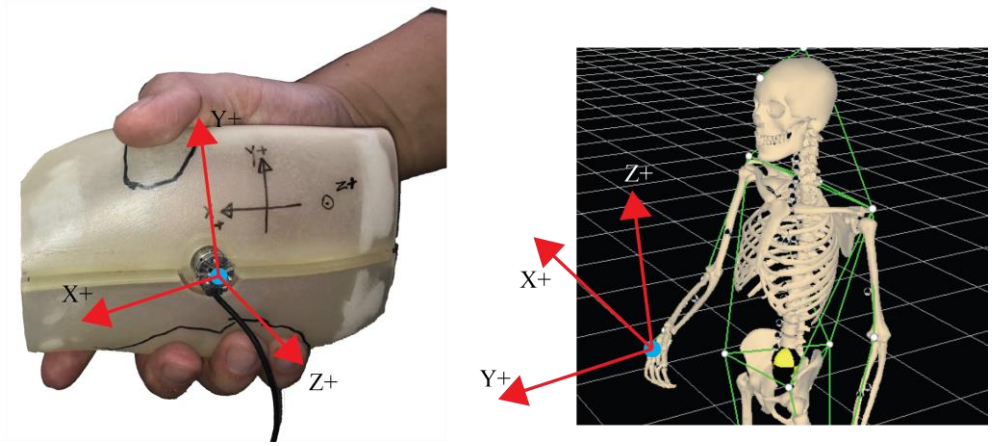

Fig. 2.20 Left: Direction of the coordinate in the measuring device
Right: Direction of the coordinate in the physical model in nMotion

$$\begin{pmatrix} X_M \\ Y_M \\ Z_M \end{pmatrix} = \begin{pmatrix} 0 & 1 & 0 \\ 1 & 0 & 0 \\ 0 & 0 & -1 \end{pmatrix} \begin{pmatrix} X_S \\ Y_S \\ Z_S \end{pmatrix} \tag{2.12}$$

Where the subscript M refers to the coordination of the musculoskeletal model, whereas the subscript S refers to the coordination of the load cell sensor.

Torque and EMG

For torque estimation, the motion capture data were first imported into nMotion, and each marker was matched to a marker on the musculoskeletal model. Then the height, weight, and shoulder-width were input into the model, and the kinetics were calculated, joint angle and angular speed were obtained at this step. After the coordinates transfer, the interaction forces measured by the measuring device were input into the model as external forces, then the whole system was solved by inverse dynamics for joint torque, muscle contraction force, etc. The graphs of one subject's data were shown in Fig. 2.21.

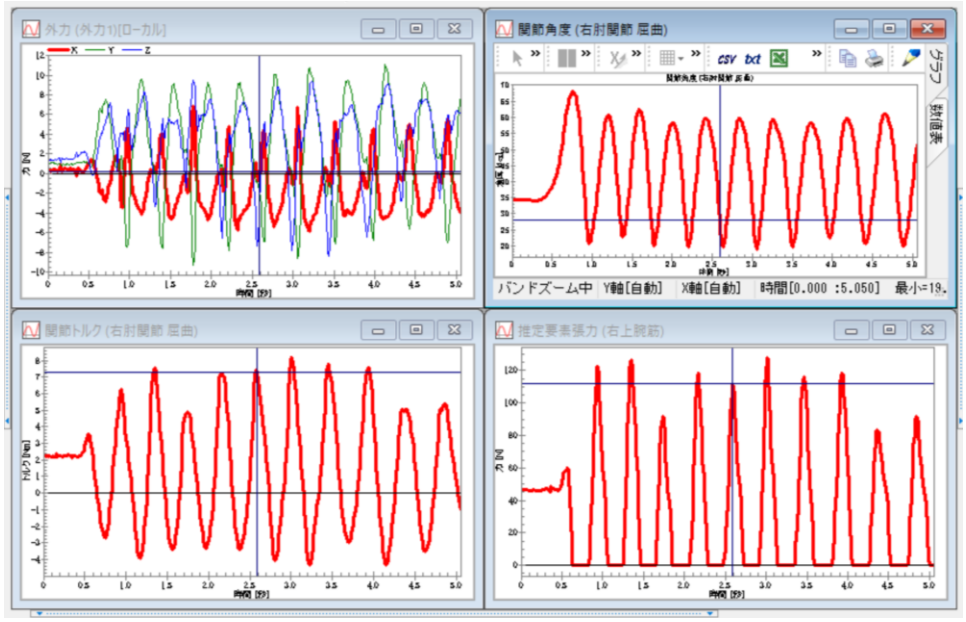

Fig. 2.21 The kinetics analysis of elbow joint in nMotion

EMG signals of the subjects' bicep and tricep were recorded by the wireless EMG sensor together with the motion capture data in Cortex and were trimmed into the same size as the motion capture data, then exported for processing. First, the DC offset of the signal was removed then the signal digitally rectified, filtered with a second-order, low-pass filter with cut-off frequency at 10 Hz, and finally sampled at 100Hz. In order to demonstrate the opposite contraction direction of bicep and tricep, the EMG signals of triceps are multiplied by -1. All the processing was done in Matlab. The EMG and torque data of subjects 1 to 5 were shown in Fig. 2.22. This data indicated that there is no correlation between the joint torque and EMG levels. And even though every subject demonstrates different torque patterns, the same subject showed a similar pattern in a firm handshake and weak handshake.

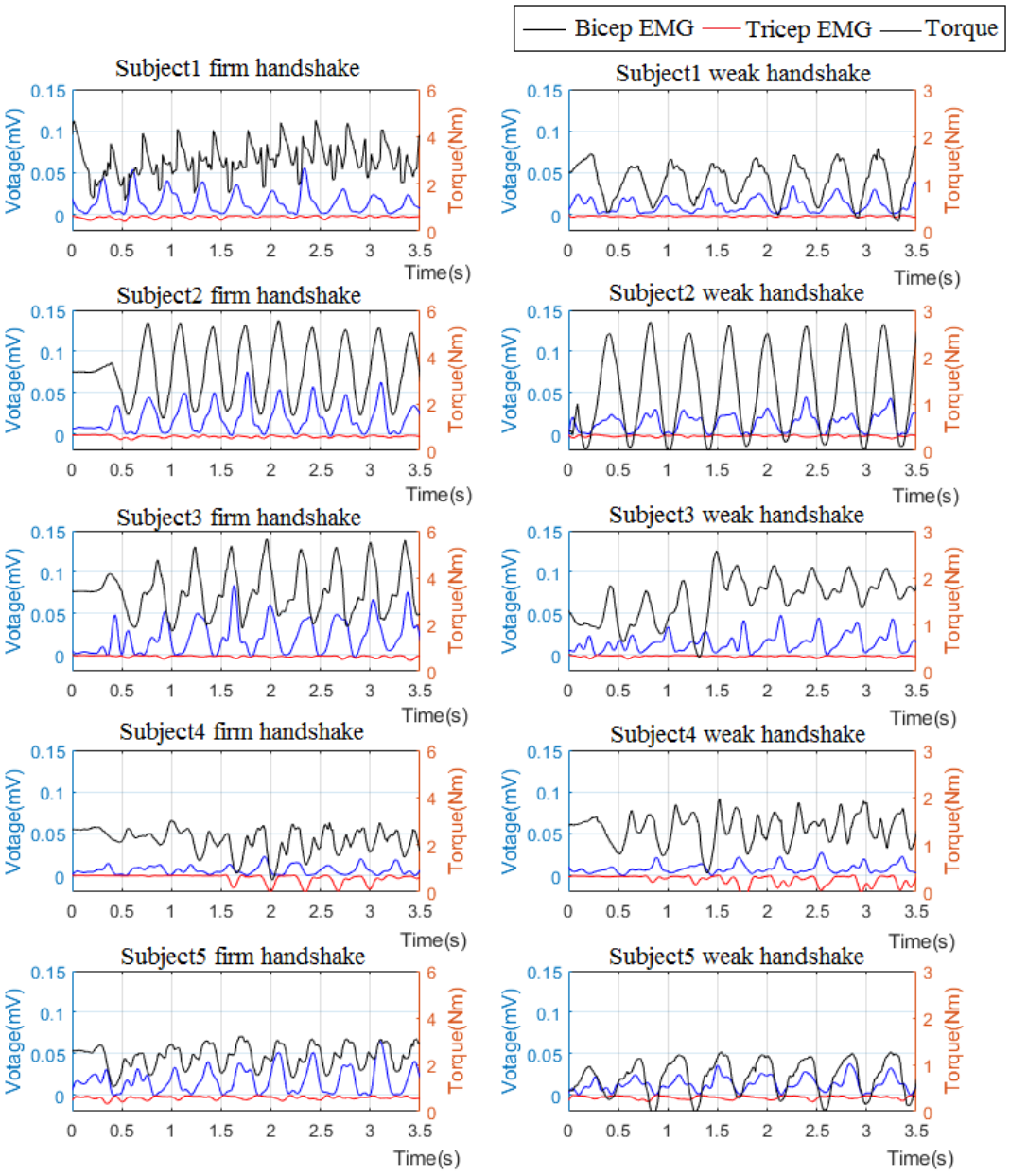

Fig. 2.22 Torque and EMG signals of 5 subjects in firm and weak handshake conditions

Joint viscosity

The joint angle, stiffness and viscosity of subject 1 were shown in Fig. 2.23. Left side of the figure is the data in firm handshake condition and right side of the figure is the data in weak handshake condition. From the graph, it can be told that the joint angle and stiffness presented clear differences under different handshake conditions, however, joint viscosity didn't appear to be much different. And the results of the multielements analysis of variance were shown in Fig. 2.24. Significant difference was found in the joint stiffness but not in joint viscosity, shown in Fig. 2.25.

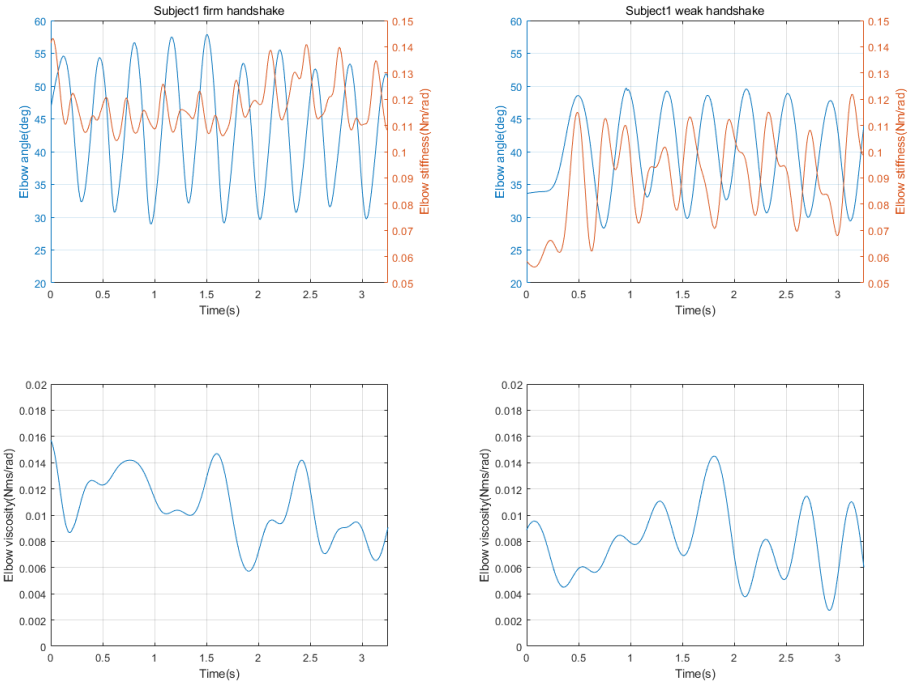

Fig. 2.23 The joint angle, stiffness and viscosity of subject 1

Analysis of Variance

Source	Sum Sq.	d.f.	Mean Sq.	F	Prob>F
X1	119.985	8	14.998	2.45	0.0287
X2	220.712	1	220.712	36.06	0
Error	250.916	41	6.12		
Total	588.557	50			

Fig. 2.24 Analysis of variance of joint stiffness

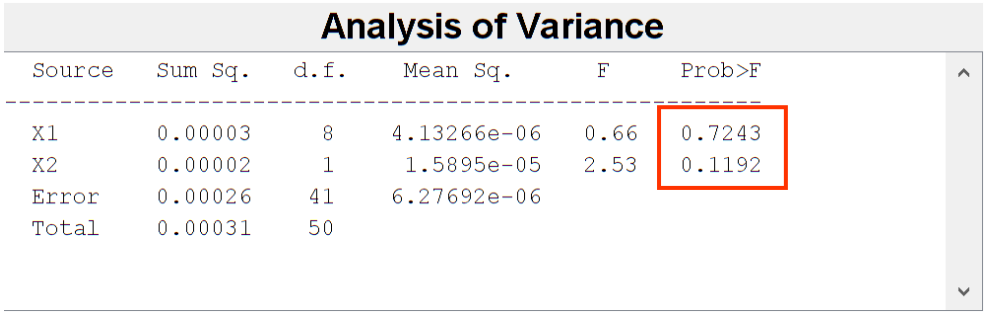

Analysis of Variance

Source	Sum Sq.	d.f.	Mean Sq.	F	Prob>F
X1	0.00003	8	4.13266e-06	0.66	0.7243
X2	0.00002	1	1.5895e-05	2.53	0.1192
Error	0.00026	41	6.27692e-06		
Total	0.00031	50			

Fig. 2.25 Analysis of variance of joint viscosity

Gripping force

Gripping force of subject 1 to 5 were shown in Fig. 2.26. It can be seen clearly from the graphs that gripping force was higher in all firm handshake conditions compared to weak handshake conditions. It suggested that the gripping force can be used as an indicator of a firm handshake. And the analysis of variance of gripping force in all trials is shown in Fig. 2.27. Significant difference was found by this analysis.

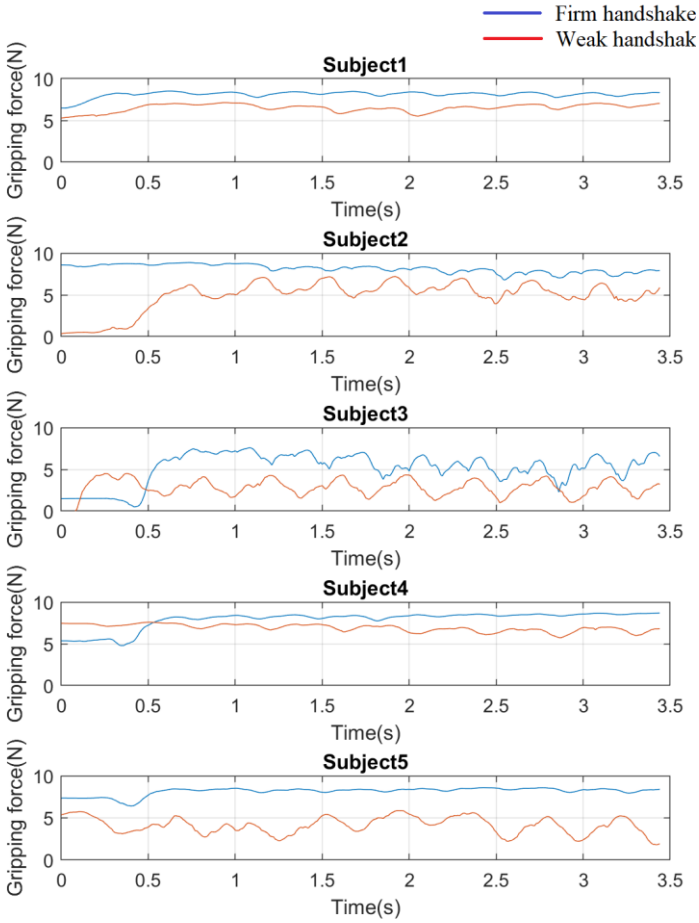

Fig. 2.26 Gripping force of subject 1 to 5

Analysis of Variance

Source	Sum Sq.	d.f.	Mean Sq.	F	Prob>F
X1	83.913	9	9.324	7.08	4.77111e-06
X2	129.429	1	129.429	98.27	2.48079e-12
Error	52.681	40	1.317		
Total	262.76	50			

Fig. 2.27 Analysis of variance of gripping force

Overall characteristics

The complete data of all the items we analyzed for human-human handshake were listed in Table 2-III. An Artificial Neural Network(ANN) with 2 hidden layers was made and trained based on this data set in order to tell if a certain handshake is a firm handshake or a weak handshake. After training the model for 100 iterations, we got a successful prediction rate of 83.57%, as shown in Fig. 2.28. Considering the relatively small data size, the performance of the model is not bad. And it has proven that the difference of handshakes can be told apart by the measured physical properties. For the details of the ANN model please refer to Appendix F.

```
Epoch 98/100
50/50 [==============================] - 0s 59us/step - loss: 0.3962 - accuracy: 0.8370
Epoch 99/100
50/50 [==============================] - 0s 60us/step - loss: 0.3960 - accuracy: 0.8354
Epoch 100/100
50/50 [==============================] - 0s 59us/step - loss: 0.3962 - accuracy: 0.8357
```

Fig. 2.28 Successful prediction rate of the handshakes

Table 2-III Complete list of the measured physical properties

No.	Physical properites	
1	Interaction force	Ave. Fx(N)
2		Ave. Fy(N)
3		Ave. Fz(N)
4	Ave. grip(N)	
5	Duration(s)	
6	Frequency(Hz)	
7	Elbow angle range(deg)	
8	Elbow angular speed range(deg/s)	
9	Elbow ave. angular speed(deg/s)	
10	Ave. torque(Nm)	
11	Viscoelasticity	Ave stiffness(Nm/rad)
12		Ave viscosity(Nms/rad)
13	EMG	Bicep EMS RMS(μV)
14		Tricep EMS RMS(μV)

2.7. Conclusions

In this chapter, a set of measuring methods were proposed for analyzing the handshake movements. Human handshake are recoded and analyzed under firm handshake and weak handshake conditions. The physical properties used for analysis include: interation forces, joint torques, gripping forces, joint angle, angular velocity, joint stiffness, joint viscosity and EMG signals.

By conducting multielements analysis of variance to different sets of data, we have come to the Conclusions:

Significant differences were found in joint sitffness and gripping force under different handshake conditions. This indicated that joint stiffness can be used as an indicator of different handshakes.

No significant differences were found in joint viscosity. This can be explained by the fact that all human joint are underdamped the joint viscosity only varies in a very small range.

2.8. Summary

In this chapter, we first stated the reason why viscoelasticity analysis of the human arm is necessary for the studies of the human-robot interaction. And according to the history of the research of handshakes introduced in section 1.2, so far there has been no research of handshakes focused on the viscoelasticity property of human arm. Based on these facts, we started our handshake research by estimating the stiffness and viscosity of human arm during handshake movements.

In order to make an accurate estimation of stiffness and viscosity of human joint, it is necessary to have an explicit definition of each characteristic and derive the estimation function based on the definition. Therefore, in section 2.2 and 2.3, we first explained in detail the definition of physical property of stiffness and viscosity, and then explained how muscle tissue presents the similar property of viscoelastic material and the attempts people have make through out the year to apply the physical property on human joint study. Even though the most fundamental mechanism of viscoelastic characterisc remains unclear, sereval commonly accepted definitions under certain circumstances have been developed. In which we chose the one that fits the purpose of our study the most and analyzed several ways to get an estimation under this definition. Considering the requirement of studying an natrual and unrepeatable handshake movement, we have chosen the estimation method that does not require multiple repetition.

The experiment section explained how the motion capture, interaction force and EMG was acquired and processed. Then the processed data was used for estimation of joint stiffness and viscosity. And all the physical properties of human arm under two different handshake conditions were compared and the

results were shown in the experiment results section.

Based on the experiment results we made the Conclusions that viscoelasticity varies according to different types of handshakes therefore verified our assumption.

Chapter 3

Variable viscoelastic handshake manipulator

Chapter 3.
Variable viscoelastic handshake manipulator

So far, a lot of handshake robots have been developed, the majority of those researches focused on the planning of the shaking motion of the robotic arm. In order to achieve high precision of position and speed control, most of the handshake robots are driven by motors and reduction gears. However, this type of structure lacks back-drivability and compliancy, therefore, we proposed a new kind of handshake manipulator which is soft, safe, and with high back-drivability.

3.1. Concept of the handshake manipulator design

Conventional industrial robots are commonly shielded from humans. However, with the development of social robots in recent years, robots are purposely put in contact with a human for interaction, such as rehabilitation or support for hard physical labor. Therefore, social and physical interactions between robots and humans are foreseeably to extend in the future [63]. The cooperation between humans and robots calls for attention to an inevitable question about the safety of the robot and how to plan the movement so that robots can interact with humans. In order to meet the foreseeably coming demands, we proposed a new type of robot arm that is driven by a soft actuator comprised of antagonistic artificial muscles and MR-brakes (shown in Fig. 3.1). The artificial muscles drive the joint by pulling a wire that is connected to the pulley of the joint. Joint angle and joint elasticity could be controlled independently by applying different air pressure to the artificial muscles. And MR brakes are used to achieve variable viscosity, also used to compensate for response overshoot of the artificial muscle. The artificial muscles represent the elastic element of human muscle and the MR-brakes represent the viscous element of human muscle. In this research, the proposed robot arm was specialized for human-robot handshake research which is why it is referred to as the handshake manipulator. Each part of the handshake manipulator and its controller are explained in detail in the following sections.

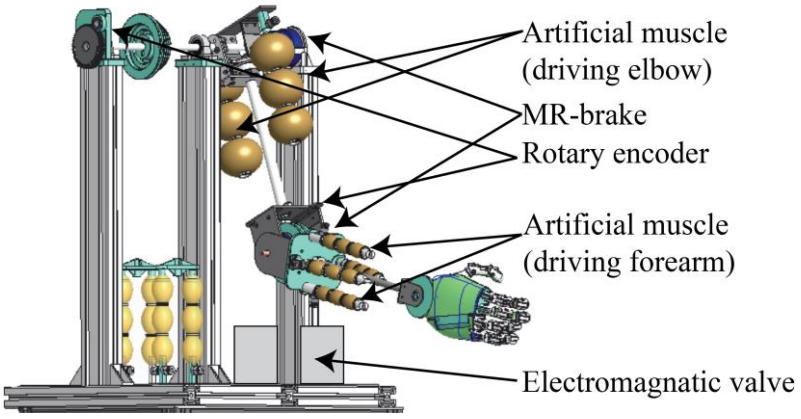

Fig. 3.1 Schematic diagram of the proposed handshake manipulator

3.2. Soft robotics

Traditional rigid robot arms are effective at precise, accurate, rapid motions. Meanwhile, there is another category of robots being developed, which is the soft robotics. It is one of the most inspiring developments in the robotics field, designed to realize safe and natural behaviors. They rely on compliant physical structures and variable impedance characteristics, which make them safe to work in the vicinity of and together with humans, instead of being isolated in a fixed working space [64]. Even though the field of soft robotic manipulators was founded in the 1960s, formal research on the design and control can be dated back to the early 1990s. The term soft robotics is associated with two distinct design approaches (1) continuum robotic manipulators; (2) compliant joint within rigid-link robots [65]. Continuum manipulators are the result of the evolution of manipulator design without rigid-links but rather with elastic structures capable of continuous bending along their length. There has been no unified method for controlling or fabricating this kind of robot. Whereas controlling the impedance of joint for the robot arm to interacting with the environment safe is a relatively more mature technology, and the variable viscoelasticity manipulator utilized in this paper can be categorized in this area [66].

Controlling rigid robots and soft robots follow two different ways of thinking. Control strategy for rigid robots is usually based on an accurate physical model, in contrary to soft robots modulating joint impedance to interact with environments. These two different attempts to control robots' movements are also a reflection of the two controversial hypotheses in the field of motor control for human movements: whether the brain requires accurate motor commands to control the body movements, or whether the brain makes use of the viscoelasticity of musculoskeletal system so accurate command is not necessary [67]. There have been proofs shown that short- and long-term motion learning may rely on different strategies of motor controls. Our research focused on replicating the impedance modulation of the human arm on a variable stiffness manipulator. The human brain learns to exploit the force and tactile contact sensation of the musculoskeletal system to control the body fulfilling all kinds of tasks by manipulating intrinsic compliance. As a result, by examining how human controls joint impedance, it may help us to understand the underlying human motor control strategy and develop control methods for robots accordingly.

3.3. The selection of soft actuator for the handshake manipulator

The manipulator is safe and flexible for human-robot interaction. Directly controlling the impedance of the joints makes it easier to synchronize with human movement. The variable stiffness and viscosity characteristics make it a better representation of human muscle, and able to generate handshakes of different feelings.

The following sections will explain in detail the structure of the manipulator and why is it resembles the real human joints. And we used the proposed manipulator to test the variable viscosity and stiffness handshake movement and verified its effectiveness in doing research on creating different feelings of handshake.

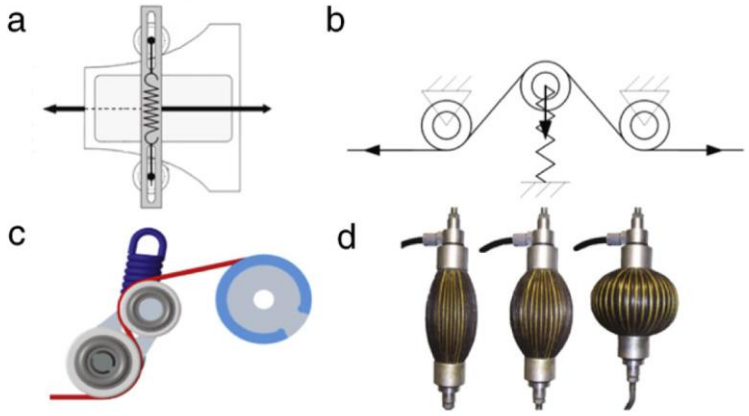

Fig. 3.2 Nonlinear springs
(a) cam mechanism (b) triangle mechanism
(c) Adapted triangle mechanism (d) pneumatic muscles

So far, there are two approaches to use as the actuator in soft robotics, the first one is the technology of torque-controlled motor, which is a relatively mature technology. The second one is variable compliance actuation that implements the soft-robotic features mainly in hardware, which is still a topic of ongoing research. Fig. 3.2 shows several possible nonlinear springs can be used as the elastic element in soft robotics [68]. Considering the resemblance to the musculoskeletal system of the human arm, I decided to use pneumatic artificial muscles as the elastic element in the manipulator.

3.4. The structure of the joint

According to the previous studies [69][70], and the introduction in section 1.3-1.4, the human joints are driven by antagonistic muscles. And the physical model of a joint comprised of two separate elements, the elastic element and the viscous element as shown in Fig. 3.3. The elastic element determines the angle and the stiffness of the joint, in which joint angle and joint stiffness can be controlled independently, while the viscous element determines the viscosity of the joint, which generates the velocity related frictional power in the joint. In this research, we made the assumption that human arms are able to perform different handshakes by controlling the viscosity and stiffness of the joints. Considering the variable viscoelastic features of the human joint, we proposed the combination of magneto-rheological fluid brakes (MR brake) and artificial muscles as the actuator for robots that aim at doing research on human-robot interaction.

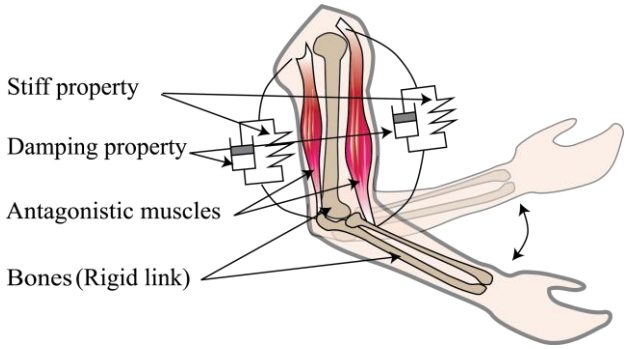

Fig. 3.3 Structure of human elbow joint

3.5. Variable viscoelastic handshake manipulator

In this section, the details of the handshake manipulator will be explained.

3.5.1. Configuration of the variable viscoelastic actuator

In this research, we proposed a soft actuator comprised of one pair of artificial muscles which resemble the elastic part of the human muscle and MR-brakes which resemble the viscous element of the human muscle. The configuration of a single actuator is shown in Fig. 3.4. The artificial muscles were installed antagonistically when air pressure was applied to the artificial muscles, they would contract and pull the tendon connected to the pulley. The rotation axis of the joint was connected to the rotor in the MR-brake, and by controlling the current applied, the MR-brake generates friction force the same as the damping element in a real human joint.

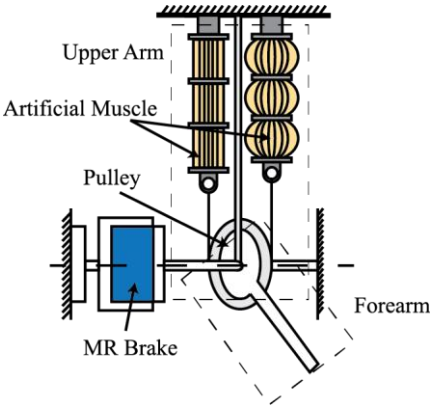

Fig. 3.4 Structure of the elbow joint

3.5.2. Straight-fiber-type artificial muscle

The artificial muscle we used in the proposed actuator is called the straight-fiber-type artificial muscle. It contracts in the axial direction and expands in radial directions when air pressure is applied. Varies by diameter, length and section number of the artificial muscle, the maximum contraction rate of a straight-fiber-type artificial muscle is between 25-30%. The schematic diagram of a straight-fiber-type artificial muscle is shown in Fig. 3.5.

The shape of the artificial muscle is a tube, and the material is natural rubber-latex liquid. When air pressure is applied, the rubber will expand, but since there is a carbon fiber layer in the axial direction, the fiber restrains the expansion so that the rubber is not extended. As a result, the artificial muscle only expands in the radial direction while contracts in the axial direction [70].

Because of the elasticity of the rubber material and the air filled within, the artificial muscle can be seen as an elastic element with a variable elastic coefficient. Fig. 3.6 shows that an approximately linear correlation was found between the stiffness and applied pressure. Artificial muscles are flexible, light in weight, and are able to generate high contraction force. When two artificial muscles are used antagonistically it makes an actuator that resembles the structure of the human joint [71]. Table 3-II shows the dimensions of the artificial muscle used in the elbow joint of this manipulator.

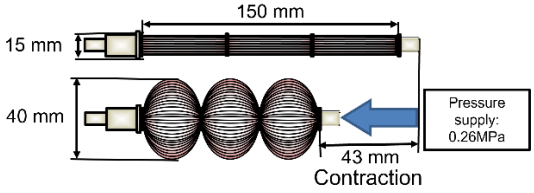

Fig. 3.5 Schematic diagram of Straight-fiber-type artificial muscle

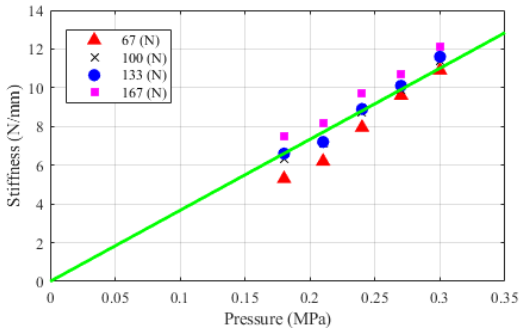

Fig. 3.6 Stiffness of the artificial muscle at different contractive forces

TABLE 3-I DIMENSIONS OF ARTIFICIAL MUSCLE

Description	Parameter Name	Dimension
Diameter of the Original Artificial Muscle (m)	$d0$	0.019
Diameter of the Inflated Artificial Muscle (m)	dm	0.046
Length of the Original Artificial Muscle (m)	$l0$	0.19
Length of the Inflated Artificial Muscle (m)	lm	0.13
Thickness of the Fiber (m)	t	0.004
Coefficient of the Fiber Tension	M	2
Number of Sections	N	3
Approximation Constant Number	α	1.85

3.5.3. MR-brake

The magneto-rheological fluid is a functional fluid which generates frictional torque when subjected to a magnetic field. MR-brake is a device that utilizes the characteristics of the MR fluid to generate controllable brake torque. Since the response of MR fluid is very fast, MR brake can reach the target output torque within approximately 10 ms [72]. MR brake is small enough in size to install in a robot arm and generates torque high enough to suspend the arm's movement, and the torque can be controlled accurately at a very high-speed response. Therefore, MR brake is ideal to use as the viscous element for the handshake manipulator.

A schematic diagram of the MR brake is shown in Fig. 3.7. And all the specifications of the MR brake used in this research are listed in Table 3-I. The MR brake mainly comprised of an outside case and an inside core. There are 8 disks attached to the inside core, and 9 disks attached to the outside case, MR fluid is fully filled between the disks. When applying a voltage to the coil planted inside the case, a magnetic field will be generated, which alters the molecular arrangement of the MR fluid and the friction torque is generated between the disks. Fig. 3.8 shows the basic property of the MR brake provided by the manufacturer. Since the intensity of the magnetic field generated by the coil is a function of input current, and the output frictional torque is determined by the intensity of the magnetic field. The output torque of the MR brake is controlled by the input current.

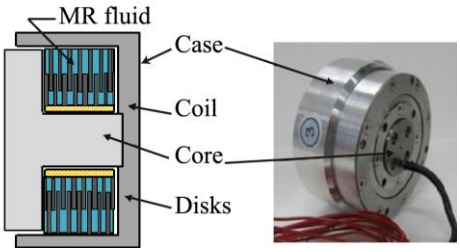

Fig. 3.7 Schematic diagram of the MR brake

TABLE 3-II DIMENSIONS OF MR BRAKE

Diameter (mm)	52.5
Width (mm)	30.6
Weight (kg)	0.277
Maximum Torque (Nm)	7.4
Minimum Torque (Nm)	0.12
Maximum current (A)	0.96
Base Friction (Nm)	0.2
Inserted MR Fluid (kg)	0.01463

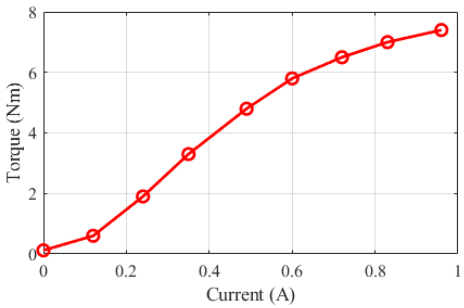

Fig. 3.8 The output torque characteristic of the MR brake

3.6. Introduction to the control method

Feed-forward controller

The mathematic model of the elbow joint was derived in the previous study [73]. With the proposed mathematic model, a feed-forward (FFW) controller can be developed. This is the most straightforward controller for the actuator comprised of artificial muscle and MR brake, which takes target angle, target stiffness and target viscosity as inputs and controls viscosity, elasticity and joint angle independently. In order to focus on studying how joint stiffness and viscosity can affect the feeling of handshake, we applied this controller in this research. This section is the deduction of the controller for the elbow joint. The model used to develop the controller of the elbow is shown in Fig. 3.9, and all the variables used in the deduction are listed in Table 3-III.

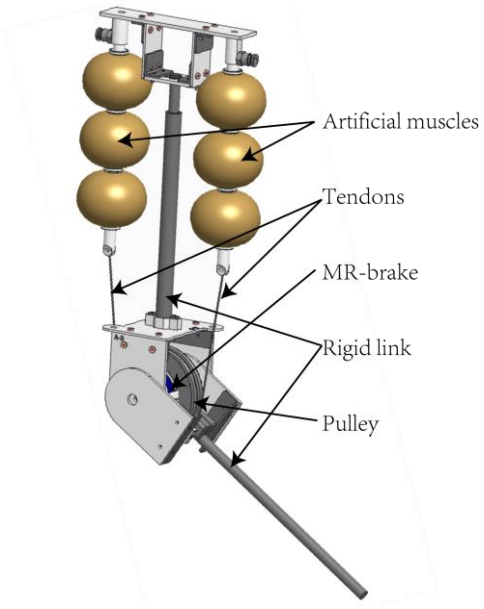

Fig. 3.9 Elbow structure of the handshake manipulator

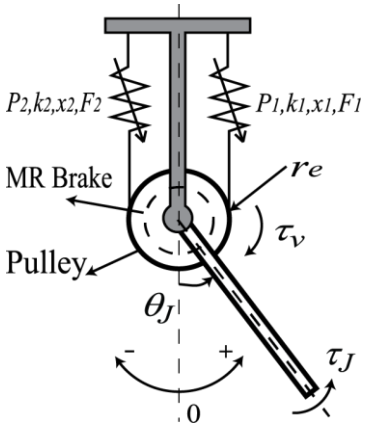

Fig. 3.10 The mathematic model of elbow joint

TABLE 3-III PARAMETERS OF THE ANTAGNOSITIC MUSCLE PHYSICAL MODEL

Description	Variable Name
Target Stiffness (Nm/rad)	K_J
Target angle (rad)	θ_J
Applied Air Pressure (Mpa)	P_1, P_2
Contraction of Artificial Muscle (m)	x_1, x_2
Coefficient of elasticity of Artificial Muscle (N/m)	k_1, k_2
Contractive Force of Artificial Muscle (N)	F_1, F_2
Radius of pulley (m)	r_e
Target torque (Nm)	τ_J
Viscous torque (Nm)	τ_v

With this controller, the pressure applied to the artificial muscles can be calculated by target contraction force and target shrinkage. In equation (3.1), P_{in} is the pressure applied, and F is the contracting force. $G_1(x)$, $G_2(x)$, $G_3(x)$ are the constants defined by shrinkage x and specifications of artificial muscle shown in Table 3-II. The detailed deduction of $G_1(x)$, $G_2(x)$, $G_3(x)$ are provided in the previous study [70].

$$P_{in}(x,F) = \frac{\{G_1(x) + FG_2(x)\}}{G_3(x)} \tag{3.1}$$

Angle and elasticity controller

This section is the detail of the FFW controller. The pressure applied is a function of the target joint stiffness K_J, target joint angle θ_J, and target joint torque τ_J.

First, the shrinkage of artificial muscle x_i is calculated as below. c_i in equations (3.2) is the slack of the wire when the joint angle is 0. Where i equals to 1 and 2 to represent each one of the antagonistic artificial muscle.

$$x_i = c_i + r_e\theta_J \tag{3.2}$$

Second, K_J is calculated by the equation below:

$$K_J = r_e^2(k_1 + k_2) \tag{3.3}$$

As explained in the earlier section, the stiffness of air muscle k_i is linear to the applied pressure. Here, k_i is defined as $k_i = k_aP_i$, where k_a is a coefficient determined by identification experiments, the details of the experiments were explained in the previous study [74]. In this experiment, k_a is approximated to be a constant. Therefore, K_J can be rewritten as below:

$$K_J = r_e^2k_a(P_1 + P_2) \tag{3.4}$$

Next, from equation (3.1), the contraction force of artificial muscle F_i can be calculated as below:

$$F_i(x_i,P_i) = \frac{\{P_iG_3(x_i) - G_1(x_i)\}}{G_2(x_i)} \tag{3.5}$$

Also, from the equilibrium of the mathematic model shown in Fig. 3.10, the following equation can be derived.

$$F_1(x_1,P_1) - F_2(x_2,P_2) - \tau_J / r_e = 0 \tag{3.6}$$

From equations (3.4), (3.5), and (3.6), the following equation is obtained:

$$P_1(K_J, x_1, x_2, \tau_J) = \{(\frac{K_J G_3(x_2) G_2(x_1)}{r_e^2 k_a} + G_2(x_2) G_1(x_1) + \frac{\tau_J G_2(x_1) G_2(x_2)}{r_e} - G_1(x_2) G_2(x_1))\} / \{G_2(x_2) G_3(x_1) + G_2(x_1) G_3(x_2)\} \quad (3.7)$$

$$P_2 = \frac{K_J}{r_e^2 k_a} - P_1 \quad (3.8)$$

According to equation (3.1), (3.7) and (3.8), the output angle, output torque and joint stiffness can be controlled independently. And the schematic of the proposed FFW controller of elbow is shown in Fig. 3.11.

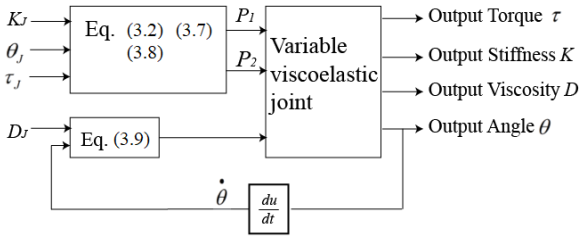

Fig. 3.11 The block diagram of FFW controller

Viscosity controller

Joint viscosity torque τ_v is defined as the multiplication of the target viscosity coefficient D_J and rotational speed $d\theta/dt$, as shown in equation (3.9). As explained in the previous section, the viscous torque is a function of the current applied on MR brake, however, for most of the microcontrollers, it's not possible to output steady controllable current. Therefore, we applied a motor driver (product of Okatech, model No. JW-143-2) to convert the control voltage into output current, in order to obtain the accurate desired frictional torque (refer to Appendix F for the detailed spec of the motor driver). Then, a controller that converts the frictional torque into joint viscosity was designed and implemented by Simulink. The block diagram of the viscosity controller is shown in Fig. 3.12.

$$\tau_v = D_J \frac{d\theta}{dt} \tag{3.9}$$

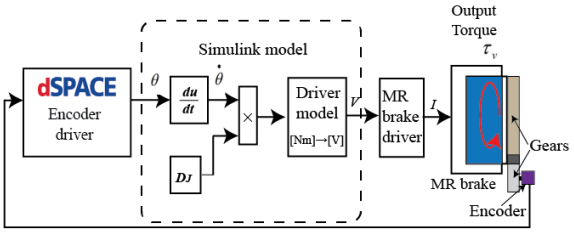

Fig. 3.12 The block diagram of MR controller

3.7. Design of the manipulator prototype

Design of the joints

The handshake manipulator has been primarily conceived for safe and performant robot arms for physically interacting with humans. Its back-drivability makes it soft and feels more natural when interacting with a human, and the variable viscoelastic characteristic is important when doing research on performing different handshakes. This section explains the detailed design of the manipulator prototype. The manipulator has 3 joints, shoulder, elbow and wrist, each joint is a 1-DOF joint, plus the fingers can be opened and closed so that the manipulator can hold hand with humans. There are totally five pairs of artificial muscles installed in this handshake manipulator. Two pairs are used to in parallel in the shoulder joint in order to generate contraction force high enough to pull up the whole arm. The elbow joint is driven by one pair of artificial muscles. The structure of the elbow joint was introduced in detail in the previous section. For the wrist joint, one pair of artificial muscles are installed vertically to drive the hand moving up and down, while another pair of artificial muscles are installed horizontally to open and close the fingers of the hand by pulling tendons go through each finger. Dimensions of the artificial muscles vary in each joint.

There are 2 MR brakes installed in the manipulator. One in the shoulder and one in the elbow. Considering the weight of the MR brake will affect the controllability of the whole arm, there is no MR brake installed on the wrist joint. The MR brakes used in this research are productions of ER-Tech. Co.

Design of the size

We designed the size of the manipulator in accordance with average Japanese adult male, we used the data that was published by AIST (National Institute of Advanced Industrial Science and Technology) in 1995. The schematic of the manipulator was shown in Fig. 3.13, and the specifications of each part are listed in Table 3-IV. And the complete diagram of the manipulator is shown in Fig. 3.14. Electromagnetic solenoid valves are used to control the air pressure applied to the artificial muscle and encoders are set on each joint to record the movement of each joint.

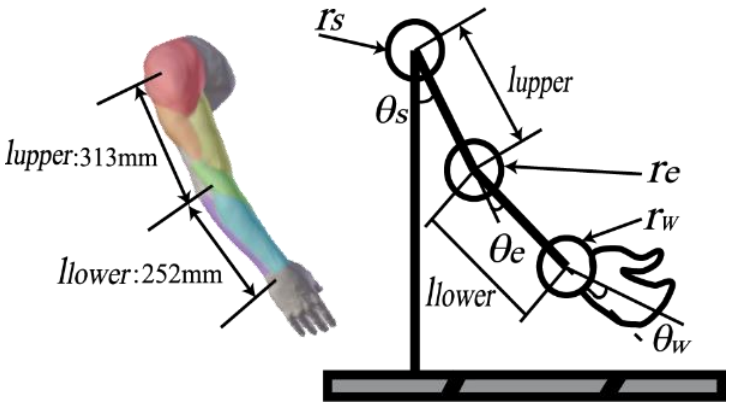

Fig. 3.13 Dimensions of the manipulator

TABLE 3-IV SPECIFICATIONS OF THE MANIPULATOR

Description	Dimension (m)
Upper Arm Length l_{upper}	0.313
Forearm Length l_{lower}	0.252
Radius of Shoulder Pulley r_s	0.085
Radius of Elbow Pulley r_e	0.065
Radius of Wrist Pulley r_w	0.03
Description	**Weight (kg)**
Upper Arm Weight m_{upper}	0.754
Forearm Weight m_{lower}	0.608
Hand Weight m_{hand}	0.351
Description	**Movable Angle Range (deg)**
Shoulder Angle θ_S	0 ~ 40
Shoulder Angle θ_E	20 ~ 75
Shoulder Angle θ_W	-40 ~ 40

Design of the hands

The shape of the hand had a great effect on the subjective feeling when handshake with the manipulator. Therefore, we work hard to make it feel like a real human hand. We designed the hand to be the size of the average adult man and utilized the 3D printer that can print with materials with different softness. Nylon tendons drive the fingers and palm to form a gripping pose, which creates the feeling of holding hands with someone. Grasping force is also a very important element in creating different handshakes, but since the focus of my research will be on the characteristics of joints, and the hand is mainly a formation for now.

Pressure sensors are placed both on top and bottom of the palm [75] worked as a trigger of the system, when someone holds hand with the manipulator, the pressure sensor would send a signal to the controller implemented by Simulink via the I/O ports provided by dSPACE. Then the controller sent out the control signal of the electromagnetic valve to actuate the artificial muscles which drove the manipulator to the target position with the target viscosity and stiffness in the

joint. And the output angles of each joint are recorded.

The overall system of handshake manipulator

In the manipulator prototype, the target torque τ_J in equation (3.10) is the torque generated by the weight of the hand and forearm. Where,

$$\tau_J = m_{forearm} g \frac{l_2}{2} \sin(\theta_s + \theta_e) + m_{hand} g \frac{l_{hand}}{2} \sin(\theta_s + \theta_e + \theta_w) \tag{3.10}$$

And the complete diagram of the handshake manipulator system was shown in Fig. 3.14. And Fig. 3.15 is the photo of the actual prototype we used in the research.

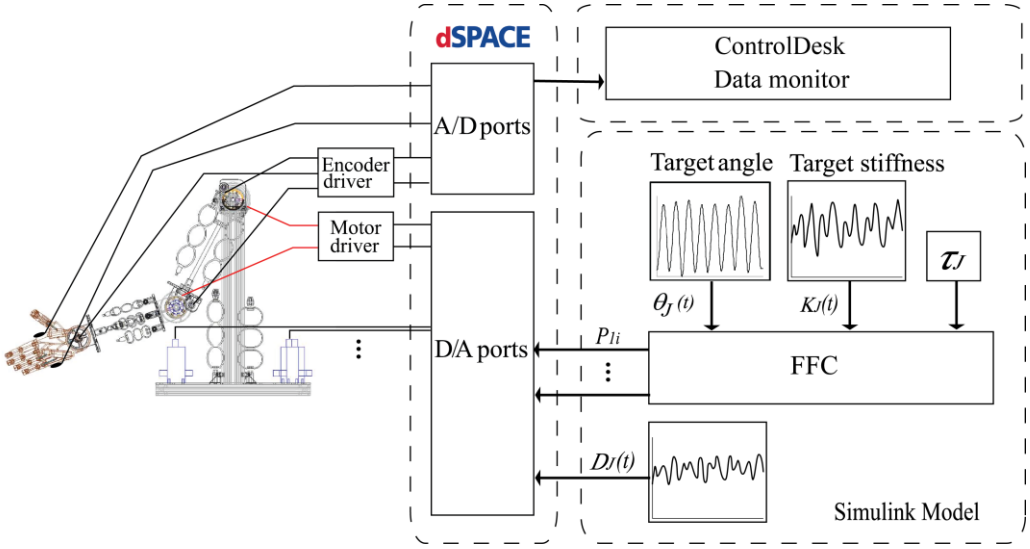

Fig. 3.14 The schematic diagram of the complete system

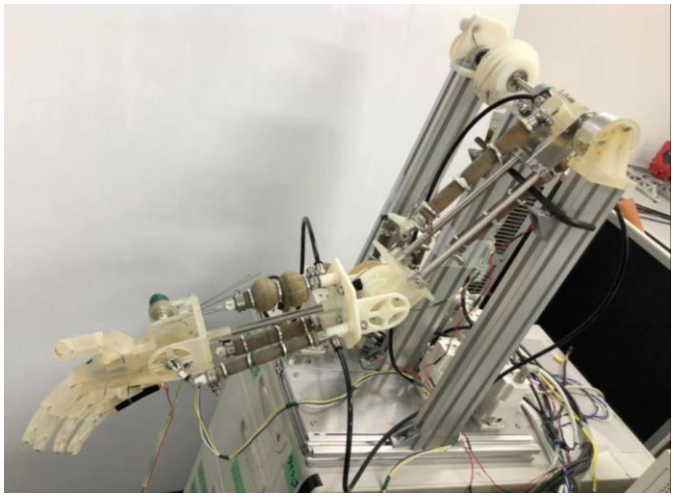

Fig. 3.15 Handshake manipulator prototype I

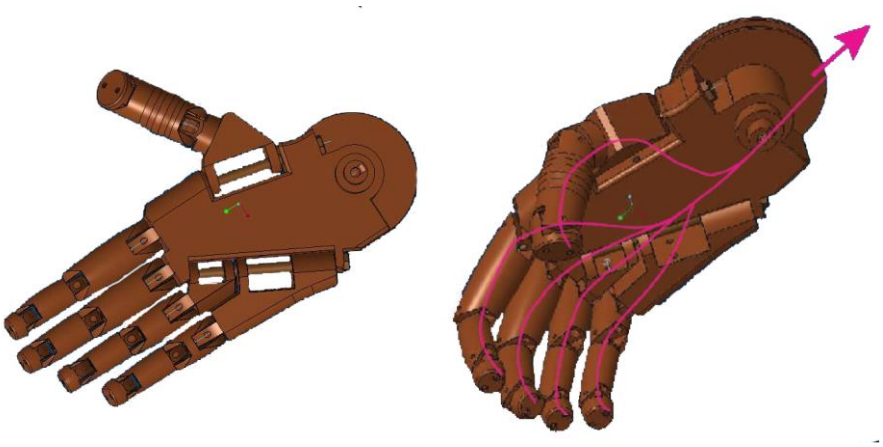

Fig. 3.16 Hand design of prototype I

3.8. Effectiveness test of the handshake manipulator

This section is devoted to verifying experimentally the performance of the proposed prototype. We designed several experiments to verify the effectiveness of variable viscoelasticity control of the manipulator. According to the previous studies [76], there is a difference between a firm handshake and a weak handshake, and different handshakes create different first impressions in social contact. Based on these social research results and the characteristic of the FFW controller, we made the assumption that varying viscosity and elasticity of the joint can affect subjective feelings when handshake with the manipulator.

3.8.1. Acquiring the target movement by analyzing human handshake

According to the previous study [76], a typical human-robot handshake's base frequency is between 1.33 Hz and 1.66 Hz, while according to social studies [77], the frequency of a human-human handshake is commonly between 1.95 Hz and 2.1 Hz. But limited by the response time of the artificial muscle, we chose to use 1.2 Hz as the frequency of the target handshake movement, a little bit slower than a human-human handshake but didn't get the feedback of feeling unnatural when tested on 5 different subjects. In order to obtain the target movement, first, we studied the business manner of an official handshake and trained the experimenter accordingly. The experimenter practiced the handshake until he was able to perform handshake movement at the constant frequency (1.2 Hz) steadily. Then we measured and recorded the experimenter's handshake by motion capture device (Fig. 3.17).

After analyzing the movement, it is noticed that the elbow joint has the largest motion range in a handshake, which is 40°-60° on average, while shoulder and wrist movements are comparatively small. Based on this result we decided to make elbow the only actively driven joint in this research while kept a constant

angle and stiffness on both shoulder and wrist joints. And we adjusted the shoulder and wrist angle so that 40°-60° are the controllable range of the elbow joint. By eliminating other influential elements, it helps us to determine the effect of variable viscoelasticity on subjective evaluation of the manipulator. The target elbow angle signal we used in the experiments is shown in the upper chart of Fig. 3.18. And the lower chart of Fig. 3.18 is the FFT of the signal, the base frequency of the signal is 1.24 Hz.

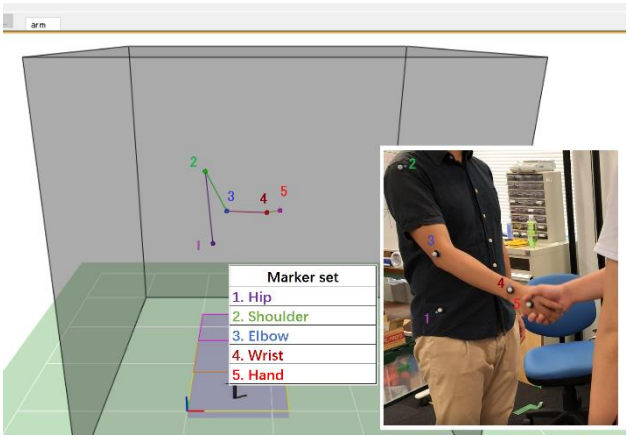

Fig. 3.17 Measuring the standard handshake

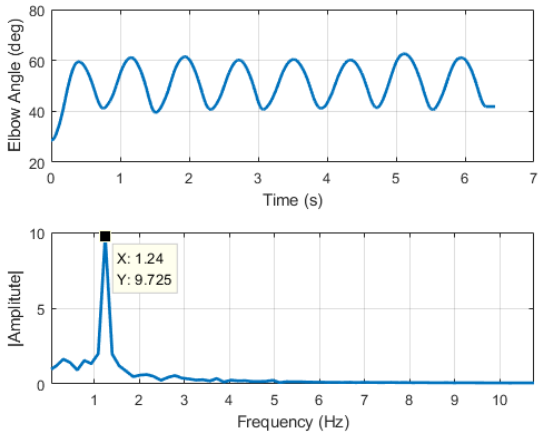

Fig. 3.18 The target elbow angle in time domain (upper chart) and frequency domain (lower chart)

3.8.2. Performance of the handshake manipulator

Before we started the handshake experiments with subjects, we tested the performance of the manipulator. First, we made the manipulator perform the handshake movement alone under different viscous conditions. The viscosity coefficient we chose were low viscosity: 0.005 Nms/deg, medium viscosity: 0.01 Nms/deg and high viscosity: 0.03 Nms/deg, plus the basic-viscosity condition, which is when no voltage is applied on MR brake, and the frictional torque is

generated by static MR fluid inside. Four conditions are designed for various viscosity experiments in total. The output elbow angle is shown in Fig. 3.19, which indicated that the positioning of the manipulator is not very accurately controlled, this is caused by the intrinsic softness of the artificial muscle. Moreover, since the viscosity control is independent from angle control, increasing viscosity can affect the output angle, in the high viscosity condition, the output curve of elbow joint has deformed greatly.

Fig. 3.20 shows the elbow angle output when the experimenter shook hand with the manipulator. The output curves under all viscosity conditions have been smoothened compared to Fig. 3.19. This result demonstrated the inherent compliancy of the manipulator when the external force applied on the manipulator, the output angle can adjust accordingly.

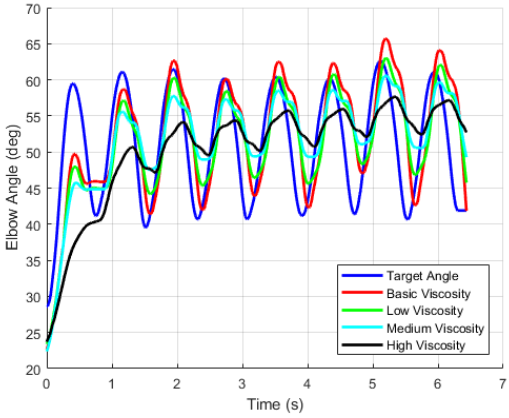

Fig. 3.19 Output elbow angle in different viscous conditions when the manipulator wave hand by itself

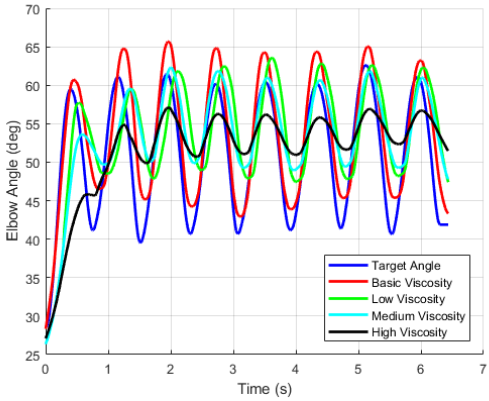

Fig. 3.20 Output elbow angle in different viscous conditions when experimenter handshake with the manipulator

Then we tested the output stiffness of the elbow joint. Fig. 3.21 shows the actual output stiffness against the theoretical stiffness. Due to the backlash of the mechanical parts and the nonlinearity of the artificial muscle's contraction amount, the measured output stiffness diverged from the theoretical value, this

has been explained by the previous study [70]. And the target stiffness lower than 0.1 Nm/deg is uncontrollable due to the looseness of the pulling wire, therefore we chose the experiment conditions as low stiffness: 0.1 Nm/deg and high stiffness: 0.15 Nm/deg. The elbow angle output of the manipulator when waving by itself (no external force applied) under each stiffness condition is shown in Fig. 3.18. The result indicated that the angle output tracks the target better under high stiffness condition, which is consistent with the previous study.

According to the results of the performance test of the manipulator, the compliancy of the actuator comprised of artificial muscle and MR brake has been demonstrated. In the following experiments, we focused on verifying the effectiveness of variable viscoelasticity on subjective feelings of handshake.

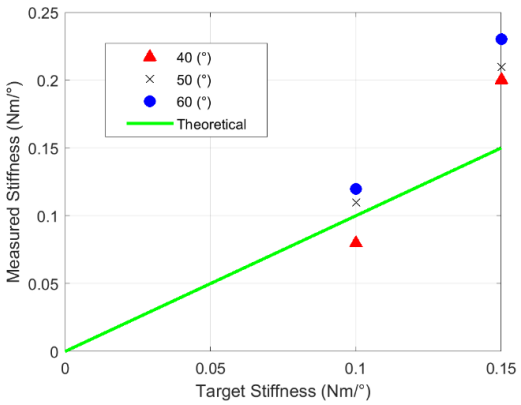

Fig. 3.21 Measured output stiffness against the theoretical value

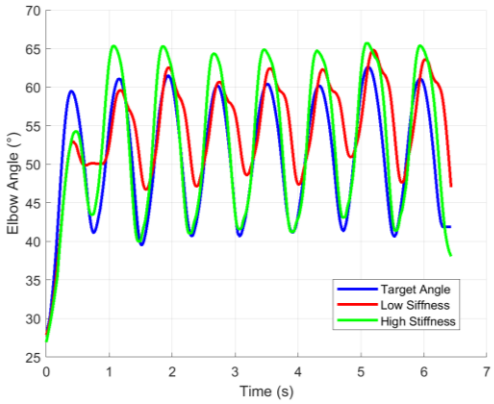

Fig. 3.22 Output elbow angle in different stiffness conditions

3.8.3. Variable stiffness and viscosity experiments

Subjects

5 male subjects (age from 22 to 26) who were moderately active participated in the study. The subjects ranged in height from 165 to 175 cm and in body mass from 67 to 75 kg. All the subjects were in good physical condition, without injuries or muscular problems. The study was approved by the Ethics Committee of Chuo University and was performed after each subject signed informed consent.

Experimental method

The following section explained the experiments to verify the effect of variable viscoelasticity on subjective feelings of a handshake. During the variable viscosity experiments, we chose three different viscosity coefficients as the experiment conditions, which are: low viscosity 0.005 Nms/deg, medium viscosity 0.01 Nms/deg and high viscosity 0.03 Nms/deg, plus the basic-viscosity condition, there were four conditions in total. Each subject shook hands with the manipulator once in each condition, and the order of the conditions was different for each subject. Then the VAS method was applied to each subject to evaluate how natural they feel about each handshake condition. The question sheet for one condition is shown in Fig. 3.23. And one scene of the experiment is shown in Fig. 3.24.

During the variable stiffness experiment, we first studied the difference between a firm handshake and a weak handshake and trained the experimenter to be able to perform both kinds of handshakes. Then we asked the experimenter to shake hands with the subject and taught them which one was the weak handshake, and which one was the firm handshake to help them understand the difference.

Then we applied high and low stiffness to the elbow joint of the manipulator and without informing the subjects experiment conditions. Subjects were asked to make a judgment of which one is the firm handshake, and which one is the weak handshake only rely on their feelings. Each subject was asked to shake hand with the manipulator 10 times, 5 were low stiffness and 5 were high stiffness conditions and their answers were recorded to calculate the percentage of the correct judgment.

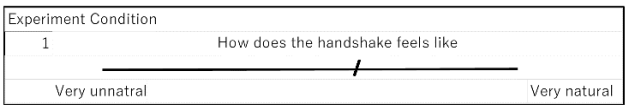

Fig. 3.23 Question sheet used in the VAS method

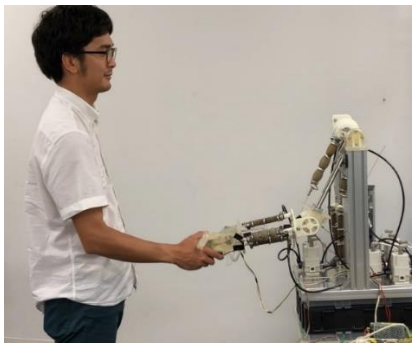

Fig. 3.24 Subject shaking hand with the manipulator

Result

The subjects' answers to VAS questionnaire were converted into scores, with 0 being very unnatural and 10 being very natural. The average score is shown in Fig. 3.25. As the bar charts indicated, the low viscosity condition received the highest evaluation score on average This result leads to the Conclusions that by adjusting the viscosity coefficient it is possible to affect how natural it feels to handshake with the manipulator.

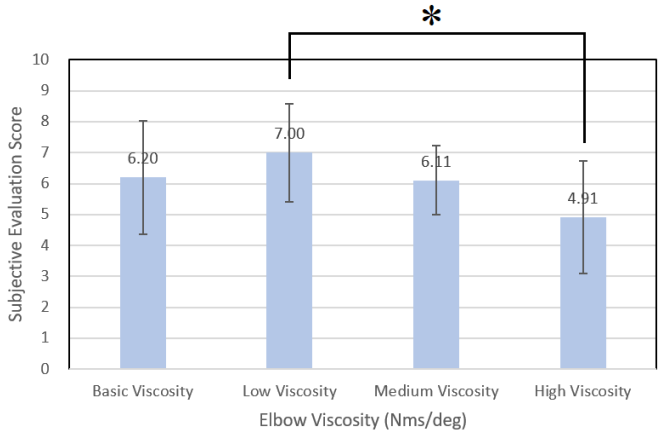

Fig. 3.25. Subjective evaluation of each handshake in different viscous conditions

The result of the correct judgment percentage of each subject is listed in Table 3-V. The correct rate was 94% in total, which indicated the high and low stiffness condition created distinctively different feelings to subjects. And the stiffness of the joint can affect the subjective feeling of the firmness of the manipulator's handshake.

TABLE 3-V CORRECT ANSWER RATE OF DETERMINING STANDARD AND FIRM HANDSHAKES

Subject No.	Correct Percentage
1	100%
2	90%
3	80%
4	100%
5	100%
Total	94%

3.9. Conclusions

In this research, we have confirmed that a combination of artificial muscle and MR brake can be used as an effective alternative actuator on robots who need to interact with humans. Even though the trajectory of the manipulator is not accurately controlled, the softness and compliancy the proposed actuator has demonstrated as a desirable characteristic when developing robots that are aimed at interacting with humans. In the case of a human-robot handshake study, we have verified that by altering the viscoelasticity of the joint, it is possible to create different feelings for the subjects. The handshake was evaluated as the most natural in low viscosity condition and the high stiffness condition was evaluated as the firm handshake, these results confirmed that variable viscosity and stiffness can affect the subjects' feeling when shaking hands with the manipulator.

In the variable viscosity experiment, each condition used a constant viscosity coefficient, but as explained in section 2.3 the actual human joint's viscosity varies all the time, along with the tension in the muscle and angle of the joint. In order to create more natural feelings of handshake, it is necessary to develop a controller to control the viscosity coefficient within different phases of handshake, and also find the viscosity coefficient of the human joint to use as a target. These are the experiments we will explain in the next chapter. We estimated the human joint in chapter 2, and in the next chapter, we would use the estimated viscoelastic properties of the subjects as the target and conduct the human-robot handshake experiments. Also, EMG was utilized as a comparison index of a human-human handshake and human-robot handshake.

3.10. Summary

In this chapter, we first explained the concept of soft robotics and explored the reason why we have chosen the combination of artificial muscle and MR-brake as the soft actuator for the handshake manipulator we proposed.

The following sections are the detailed explanations of the manipulator's joint design, the structures of artificial muscle and MR-brake and the controller design used for the position and viscoelasticity property control was derived from the physical model of the joint. Then the size design and the overall system was explained.

In the experiments section, we conducted two types of experiments to verify the effectiveness of the proposed manipulator. The first was the performance test of the manipulator, in which the manipulator performed the handshake movement on its own when no one was interacting with it. The result verified that the manipulator was able to make a handshake movement and by adding the viscous element, the performance of the manipulator was improved. The second type was the human-robot handshake experiments, which were done under different stiffness and viscosity conditions. The results verified that by controlling the viscoelastic property of the manipulator it was capable of generating distinctively different feelings of handshakes.

Chapter 4

Human-robot handshake experiments

Chapter 4.
Human-robot handshake experiments

In this chapter, we first upgraded the proposed handshake manipulator to make it capable of generating a wider range of stiffness for the human-robot experiments. Then applied the stiffness and viscosity measured in the previous human handshake experiments as the target value for the handshake manipulator. Next, human-robot handshake experiments were performed, subjective evaluations were taken and physiological data of the experimenter were compared when he shook hands with human subjects.

4.1. Upgraded handshake manipulator

We have built 2 prototypes for this research. These 2 prototypes have the same arm length and palm-size, but prototype II had an improved elbow joint, which used metal parts to replace the 3D printed parts in the prototype I so that it generated more stable movement and had the ability to output higher stiffness (Fig. 4.1). What's more, because we noticed that subjects with different heights may act differently when handshake with the prototype I, we mounted prototype II on a height-adjustable stand with 4 casters so that it can fit subjects in different heights and also can be moved around to be better captured with the motion capture device.

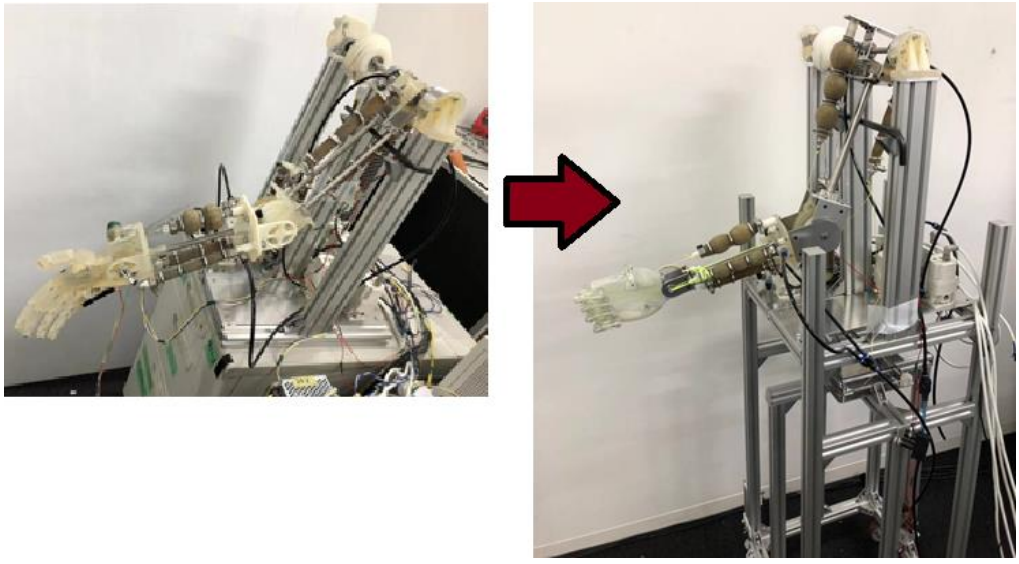

Fig. 4.1 Handshake manipulator prototype I and prototype II

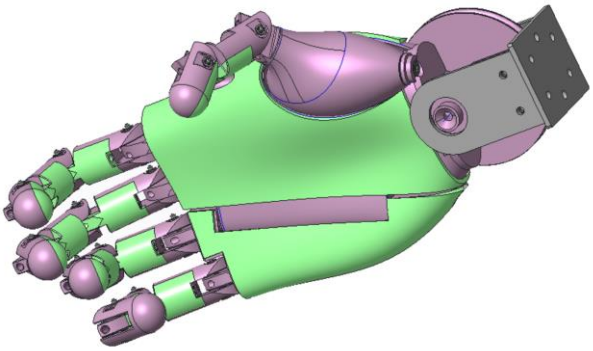

Fig. 4.2 Hand design of prototype II

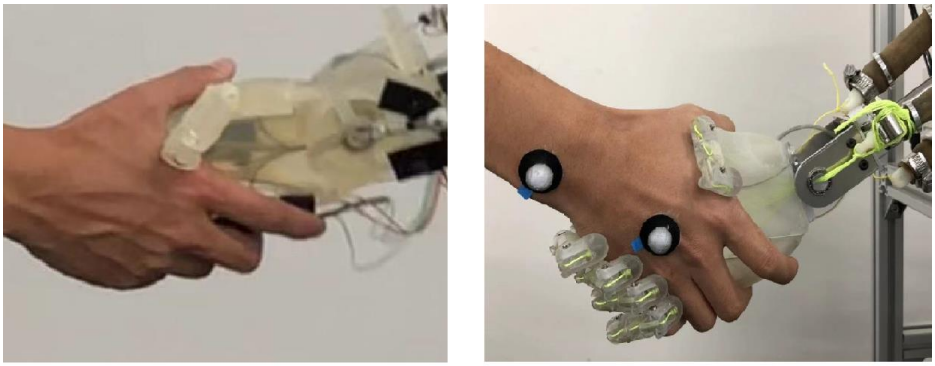

Prototype I hand Prototype II hand

Fig. 4.3 Different grippings of the prototype I and II

4.2. Joint stiffness measurement of the handshake manipulator

In the performance test of prototype I, we found out the actual joint stiffness is diverted from the theoretical stiffness and the maximum joint stiffness of the manipulator is much lower than a real human arm. This was partially caused by the intrinsic property of artificial muscles but also affected by the structure and material used to make the elbow joint of the manipulator. In prototype I the parts in the elbow joint are mainly made by 3D printer. Due to the softness of the 3D printed material, the joint deforms when the artificial muscles apply large contraction force on the joint, therefore the actual stiffness of the joint was lower than it was designed. In prototype II, we remade the elbow joint with all aluminum parts so that it achieved higher strength without increasing in weight as shown in Fig. 4.4. After remaking the elbow joint we measured the output stiffness of the manipulator again, and the result was shown in Fig. 4.5.

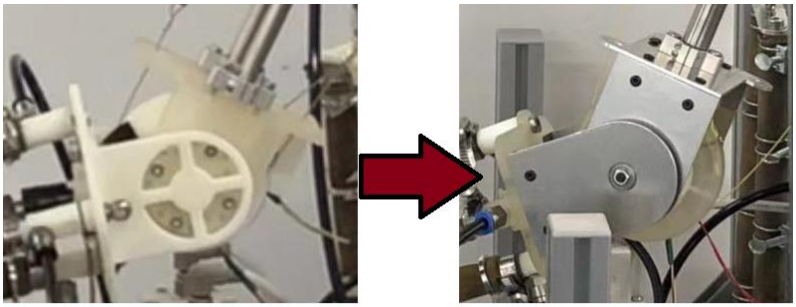

Prototype I elbow Prototype II elbow

Fig. 4.4 Upgraded design of the elbow

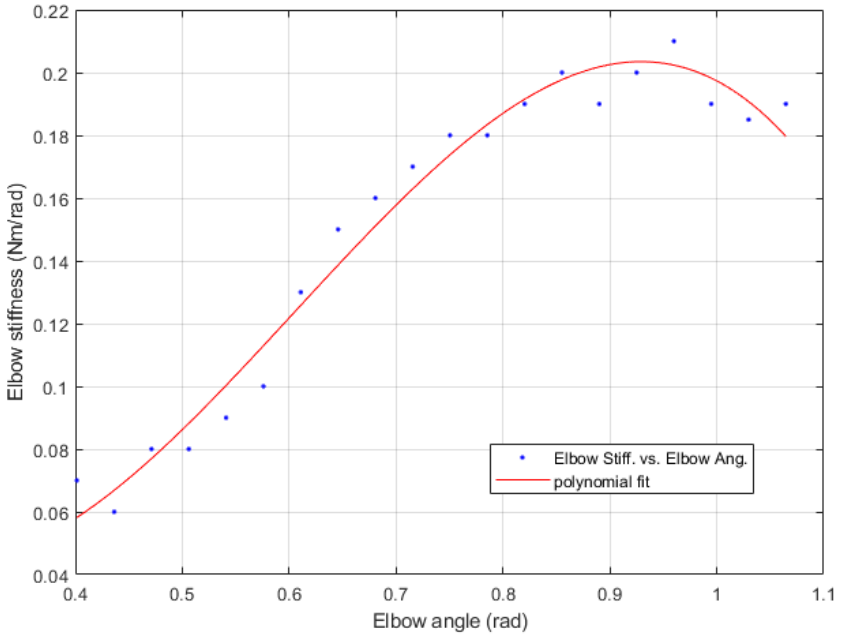

Fig. 4.5 Measured joint stiffness of the handshake manipulator prototype II

4.3. The first human-robot handshake experiment

In the first human-robot handshake experiment, we estimated the joint stiffness of human elbow by using the EMG signals. First, we performed a human-human handshake experiment, recorded the EMG signals of both the subject and the experimenter, then used the experimenter's EMG signal as an estimation of the elbow joint stiffness, and the subject was required to handshake with the manipulator and the performance of the subject was compared when he handshake with the experimenter. Viscosity was not taken into consideration in this experiment.

4.3.1. Acquiring the target stiffness for the manipulator by EMG signals

In the human-human handshake experiments, the EMG signals of the bicep, tricep, forearm exterior, and forearm interior were recorded by the Delsys wireless EMG sensor as shown in Fig. 4.6. The bicep and tricep EMG signals of the experimenter were used to estimate the target stiffness value for the handshake manipulator. The forearm exterior and interior EMG signals were used as an indicator of the gripping force. And the movement of the experimenter was recorded by the motion capture device to get the target elbow angle for the handshake manipulator.

6 trials of handshakes were performed, 3 times each under the firm handshake and weak handshake conditions. We then chose the value in the middle to use for estimating the elbow joint stiffness. According to the result of previous research [76], the estimated joint stiffness has a linear relationship with the processed EMG signal. Therefore, we added the biceps and triceps EMG signal together to be used as the estimation of the joint stiffness. And considering the controllable joint stiffness of the manipulator is between 0.1 Nm/deg and 0.15 Nm/deg, we normalized the signal between this range. And because of the respond time of the artificial muscles, we filtered the processed EMG signal one more time, with a low-pass filter of 2 Hz, and used the filtered signal as the target stiffness signal for the manipulator. The processed EMG signals of the experimenter are shown in Fig. 4.7(a), and Fig. 4.7(b) showed the targeted elbow stiffness used in the human-robot handshake experiment. Fig. 4.7(c) showed the elbow angle recorded by the motion capture device, which is used as the target angle in the experiments.

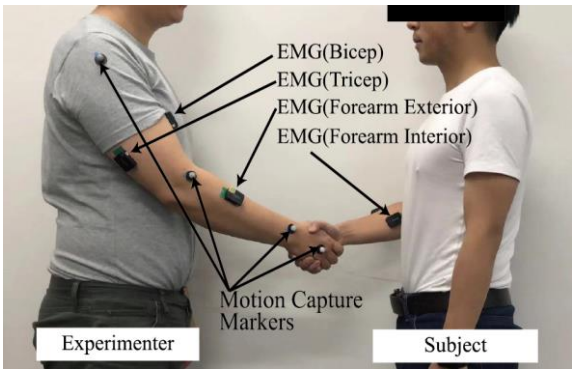

Fig. 4.6 Human-human handshake experiment

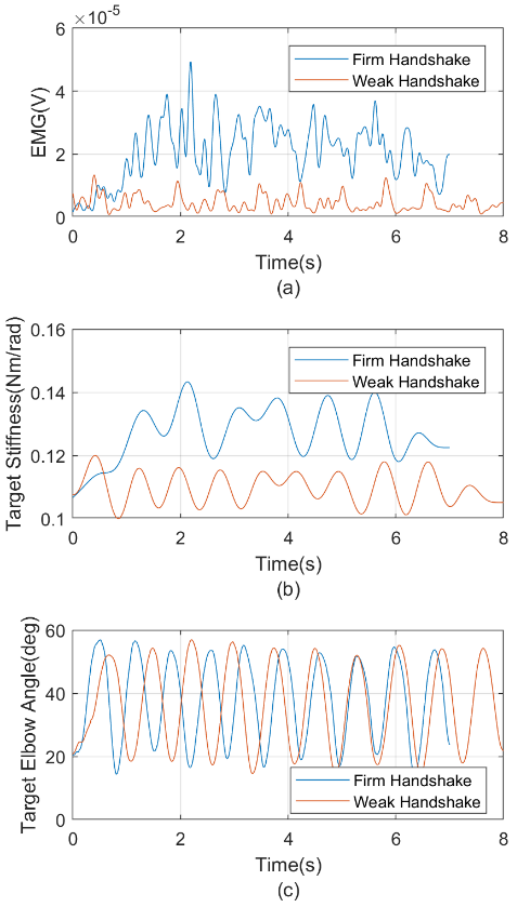

Fig. 4.7. Target stiffness and target elbow angle in different conditions

4.3.2. Experimental method

This section explained the first human-robot handshake experiments. During the experiments, we asked the subject to handshake with the handshake manipulator prototype II naturally. The subject was not aware of the experiment's conditions and shook hands with the manipulator 5 times under each stiffness condition (firm handshake and weak handshake) in random order. The subject was asked to answer whether he thinks the handshake was firm or weak after each handshake, and the EMG signal was recorded.

4.3.3. Results and Conclusions

Results

The subjects' answer to the experimental conditions was 100% correct, which indicated the firm handshake and the weak handshake can be clearly distinguished by subjective feelings. The EMG signal of the subject's bicep when he handshake with the experimenter was shown in Fig.4.8(a) and (b), while the EMG signal of the subject's bicep when he handshake with the proposed manipulator was shown in Fig.4.8(c) and (d). The RMS of the EMG signals are listed in Table 4-I, from this table, it is clear that both the human-human handshake experiments and the human-robot experiments presented the same tendency, which is, the subject's muscle activation level was higher in a firm handshake condition, and much lower in a weak handshake condition. But the overall muscle activation was lower in the human-robot handshake experiment. This can be explained by the fact that the output stiffness of the manipulator's joint was much lower than the real human elbow joint.

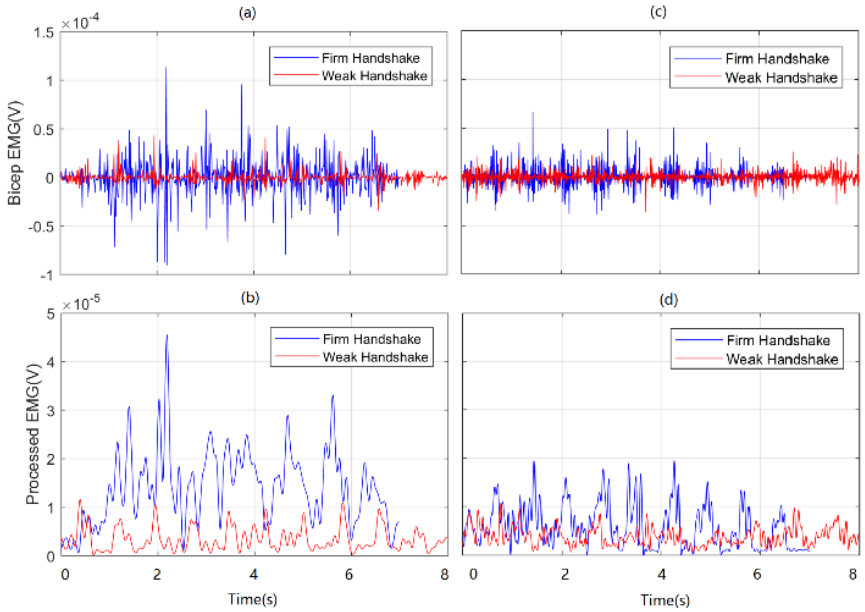

Fig. 4.8 Comparison of the subject's EMG signals in the human-human handshake and human-robot handshake under different stiffness conditions

TABLE 4-I RMS OF THE EMG SIGNALS

RMS of biceps EMG signal (μV) Human-human handshake							
Experiment No.		1	2	3	4	5	Average
Experiment condition	Firm (RMS_f)	12.53	13.72	13.30	14.45	12.89	13.38
	Weak (RMS_w)	3.50	4.64	4.77	3.85	4.53	4.26
Rate (RMS_f/RMS_w)		3.58	2.96	2.79	3.75	2.85	3.14

RMS of biceps EMG signal (μV) Human-robot handshake							
Experiment No.		1	2	3	4	5	Average
Experiment condition	Firm (RMS_f)	7.36	6.98	7.52	7.08	7.43	7.27
	Weak (RMS_w)	3.36	3.24	4.02	3.58	3.95	3.63
Rate (RMS_f/RMS_w)		2.19	2.15	1.87	1.98	1.88	2.00

Conclusions

In this experiment, we established the fact that the firmness of the handshake is related to the stiffness of the elbow joint, and estimated the joint stiffness by EMG signals. And then utilized a handshake manipulator using artificial muscle as the actuator proposed in the previous study to replicate both firm handshake and weak handshake. In the human-human handshake experiments, we analyzed the muscle activations of the experimenter in both firm handshake and weak handshake conditions, then used the EMG signal of bicep and triceps as the estimated target stiffness signal for the handshake manipulator. In the human-robot handshake experiments, we measured the muscle activations of the subject and compared it to the subject's muscle activations in human-human handshake experiments. It has been demonstrated that even though the subject was not aware of the experiment conditions, the muscle activations are higher in the firm handshake conditions, which indicated that the EMG signal may be used as an evaluation of different handshakes.

4.4. The second human-robot handshake experiment

In the second human-robot handshake experiment, we estimated the joint stiffness of human elbow by using the joint torque. First, we obtained the estimated joint stiffness of different subjects through the experiment introduced in Chapter 2, then used the measured subjects' interaction forces for joint stiffness estimation. Finally, the experimenter in the human-human handshake experiment became the subject in the human-robot experiment. Viscosity was also taken into consideration in this experiment.

4.4.1. Experiment concept

In the human-human handshake experiment explained in Chapter 2, all kinds of physical properties were taken including interaction force and motion capture data. The recorded data was then used to estimate the joint stiffness and viscosity

of each subject and the results were presented in section 2.6. In the following human-robot utilized the experiment results of Chapter 2 by applying the estimated joint stiffness and viscosity of different subjects to the handshake manipulator in the expectation of creating the feeling of shaking hand with different persons. The experimenter in the human-human handshake experiment was asked to be the subject in the human-robot handshake experiment. His muscle activation and subjective evaluations were taken to be compared when handshake with the manipulator and with different human subjects.

The concept of this experiment was that by changing the viscoelasticity properties of the handshake manipulator, the manipulator can perform handshakes like different persons. The concept and process of the experiment was shown in Fig.4.9

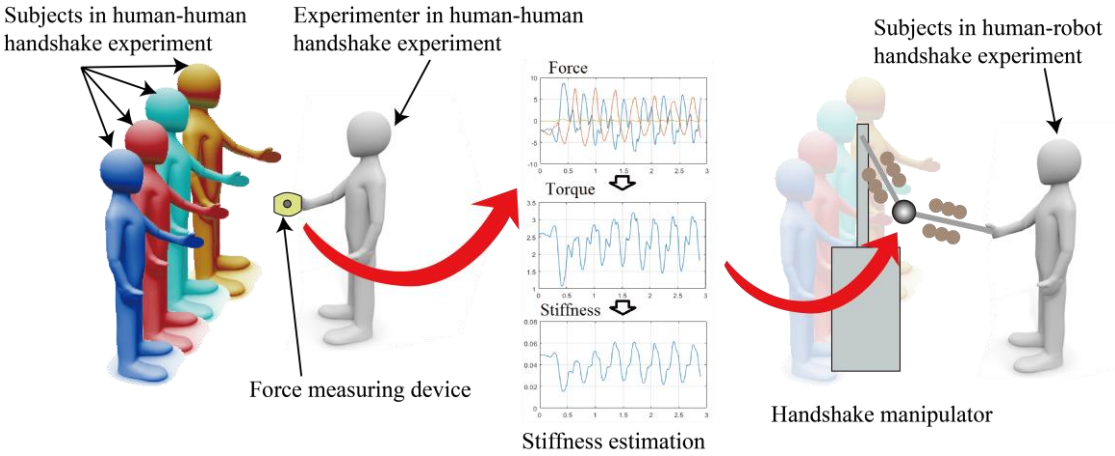

Fig. 4.9 The concept and process of the human-robot handshake experiment

4.4.2. Experiment setup

In the human-robot handshake experiment, the same person who was acting as the experimenter in the human-human handshake experiment was asked to be the subject. EMG signals of his bicep and tricep were recorded by the Delsys wireless EMG sensor. His movement was captured by the motion capture device. The interaction forces and gripping force when he handshake with the manipulator were also recorded to be compared with the interaction forces and gripping force in the human-human handshake experiment.

In order to measure the necessary data for the experiment, we modified the hand of handshake manipulator prototype II. The hand is shown in Fig. 4.3 which was used on prototype II was replaced with a design similar to the interaction force measuring device as shown in Fig.4.10. The hand was separated into upper and lower 2 parts, with a pressure sensor installed in the middle. And the hand was connected to the pulley which was driven by the artificial muscles via the

load cell so that the interaction force between the subject and the handshake manipulator was measured.

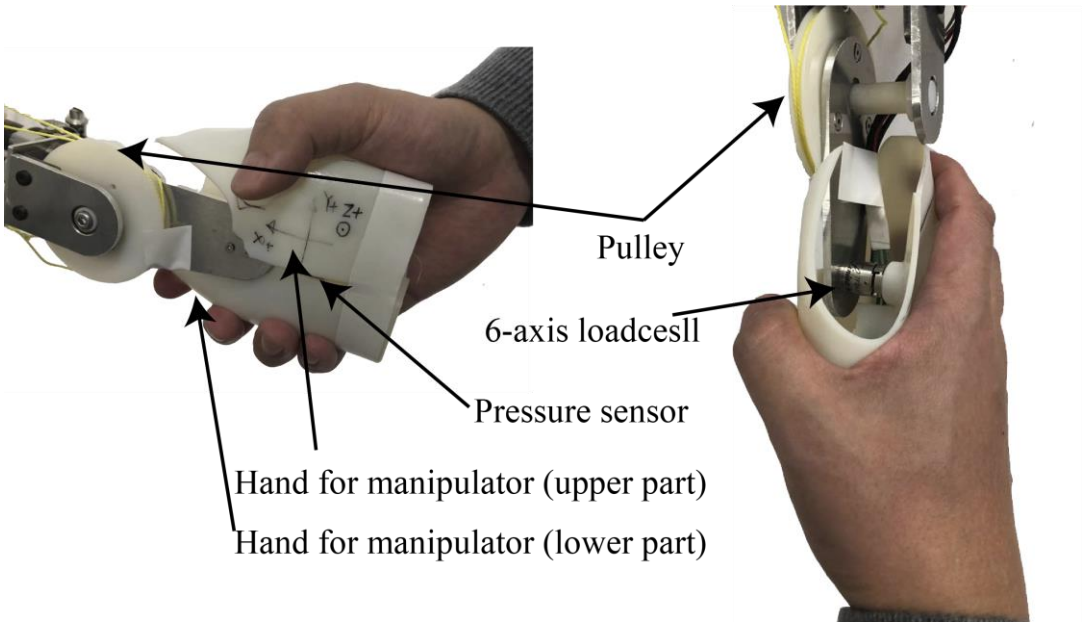

Fig.4.10 The hand design for the human-robot handshake experiment

3 subjects's data in the human-human experiment was elected to be used as the target value in the human-robot experiment. The estimated stiffness and viscosity were normalized to fit the output range of the handshake manipulator. 10 trials of human-robot handshake experiments were performed in total. In which, 6 trials used the subjects' data from the human-human handshake experiment as the target with 3 trials each under the firm handshake and weak handshake conditions. The other 4 trials are under constant stiffness conditions 2 trials each with high and low stiffness constant, in which 2 trials didn't activate viscosity control and 2 other trials applied low viscosity. The trial list is shown in Table 4-II.

TABLE 4-II Conditions of human-robot handshake experiment

Trial No.	Stiffness	Viscosity
1	Subject 1's estimated elbow stiffness firm	Subject 1's estimated elbow viscosity firm
2	Subject 1's estimated elbow stiffness weak	Subject 1's estimated elbow viscosity weak
3	Subject 2's estimated elbow stiffness firm	Subject 2's estimated elbow viscosity firm
4	Subject 2's estimated elbow stiffness weak	Subject 2's estimated elbow viscosity weak
5	Subject 3's estimated elbow stiffness firm	Subject 3's estimated elbow viscosity firm
6	Subject 3's estimated elbow stiffness weak	Subject 3's estimated elbow viscosity weak
7	Constant stiffness high	0
8	Constant stiffness high	Constant viscosity low
9	Constant stiffness low	0
10	Constant stiffness low	Constant viscosity low

* Subject number refer to the number in the human-human handshake experiment

A part of the target values used for the human-robot handshake experiment were shown in Fig.4.11. The left side of Fig.4.11 are the normalized elbow angle, stiffness and viscosity of subject1's firm handshake, and right side of Fig.4.11 are the normalized elbow angle, stiffness and viscosity of subject1's weak handshake. It can be told from the graph that the elbow angle range and stiffness in a firm handshake condition differs clearly to those in a weak handshake condition. And this distinction can be subjectively told apart by the subject in the human-robot handshake experiment.

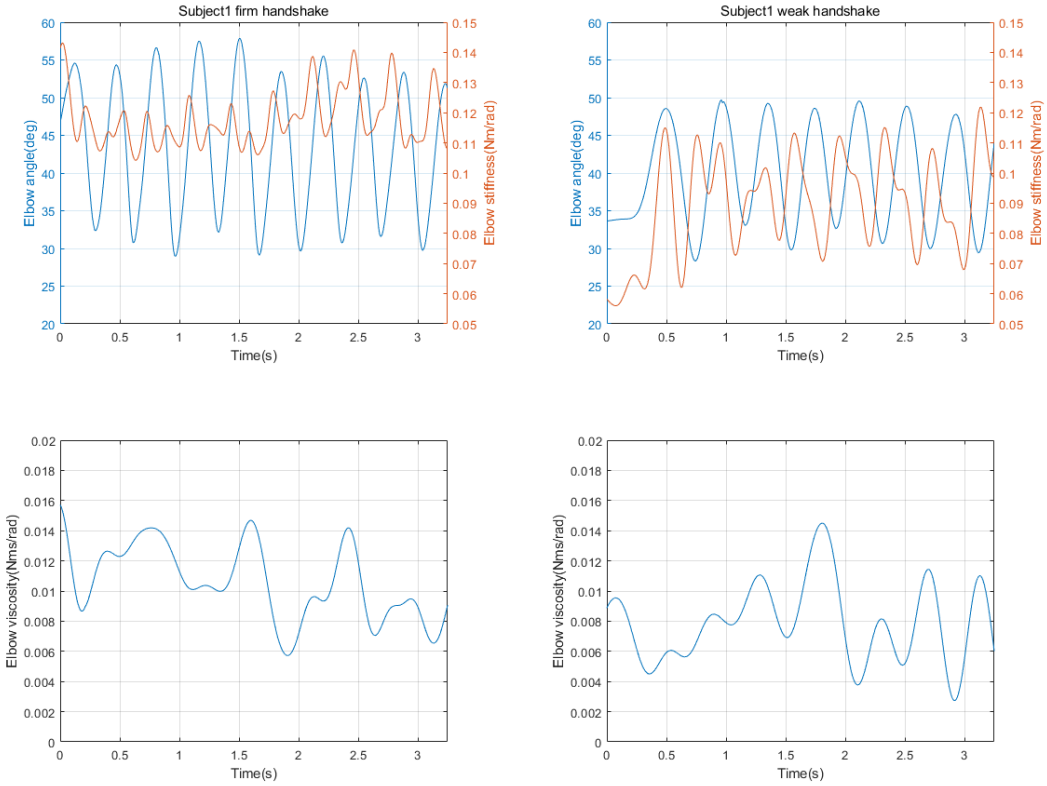

Fig. 4.11 Targe elbow angle stiffness and viscosity of subject1 for the human-robot handshake experiment

4.4.3. Performance test under different viscosity conditions

In the experiment explain in section 3.8, it has been verified that under the constant viscosity conditions applying low viscosity to the elbow joint generated the most natural feeling of a human-robot handshake, also reduced the overshoot of the elbow angle compared to no viscosity condition. In this section, the performance of the handshake will be compared under constant viscosity and variable viscosity conditions in terms of the elbow joint overshoot. The target elbow angle and the actual elbow angle under different viscosity conditions were shown in Fig. 4.12. In all trials, the target stiffness of the handshake manipulator

was set to a constant 0.1 Nm/rad. All the tests were done when the manipulator was moving by itself, that is there was no one shaking hand with the manipulator.

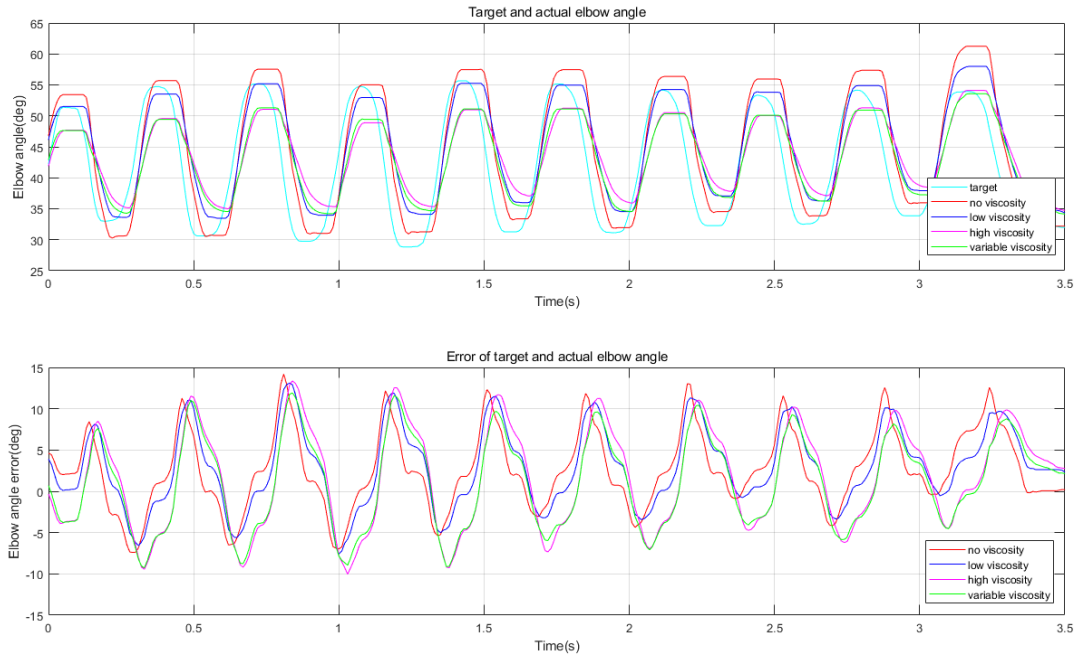

Fig. 4.12 Performance of the handshake manipulator

TABLE 4-III Error of elbow angle in different viscosity conditions

Target angle	Experiment condition	Viscosity	Error (mean)	Error (std.)
Subject1	Firm handshake	0	2.58	4.71
		constant low	2.93	4.72
		constant high	1.63	6.06
		variable	1.07	5.48
Subject1	Weak handshake	0	2.16	5.31
		constant low	1.97	4.96
		constant high	2.31	5.68
		variable	2.04	4.37
Subject2	Firm handshake	0	3.21	5.84
		constant low	2.79	6.32
		constant high	3.66	5.47
		variable	2.87	5.39
Subject2	Weak handshake	0	2.54	4.88
		constant low	2.96	5.13
		constant high	1.07	4.23
		variable	2.16	4.87
Subject3	Firm handshake	0	2.97	4.84
		constant low	3.05	5.65
		constant high	2.69	4.97
		variable	3.11	4.59
Subject3	Weak handshake	0	1.96	4.62
		constant low	2.15	5.13
		constant high	2.06	5.37
		variable	2.40	4.29

4.4.4. EMG comparison

The EMG signals of the subject handshake with a human and with the manipulator were shown in Fig. 4.13.

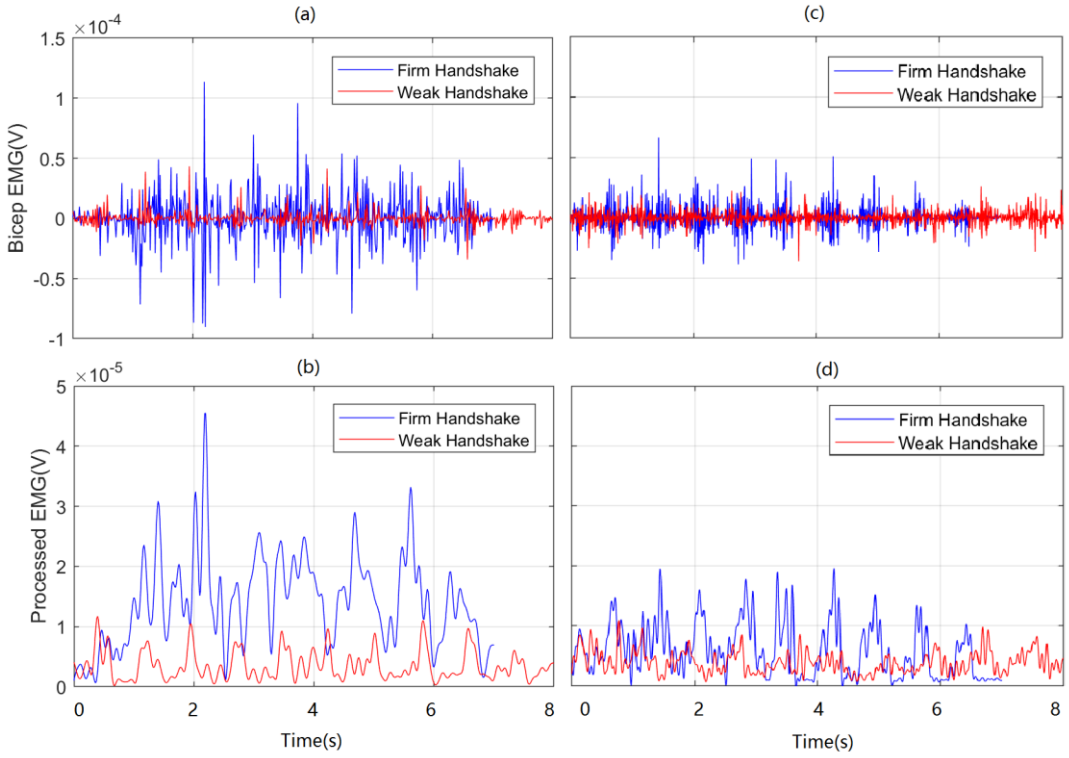

Fig. 4.13 EMG signals of the subject when handshake with human and robot

4.4.5. Subjective evaluation of viscoelasticity control

Subjective evaluations were taken after each trial in the form of a questionnaire. The questionnaire was shown in Fig. 4.14. It asked the subject about how did he think the experiment condition was. And the questionnaire was comprised of 2 parts about the stiffness condition and viscosity condition separately. The correct answer rate of the questionnaire as shown in Fig. 4.15. It can be seen from the graph that different stiffness conditions caused distinctively different feelings of handshake, and the subject had no problem to tell them apart, hence the correct answer rate is close to 100%. However, the difference between different viscosity conditions was much more difficult to tell. Except for the high viscosity conditions in which the motion of the robot arm stopped abruptly, the low viscosity condition and variable viscosity conditions were unable to separate by the subject.

Can you tell the stiffness and viscosity condition of this handshake?

Stiffness condition

☐ Firm ☐ Weak ☐ Can't tell

Viscosity condition

☐ No viscosity ☐ Low viscosity ☐ High viscosity ☐ Variable viscosity ☐ Can't tell

Fig. 4.14 Questionnaire of subjective feelings of each handshake condition

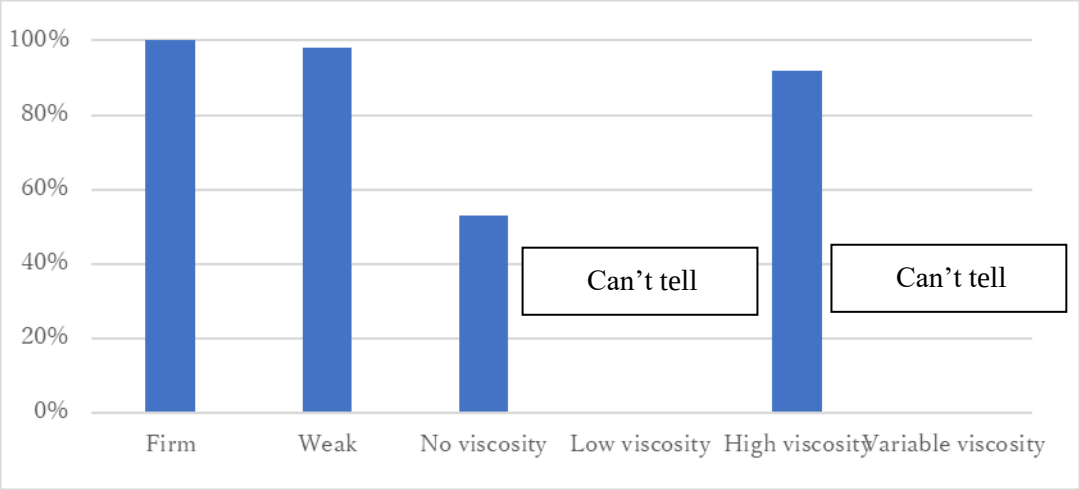

Fig. 4.15 Correct answer rate of each handshake condition

4.5. Subjective evaluation of the handshake manipulator

Experiment method

10 male subjects participated in this experiment, age range from 22 to 25, all physically healthy young students from our research lab. 4 different experimental conditions were selected according to the subjective evaluation results from the previous experiment. The 4 conditions are the combination of variable stiffness (firm handshake), variable stiffness (weak handshake), and high viscosity, variable viscosity (weak handshake). All subjects were shown the instruction video to explain that different handshakes convey different emotions. Each subject was first asked to handshake with the manipulator under the condition without stiffness or viscosity control to obtain the general feeling of the manipulator movement and use it as the baseline of the evaluation. Then each subject handshake with the manipulator 4 times, after each handshake, the subject was asked to evaluate the handshake on 2 different aspects, how natural is the handshake and what emotion does this handshake convey. The questionnaire used in this experiment was shown in Fig. 4.16. VAS method was applied in this evaluation.

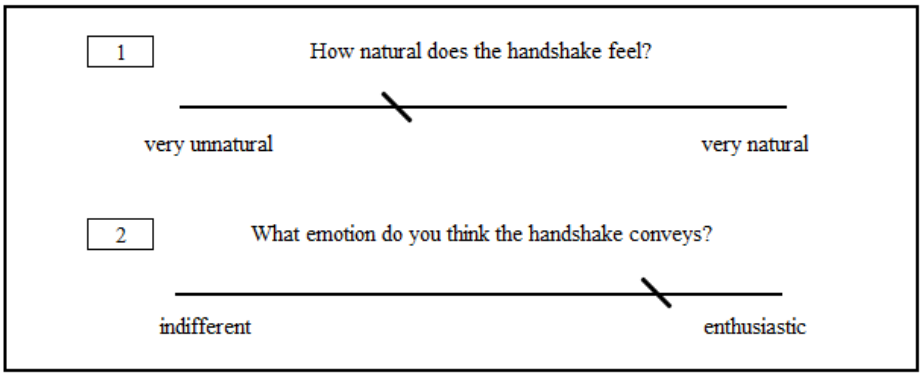

Fig. 4.16 VAS questionnaire for the subjective evaluation

Result

The evaluation of each subject was converted into a score with a range of 0 to 10. For the first question, 0 means the handshake movement feels very unnatural whereas 10 means the movement is very natural. For the second question, score 0 means the handshake makes people feel low or no emotion, also known as the "bad handshake" in the previous research [11]. On the contrary, score 10 means the handshake feels energetic and enthusiastic, which is called the "good handshake" in the previous research. The result of the first question was shown in Fig. 4.17(a), and the result of the second question was shown in Fig. 4.17(b). For the question about the emotion of the handshake, no matter what the

viscosity level is, subjects felt a stronger emotion during a high stiffness handshake condition. And significant differences were found between the high stiffness condition and the low stiffness condition. For the question of how natural the handshake feels, a tendency of the variable viscosity condition feels more natural, however, the significant difference was only found under the low stiffness condition, this can be explained by the fact that under high stiffness condition, the handshake generally moves in a wider range and faster, which eliminated the effect of viscosity control.

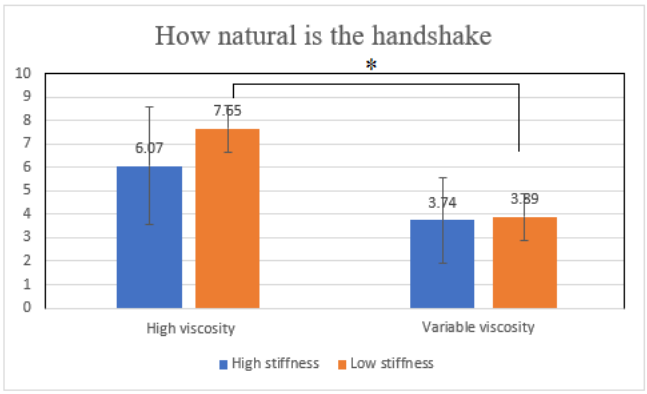

(a)

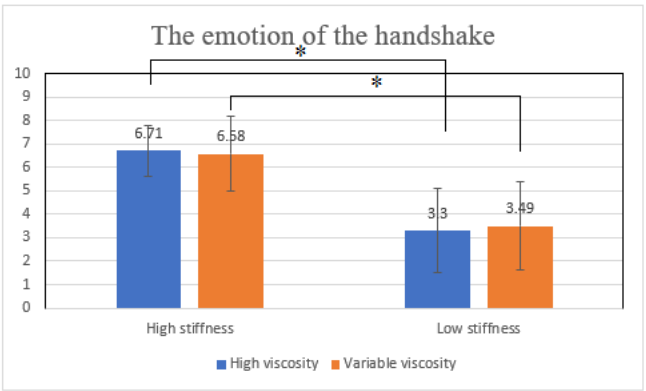

(b)

Fig. 4.17 Result of the subjective evaluation

4.6. Conclusions

In the human-robot handshake experiment, the estimated stiffness and viscosity values from the human-human handshake experiments were used as the target value for the handshake manipulator. And the subject was asked to handshake with the handshake manipulator. EMG signals and subjective evaluations were taken. According to the experiment results, viscosity variation didn't affect the feelings of a handshake as much as stiffness. It was easier for the subject to tell the difference between different stiffness conditions than the different viscosity conditions. And the performance of the handshake manipulator was also evaluated in the term of error of the elbow angle. It was verified that viscosity conditions can affect the performance of the manipulator

4.7. Summary

In this chapter, the interaction force measuring device was combined with the handshake manipulator to analyze the human-robot handshakes. The performance of the handshake manipulator was evaluated under different viscosity conditions. And different stiffness and viscosity target values were applied to conduct the human-robot handshake experiments. Physical properties of the subject was compared when he handshake with the human experimenter and the handshake manipulator. And subjective evaluations were taken after each trial. To sum it up, significant difference was found under different stiffness conditions, however, no significant difference was found under different viscosity conditions. And the same tendency was found in subjective evaluations, different stiffness conditions were easy to tell, but different viscosity conditions were much subtle to the subjective feelings. These maybe caused by the fact that human lacks receptors for viscosity and also the all human joints are underdamped, the viscosity varies with such subtlety that almost impossible to feel, however, it smoothened the movement of human arm to a level no robot arm can compare.

Chapter 5

Conclusions and future work

Chapter 5. Conclusions and future work

5.1. Conclusions

In this research, we proposed a new variable viscoelastic handshake manipulator to research the human-robot handshakes and built the prototypes. The manipulator has been proven to have high compliancy and back-drivability, it's effectiveness as a handshake research device has been demonstrated by experiments. The experiment results indicated that by controlling the viscoelasticity of the joint it is possible to generate different type of handshakes. In the performance test experiment, we have confirmed that the combination of artificial muscle and MR brake can be used as an effective alternative actuator on robots who need to interact with human. Even though the trajectory of the manipulator is not accurately controlled, the softness and compliancy the proposed actuator has demonstrated as a desirable characteristic when developing robots that are aimed at interacting with humans. In the case of a human-robot handshake study, we have verified that by altering the viscoelasticity of the joint, it is possible to create different feelings for the subjects. The handshake was evaluated as the most natural in low viscosity condition and the high stiffness condition was evaluated as the firm handshake, these results confirmed that variable viscosity and stiffness can affect the subjects' feeling when shaking hands with the manipulator.

In the variable viscosity experiment, each condition used a constant viscosity coefficient, but the actual human joint's viscosity varies all the time, along with the tension in the muscle and angle of the joint. In order to create more natural feelings of handshake, it is necessary to develop a controller to control the viscosity coefficient within different phases of handshake, and also find the viscosity coefficient of the human joint to use as a target. These are the experiments we will do in future research. We are planning to analyze human in different methods, for example, utilize EMG to analyze the activity of muscle and the 6-axis loadcell to do a more detailed research on the interaction force of human-human handshake and human-robot handshake, to determine the role of stiffness in creating the feeling of firm handshake. And reproduce the different handshakes on the proposed manipulator.

In the human-human handshake analysis, a set of handshake measurement methods were proposed and the complete measure system was built. Then multiple subjects participated in the experiments and their handshakes under different social conditions were measured and analyzed from the joint viscoelasticity point of view. The experiment results indicated that joint stiffness was different under different handshake conditions and significant differences were found. However, viscosity may perform a less important role in changing

the handshake feelings. No significant difference were found in joint viscosity.

In the human-robot handshake experiments, the measured joint viscoelasticity was used as the target value for the handshake manipulator, the subject was asked to handshake with the manipulator, and the subject's physical properties were compared when he handshake with human and handshake manipulator. Also, the subjective evaluation was taken after each trial. The result indicated that the difference under different stiffness conditions was obvious to the subject, however, the difference in viscosity is difficult to tell. And the significant difference was found in the comparison of the gripping force and interaction force.

5.2. Discussion

The experiment results of the human-human and human-robot handshake experiments all indicated that stiffness plays a more important role in the subject perspective of a movement, however that variation in viscosity is not so obvious. This may be caused by several reasons. The first one is that all human joints are underdamped system, skeletalmuscles can achieve the target position or stiffness in a instant without any noticeable oscillation which is much more superior than any of the mechanical speing-damper system. The damping mechanism of the muscle is still unclear, and it's very difficult to be compared to the physical property of viscosity.

The second reason could be that human being lacks the receptor to sense variation of viscosity. Not considering the affect of temperature, force and viberation are the main sensing ability of the skin to tell the difference in a physical. The increase of stiffness and viscosity all present as the increase in resistant force. Therefore, when we use the word "firm" and "weak" we usually refer to the force we fill which are interpreted into stiffness in this research. The lack of ability of feeling the variation in viscosity also lead to the lack of word to describe the difference in feeling.

5.3. Future work

In the foreseeable future it is reasonable to believe more and more robots can be found in our life around us. Other than the verbal communication, the non-verbal communication is envitably the next thing people are expecting from the robots. This study if viscoelascity control of robot arms may serve as a possible solution for future human-robot physical interaction. And I will persue the work of applying the viscoelascity control technology into practical uses.

Reference

[1] Sankei News Digital: *Estimated annual worldwide supply of industrial robot arms,* https://www.sankei.com/economy/news/ecn1812160011-n1.html, 2018

[2] Feil-Seifer D, Mataric MJ, "Defining socially assistive robotics," 9th International Conf. on Rehabilitation Robotics, (ICORR2005), p465- 468, 2005.

[3] A. De Santis, B. Siciliano, A. De Luca, and A. Bicchi, "An atlas of physical human–robot interaction," Mechanism and Machine Theory, Vol. 43, No. 3, p253–270, 2008.

[4] Argyle, M. Non-verbal communication in human social interaction. In R. A. Hinde, *Non-verbal communication.* Cambridge U. Press. Page 107-12, 1972

[5] Burgoon, M. and Ruffner, M., *Human Communication,*Holt, Rinehart and Winston, New York. Pages 130-3, 1978

[6] Heslin, R., *Non-verbal Behaviour and Social Psychology,*Plenum Press, New York. Pages 75-7, 1982

[7] Heslin, R. and Alper, T., "Touch, a Bonding Gesture", in Wiemann, J.M. and Harrison R.P. (Eds), *Non-verbal Interaction,* Sage Publications, London. Pages 47-7, 1983

[8] P. M. Hall and D. A. S. Hall, "The handshake as interaction," Semiotica. 45(3-4): 191-379. doi:10.1515/semi.45.3-4.249, 1983

[9] David A. Wesson, "The Handshake as Non-verbal Communication in Business", *Marketing Intelligence & Planning*, Vol. 10 Issue: 9, pp.41-46, 1992

[10] Greg L. Stewart and Susan L. Dustin, "Exploring the Handshake in Employment Interviews", *Journal of Applied Psychology*, Vol. 93, No. 5, 1139–1146, 2008

[11] Pierre-Henri Orefice, et. al., "Let's Handshake and I'll Know who You Are: Gender and Personality Discrimination in Human-Human and Human-Robot Handshaking Interaction", *IEEE-RAS 16th International Conference on Humanoid Robots (Humanoids),* Cancun, Mexico, Nov 15-17, 2016

[12] Artem A. Melnyk, Viacheslav Khomenko, "Sensor Network Architecture to Measure Characteristics of a Handshake Between Humans", *IEEE 34th International Scientific Conference on Electronics and Nanotechnology (ELNANO),* 2014

[13] A. A. Melnyk, V. Ph. Borysenko, P. Hénaff, "Analysis of synchrony of a handshake between humans", Advanced Intelligent Mechatronics (AIM) IEEE/ASME International Conference on, pp. 1753-1758, 2014.

[14] Pierre-Henri Orefice, Mehdi Ammi, "Pressure Variation Study in Human-Human and Human-Robot Handshakes: Impact of the Mood", Proceedings of the 27th IEEE International Symposium on Robot and Human

Interactive Communication, Nanjing, China, August 27-31, 2018

[15] M. Jindai and T. Watanabe, “Development of a handshake robot system based on a handshake approaching motion model,” in *Advanced intelligent mechatronics, IEEE/ASME international conference on IEEE*, p1–6, 2007

[16] Dimitrios Papageorgiou and Zoe Doulgeri, “A Kinematic Controller for Human-Robot Handshaking using Internal Motion Adaptation,” *IEEE Int. Conf. on Robotics and Automation (ICRA)*, p5622-5627, 2015

[17] T. Kasuga and M. Hashimoto, “Human-Robot Handshaking using Neural Oscillators,” *IEEE Int. Conf. on Robotics and Automation*, p3802-3807, 2005

[18] Melanie Jouaiti, Patrick Hénaff. “CPG-based Controllers can Trigger the Emergence of Social Synchrony in for Human-Robot Interactions”, *ARSO – IEEE International Workshop on Advanced Robotics and its Social Impacts*, Sep. 2018

[19] Melanie Jouaiti, Lancelot Caron and Patrick Hénaff., “Hebbian Plasticity in CPG Controllers Facilitates Self-Synchronization for Human-Robot Handshaking”, *Front Neurorobot*, 2018

[20] Haider A.F. Almurib, “Design of Human Elbow Joint Mechanism”, *Australian Journal of Basic and Applied Sciences*, 5(7): 976-981, 2011

[21] Rieko Osu, David W. Franklin, Hiroko Kato et al, “Short- and Long-Term Changes in Joint Co-Contraction Associated with Motor Learning as Revealed from Surface EMG,” *Journal of Neurophysiology*, 88: 991-1004, 2002

[22] Latash, M. L., Muscle coactivation: definitions, mechanisms, and functions, (2018). *Journal of Neurophysiology*, 120(1), 88–104. 2018

[23] Arndt, K.H., *Achillesehnenruptur and Sport*. Leipzig: Johann Ambrosius Barth. 1976.

[24] Woledge, R.C., N.A. Curtin and E. Homsher, Energetic aspects of muscle contraction. *Monographs of the Physiological Society*, No. 41. London: Academic Press. 1985.

[25] Morgan, D.L., U. Proske and D. Warren. Measurements of muscle stiffness and the mechanism of elastic storage of energy in hopping kangaroos. *Journal of Physiology*, vol 282. 253-261. 1978.

[26] Proske, U. and D.L. Morgan, Stiffness of cat soleus muscle and tendon during activation of part of muscle. *Journal of Neurophysiology*, vol. 52, 459-468. 1984.

[27] Hill, A.V., Production and absorbtion of work by muscle. *Science*, vol. 131, 897-903. 1960.

[28] Hill, A.V., *First and last experiments in muscle mechanics*. Cambridge University Press. 1970.

[29] Jewell, B.R. and D.R. Wilkie, An analysis of the mechanical components of frog’s striated muscle. *Journal of Physiology* 143, 515-540. 1958.

[30] Bahler, A.S., Series elastic component of mammalian skeletal muscle. *American Journal of Physiology,* vol. 213, 1560-1564. 1967.

[31] Huxley, A.F. and R.M. Simmons, Rapid 'give' and the tension 'shoulder' in the relaxation of frog muscle fibres. *Journal of Physiology,* vol. 210, 32-33. 1970.

[32] Gottlieb, G.L. and G.C. Agarwal, Compliance of single joints: Elastic and plastic characteristics. *Journal of Neurophysiology*, vol. 59, 937-951. 1988.

[33] Hof. A.L. and J.W. van den Berg, EMG to force processing. II. Estimation of parameters of the Hill muscle model for the human triceps surae by means of a calf ergometer. *Journal of Biomechanics*, vol. 14. 759-77, 1981.

[34] Hof, A.L., 'Effects of muscle elasticity in walking and running'. In: J.M. Winters and S.L.-Y. Woo teds.), *Multiple muscle systems: Biomechanics and movement organization* (pp.591-607). Berlin: Springer-Verlag. 1990.

[35] Mark L. Latash, Vladimir M. Zatsiorsky, Joint stiffness: Myth or reality? *Human Movement Science*, vol. 12, 653-692, 1993.

[36] Palazzolo JJ, Ferraro M, Krebs HI, Lynch D, Volpe BT, et al. Stochastic estimation of arm mechanical impedance during robotic stroke rehabilitation. *IEEE Engineering in Medicine and Biology Society*, 15: 94–103. 2007.

[37] Perreault EJ, Kirsch RF, Crago PE, Effects of voluntary force generation on the elastic components of endpoint stiffness. *Experimental Brain Research* 141: 312–323. 2001.

[38] Perreault EJ, Kirsch RF, Crago PE, Multijoint dynamics and postural stability of the human arm. *Experimental Brain Research* 157: 507–517. 2004.

[39] Dolan JM, Friedman MB, Nagurka ML, Dynamic and loaded impedance components in the maintenance of human arm posture. *IEEE Transactions on Systems, Man, and Cybernetics* 23: 698–709. 1993.

[40] Tsuji T, Morasso PG, Goto K, Ito K, Human hand impedance characteristics during maintained posture. *Biological cybernetics* 72: 475–485. 1995.

[41] Darainy M, Malfait N, Gribble PL, Towhidkhah F, Ostry DJ, Learning to control arm stiffness under static conditions. Journal of neurophysiology, vol. 92: 3344–3344. 2004.

[42] Franklin DW, Liaw G, Milner TE, Osu R, Burdet E, et al., Endpoint stiffness of the arm is directionally tuned to instability in the environment. *Journal of Neuroscience,* vol. 27: 7705–7705. 2007.

[43] Wong J, Wilson ET, Malfait N, Gribble PL, Limb stiffness is modulated with spatial accuracy requirements during movement in the absence of destabilizing forces. *Journal of neurophysiology*, vlo. 101: 1542–1549. 2009.

[44] Ludvig D, Starret Visser T, Giesbrecht H, Kearney R, Identification of Time-Varying Intrinsic and Reflex Joint Stiffness. *IEEE transactions on biomedical engineering*. 2011

[45] Milner TE, Dependence of elbow viscoelastic behavior on speed and loading in voluntary movements. Experimental Brain Res 93: 177–180. 1993.

[46] Wong J, Wilson ET, Malfait N, Gribble PL, The influence of visual perturbations on the neural control of limb stiffness. *Journal of neurophysiology*, vol. 101: 246–257. 2009.

[47] Ravichandran VJ, Perreault EJ, Westwick DT, Cohen N, Nonparametric identification of the elbow joint stiffness under compliant loads. *Annual International Conference of the IEEE Engineering in Medicine and Biology*, 7: 4706–4709. 2004.

[48] Piovesan D, Pierobon A, DiZio P, Lackner JR, Measuring Multi-Joint Stiffness during Single Movements: Numerical Validation of a Novel Time-Frequency Approach. *PLoS ONE* 7(3): e33086. 2012.

[49] Zatsiorsky VM, On muscle and joint viscosity. *Motor Control* 1:299-309, 1997

[50] Milner TE and Cloutier C. Damping of the wrist joint during voluntary movement. *Exp. Brain Res.* 122: 309–317, 1998

[51] Ford LE, Huxley AF, Simmons RM, Tension during steady shortening of frog muscle fibers. J Physiol (Lond) 361:131-150, 1985

[52] Milner TE, Cloutier C., Compensation for mechanically unstable loading in voluntary wrist movement. *Exp. Brain Res.*, 94:522-532, 1993

[53] : Hyun K. Kim, Byungduk Kang, Byungchan Kim, and Shinsuk Park, "*Estimation of Multijoint Stiffness Using Electromyogram and Artificial Neural Network*," IEEE TRANSACTIONS ON SYSTEMS, MAN, AND CYBERNETICS—PART A: SYSTEMS AND HUMANS, VOL. 39, NO. 5, 2009

[54] Minoru Hashimoto, Yoshihide Kiyosawa, Richard P. Paul, A Torque Sensing Technique for Robots with Harmonic Drives, *IEEE Transactions on Robotics and Automation*, Vol. 9, No. 1, 108-116, 1993

[55] Navvab Kashiri, Jorn Malzahn and Nikos G. Tsagarakis, On the Sensor Design of Torque Controlled Actuators: A Comparison Study of Strain Gauge and Encoder Based Principles, *IEEE ROBOTICS AND AUTOMATION LETTERS*, 2017

[56] Albert G. Crenshaw, Stefan Karlsson, Jorma Styf, Tomas Backlund, Jan Friden, Knee extension torque and intramuscular pressure of the vastus lateralis muscle during eccentric and concentric activities, *Eur. J. Appl. Physiol*. Vol. 70, 13-19, 1995

[57] Khalil Ullah, Jung-Hoon Kim, A Mathematical Model for Mapping EMG Signal to Joint Torque for the Human Elbow Joint using Nonlinear Regression, *4th International Conference on Autonomous Robots and Agents*, Feb 10-12, Wellington, New Zealand, 2009

[58] Pierre-Henri Orefice, Mehdi Ammi, Moustapha Hafez, Adriana Tapus, Pressure Variation Study in Human-Human and Human-Robot Handshakes:

Impact of the Mood, *27th IEEE Int. Symposium on Robot and Huamn Interactive Communication*, pp247-254, 2018

[59] A. Melnyk, V. Khomenko, V. Ph. Borysenko, and P. Henaff, Sensor network architecture to measure characteristics of a handshake between humans, *Proc. of IEEE XXXIV Int. Sci. Conference Electronics and Nanotechnology (ELNANO'2013)* pp. 264-268.

[60] E. Knoop, M. Bacher, V. Wall, R. Deimel, O. Brock, and P. Beardsley. Handshakiness: Benchmarking for human-robot hand interactions. *IEEE/RSJ International Conference on Intelligent Robots and Systems (IROS)*, p4982–4989. 2017.

[61] Human Body Properties Database, Japanese Body Size Data 1992-1994, Available: http://www.hql.jp/project/size1992/

[62] Duk Shin, Jaehyo Kim, and Yasuharu Koike, A Myokinetic Arm Model for Estimating Joint Torque and Stiffness From EMG Signals During Maintained Posture, *J. Neurophysiol* 101: 387–401, 2009.

[63] Feil-Seifer D, Mataric MJ, "Defining socially assistive robotics," 9th International Conf. on Rehabilitation Robotics, (ICORR2005), p465- 468, 2005.

[64] A. De Santis, B. Siciliano, A. De Luca, and A. Bicchi, "An atlas of physical human–robot interaction," Mechanism and Machine Theory, Vol. 43, No. 3, p253–270, 2008.

[65] Albu-Schaffer, A., Eiberger, O., Grebenstein, M., Haddadin, S., Ott, C., Wimbock, T., Wolf, S. and Hirzinger, G., "Soft robotics." IEEE Robotics & Automation Magazine, 15(3), 2008.

[66] C. Laschi, B. Mazzolai, M. Cianchetti, "Soft robotics: Technologies and systems pushing the boundaries of robot abilities." Sci. Robot., eaah3690, 2016

[67] Rieko Osu, David W. Franklin, Hiroko Kato et al, "Short- and Long-Term Changes in Joint Co-Contraction Associated with Motor Learning as Revealed from Surface EMG," Journal of Neurophysiology, 88: 991-1004, 2002

[68] T. George Thuruthel, Y. Ansari, E. Falotico, and C. Laschi, "Control strategies for soft robotic manipulators: A survey," Soft Robotics, vol. 5, no. 2, pp. 149–163, 2018

[69] T. Kozuki, Y. Motegi, T. Shirai, "Design of Upper limb by Adhesion of Muscles and Bones -Detail Human Mimetic Musculoskeletal Humanoid Kenshiro-," *IEEE Int. Conf. on Intelligent Robots and Systems (IROS)*, p935-940, 2013

[70] Taro Nakamura, Hitomi Shinohara, "Position and Force Control Based on Mathematical Models of Pneumatic Artificial Muscles Reinforced by Straight Glass Fibers," *IEEE Int. Conf. on Robotics and Automation*, p4361-4366, 2007

[71] H. Maeda, H. Nagai, H. Saito, et al. "Position and compliance control of an artificial muscle manipulator using a mechanical equilibrium model," *Proceedings of 34th annual conference of IEEE Industrial Electronics Society*

(IECON), Orlando, FL, p3431–3436, 2008

[72] Edward J. Park, Luis F. da Luz, Afzal Suleman, "Multidisciplinary design optimization of an automotive magnetorheological brake design," Computers and Structures 86, p207-216,2008

[73] M. Okui, S. Iikawa, Y. Yamada, T. Nakamura, "Fundamental characteristic of novel actuation system with variable viscoelastic joints and magneto-rheological clutches for human assistance," *Journal of Intelligent Material Systems and Structures*, Special Issue Article, p1-9, 2017.

[74] Ryuji Suzuki, Manabu Okui, Shingo Iikawa et al, "Novel Feedforward Controller for Straight-Fiber-Type Artificial Muscle Based on an Experimental Identification Model," IEEE Int. Conf. on Soft Robotics (RoboSoft), p31-38. 2018.

[75] Human Body Properties Database, Japanese Body Size Data 1992-1994, Available: http://www.hql.jp/project/size1992/

[76] E. Knoop, M. Bacher, and P. Beardsley, "Contact pressure distribution as an evaluation metric for human-robot hand interactions," HRI 2017 workshop - Towards reproducible HRI Experiments: Scientific endeavors, benchmarking and standardization

[77] Gilles Yange, Patrick Henaff and Nicolas Gregori, "Measurement and Analysis of Physical Parameters of the Handshake Between two Persons According to Simple Social Contexts," 2016, IEEE Int. Conf. on Intelligent Robots and Systems (IROS), p674-679

Research achievement

- Journal paper

Variable viscoelasticity handshake manipulator for physical human–robot interaction using artificial muscle and MR brake
DOI: https://doi.org/10.1088/1361-665X/ab0d9b
Smart Materials and Structures, Volume 28, Number 6, Published 1 May 2019

- Conference paper

Research of human-robot handshakes under variable stiffness conditions
Published in: 2019 IEEE 4th International Conference on Advanced Robotics and Mechatronics DOI: 10.1109/ICARM.2019.8833897
Proposal of the interaction force measuring device for human handshakes
The Proceedings of JSME annual Conference on Robotics and Mechatronics (Robomec)
DOI: 10.1299/jsmermd.2019.2P1-K09

- International conference

16th Electrorheological Fluids and Magnetorheological Suspensions (ERMR2018)
IEEE 4th International Conference on Advanced Robotics and Mechatronics (ICARM2019)
17th Electrorheological Fluids and Magnetorheological Suspensions (ERMR2019)

- Japanese conference

The Proceedings of JSME annual Conference on Robotics and Mechatronics (Robomec2019)

Acknowledgments

The author would like to express the deepest gratitude to his supervisor, Professor Taro Nakamura, for guiding him and many pieces of advice. The author was always encouraged and given a lot of chances to grow by him. This thesis could not be completed without his support.

The author is deeply grateful to Assistant Professor Manabu Okui and Rie Nishimura who provided him insightful pieces of advice and supported him during his doctor course.

The author would like to thank the members of his Ph.D. dissertation committee: Professor Nituma, Professor Hiraoka, Professor Moromugi and Professor Wan from Osaka University, for their valuable comments on the revision of this thesis.

The author would like to express his sincere gratitude to the staff in Biomechanics Lab., Chuo University for their support. Finally, the author is deeply grateful to his family. The author could not have done it without their supports and encouragement.

Appendix A: Artificial muscle characteristic identification experiment

A-1 Background

Considering the response time delay of the artificial muscles and based on the antagonistic structure of the artificial muscle actuator a feedforward controller has been proposed in the previous research. And according to the performance test result of the handshake manipulator in section 3.8, it has been verified that the controller is capable of achieve steady control of the handshake manipulator without being affected by the response delay the same as in a feedback controller. The feedforward controller is designed based on the force equilibrium model of the artificial model, and some of the parameters are not directly measurable. Therefore, the system identification method was applied to determine artificial muscle characteristics.

A-2 Force equilibrium model of artificial muscle

In order to control artificial muscles, modeling of artificial muscles is required. In the system identification experiment, a mechanical force equilibrium model of the artificial muscle was developed. From the shape of the axial fiber reinforced artificial muscle, it is known that the applied pressure to the artificial muscle can be calculated from the target contraction amount. Figure A1 shows the shape model of the artificial muscle, and Table A1 shows the definition of each parameter.

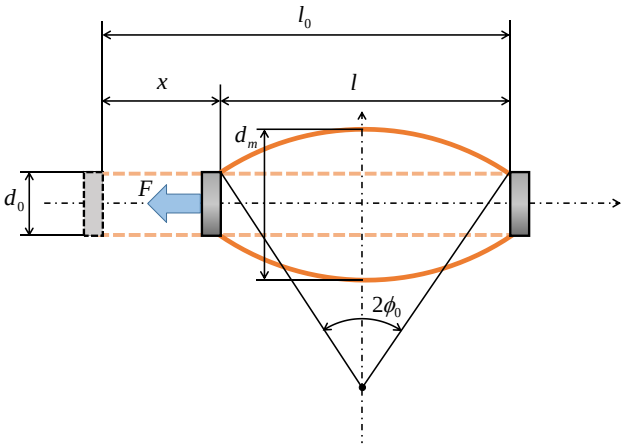

Fig. A1 The model of an artificial muscle

Table A1: List of symbols used in the model of a mechanical equilibrium of an artificial muscle

Diameter of the artificial muscle [m]	d_0
Diameter of the artificial muscle after deformation [m]	d_m
Displacement of the artificial muscle [m]	x
Length of the artificial muscle [m]	l_0
Length of the artificial muscle after deformation [MPa]	l
The central angle of the artificial muscle [rad]	φ_0
Longitudinal modulus of the rubber [Pa]	K
The thickness of the fiber [mm]	t
Coefficient about the tension of the fiber	M
The number of fiber	n
The width of the fiber	b

As shown in Fig. A1, it is assumed that the deformation of the artificial muscle can be circularly approximated. In the axial direction, the balanced relationship between the contraction force, force by pressure, and fiber tension is established. In the radial direction, the balanced relationship of fiber tension, pressure force, and rubber tension is established. By solving these balancing equations, the following equations (A.1)-(A.5) are derived.

$$P(x, F) = \frac{G_1(\phi_0) - FG_2(\phi_0)}{G_3(\phi_0)} \tag{A.1}$$

$$\phi_0 = \frac{2\alpha l_0^{1.5} x_d^{0.5}}{(l_0 - x)^2 + \alpha^2 x_d l_0} \tag{A.2}$$

$$G_1(\phi_0) = \frac{2Kt}{d_0}\left(\frac{l_0}{d_0}\right)^2\left(\frac{\sin\phi_0 - \phi_0\cos\phi_0}{\phi_0^2}\right) \tag{A.3}$$

$$G_2(\phi_0) = \frac{M\tan\phi_0}{d_0 nb} \tag{A.4}$$

$$G_3(\phi_0) = \left(\frac{l_0}{d_0}\right)^2\left(\frac{\phi_0 - \sin\phi_0\cos\phi_0}{\phi_0^2}\right) + 2\left(\frac{l_0}{d_0}\right)\frac{\sin\phi_0}{\phi_0} - \frac{\pi M d_0}{4nb}\tan\phi_0 \tag{A.5}$$

A-3 Experimental method

In order to identify the parameters shown in Table A1, which are used to solve the force equilibrium equations, an experiment was designed to measure the static characteristic of an artificial muscle. The relationships between the contraction amount and the contraction force were measured under different air

pressure conditions. A platform was designed to install an artificial muscle, and rails are applied to a moving plate, which slides when the artificial muscle contracts. A laser distance sensor was used to measure the contraction amount of the artificial muscle. The same measurement was conducted under different air pressure conditions. The experiment device was shown in Fig. A2, and the diagram of the system as shown in Fig. A3.

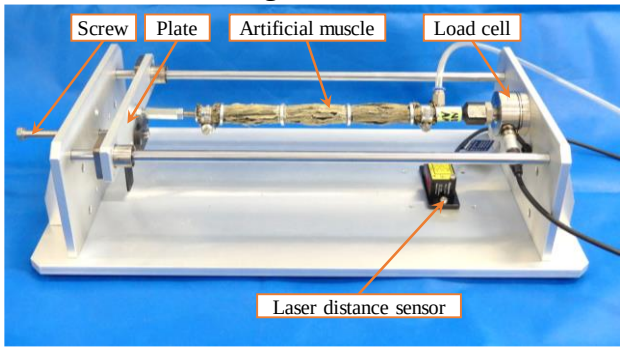

Fig. A2 A photograph of the experimental device

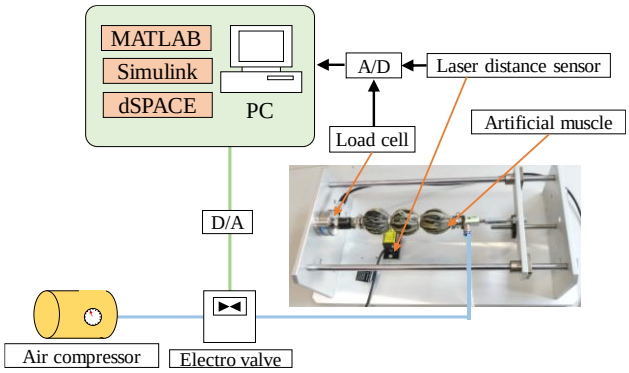

Fig. A3 The system of an isometric experiment

The measured data of the air pressure and the contraction amount was shown in Table A1. Both the theoretical relationships of the contraction force and contraction amount under different air pressure conditions and the measured relationships were displayed in Fig. A4, representing by a solid line and dots respectively. By adjusting the system parameters, each artificial muscle can be estimated by a set of parameters accurately. Therefore, the feed-forward controller can control the movement of the artificial muscle driven actuator without obvious output error.

Table A1 Relationship of contraction force and displacement

Contraction force (N)	Air pressure (MPa)								
	0	0.03	0.06	0.09	0.12	0.15	0.18	0.21	0.24
	Displacement (mm)								
0.0	175.5	175.0	173.8	170.0	145.3	132.1	125.0	120.6	117.6
33.3	176.0	175.7	174.9	172.0	155.3	140.5	132.1	126.8	123.3
66.6	176.4	176.2	175.5	172.9	162.4	148.1	138.8	132.4	128.2
100.0	176.7	176.6	176.1	173.9	167.8	154.9	144.8	137.7	132.8
133.3	176.9	176.7	176.3	174.6	170.5	159.9	149.8	142.6	137.1
166.6	176.9	176.8	176.5	175.5	172.6	163.3	154.8	147.7	141.8

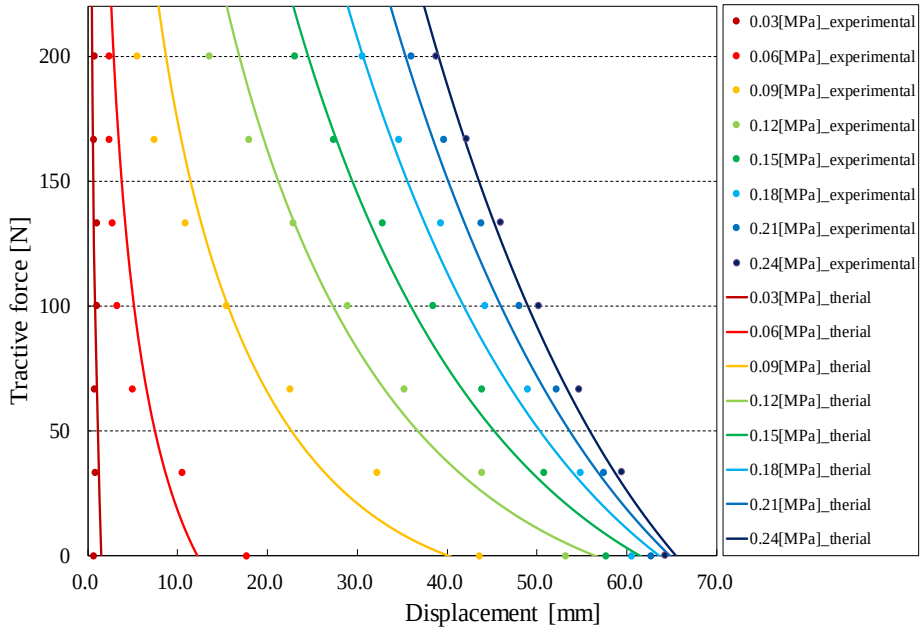

Fig. A4 Static characteristic of an artificial muscle

A-4 Result and conclusion

Fig. A5 shows the results of the isometric stiffness experiment in this experiment. The results shows that the stiffness of the artificial muscle depends on the displacement from the neutral length and the applied pressure. In addition, Fig. A6 plots the slope of the straight line when the applied pressure and stiffness of each displacement are linearly approximated by the least-squares method in Fig. A5. In Fig. A6, the relationship between displacement and stiffness can be approximated by a logarithmic function,

$$k_a = -0.26\ln(x) + 0.13 \tag{A.6}$$

In this particular example, the correlation coefficient at this time is 0.96. From the above, it was found that the stiffness of the artificial muscle changes according to the applied pressure for a certain amount of contraction.

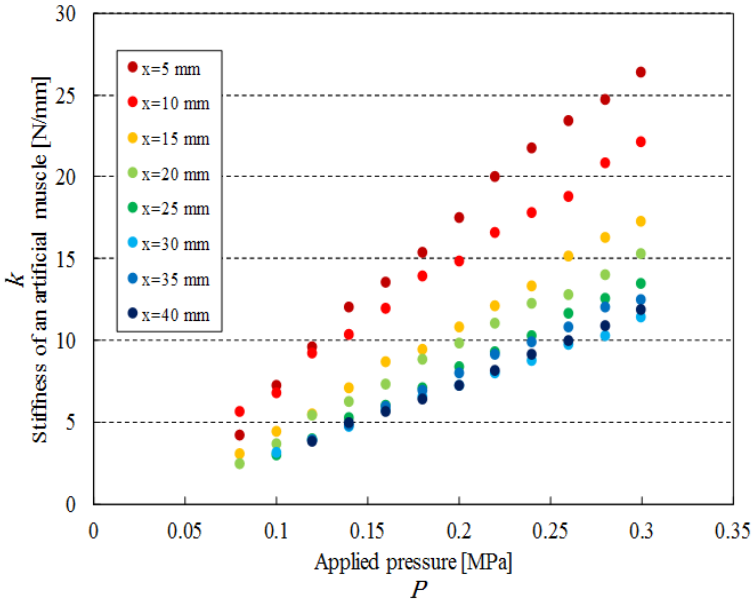

Fig. A5 The result of an isometric experiment

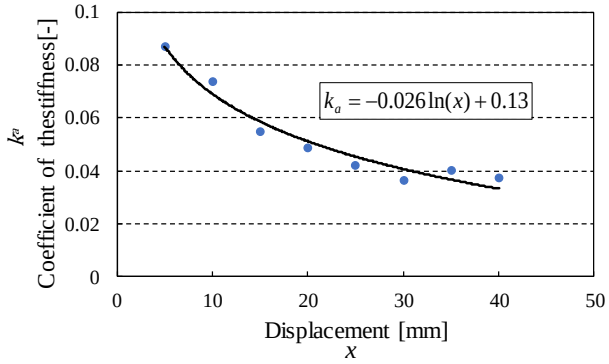

Fig. A6 The relationship of artificial muscle stiffness and displacement

Appendix B: Motion capture device and Cortex

In this research, a motion capture system was used for capturing the movement of the subjects. The system we selected for this purpose is called the MAC3D system, and the software for the captured data analysis is Cortex.

B-1 MAC3D System

The MAC3D System is an optical motion capture system that attaches markers to humans and robots and can measure three-dimensional positions in real-time. The MAC3D System is active in a wide range of fields such as sports, biomechanics, robotics, ergonomics, and VR. It is the only all-in-one package system in the optical motion capture industry. All processes from camera installation to measurement and analysis can be performed with one software. It has excellent real-time properties. And all types of MAC3D System digital cameras released so far can be used together. In this research, we have the setup of 8 cameras of 2 different types, the setting position of the cameras can be seen in Fig. B1.

Fig. B1 The camera settings of the motion capture device

B-2 Analysis software Coretex

MAC3D System software Cortex supports measurement and analysis such as sports, rehabilitation, robotics, object behavior analysis, and biomechanics. It has a reputation for stable connection to external devices and a large lineup of optional software specialized in each field, and has been chosen by many people.

Cortex was developed based on the concept of "simplifying motion analysis", it greatly improved the quality and quantity of analysis. Tools for analyzing batting, pitching, golf, walking, jumping, running, and lifting motions are available. By attaching a marker at a specified position, the coordinates of the markerset can be exported to an Excel file with a few clicks.

B-3 Process of motion capture data analysis

The processing window of the captured data was shown in Fig. B2. In order to start the analysis, a predefined markerset has to be imported first as shown in Fig. B2. For this research, we applied the Helen-hayes markerset, which was explained in section 2.6.

First, each recorded marker was assigned to a name in the markerset, for example, head front, right shoulder, left elbow etc. As shown in Fig. B3. When all the markers are assigned, a whole-body model will be created. In order to synchronize the motion capture data with the interaction force measurement device, a start trigger signal was sent to the A/D port of the MAC3D system, which was recorded together with the marker data. In order to reduce the amount of data for processing and synchronize the starting point of each data, each record was strimmed at the rising edge of the start trigger and the end of each handshake motion, as shown in Fig. B4. Finally, xyz coordinates of each marker were examed for discontinuity, connected and filtered by a low-pass filter, as shown in Fig. B5.

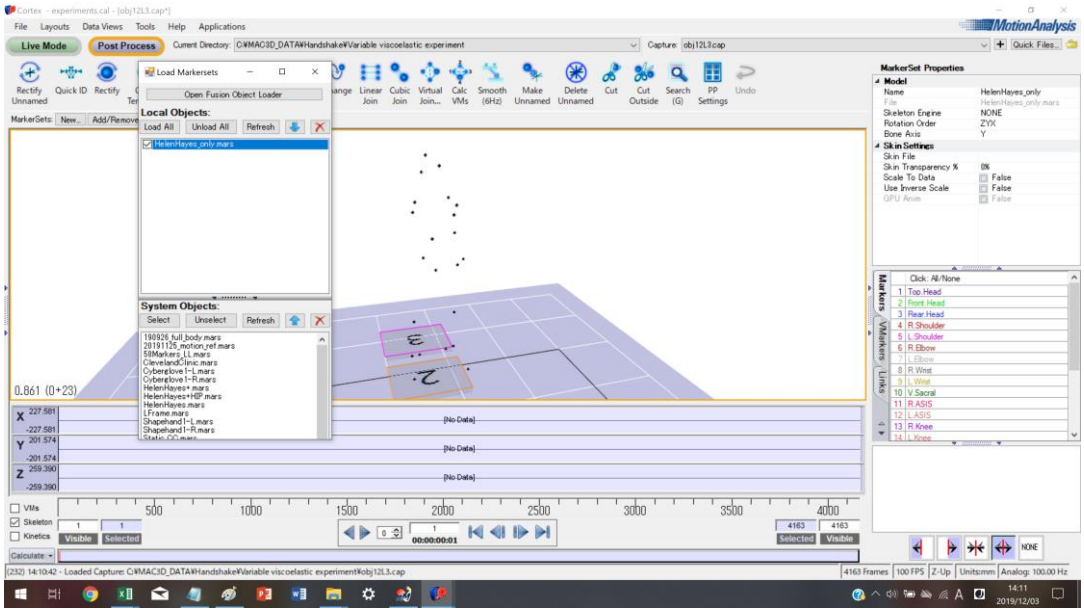

Fig. B2 Process window of Cortex and markerset

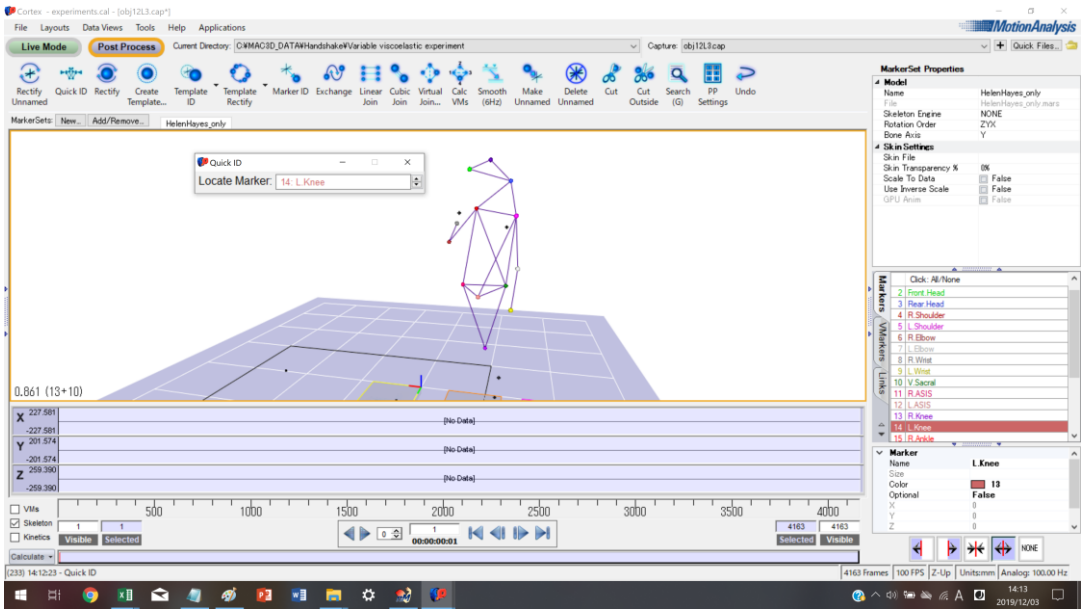

Fig. B3 Assign each marker to the markerset

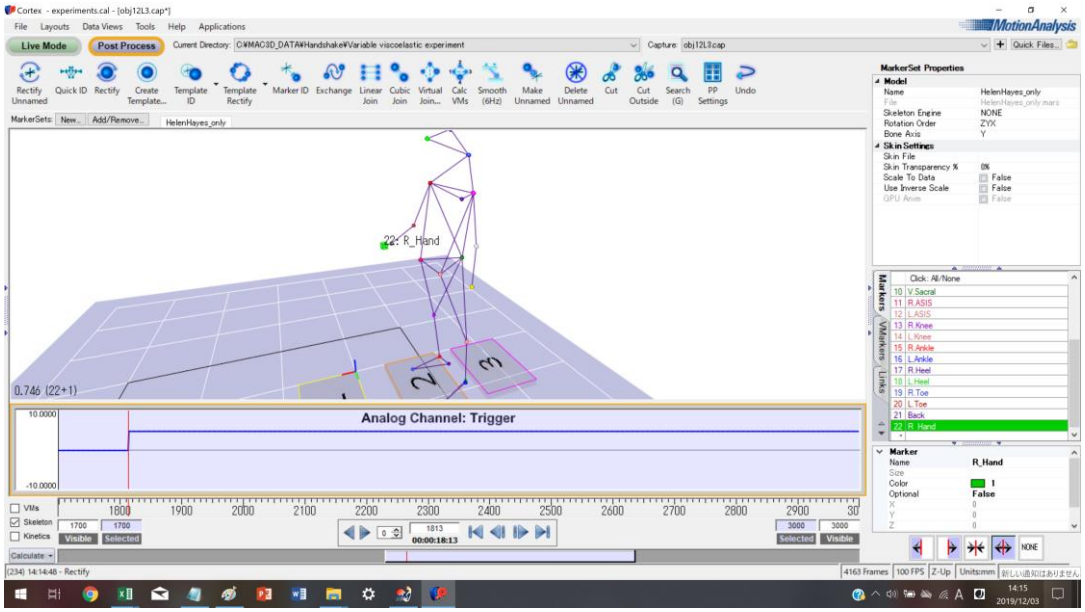

Fig. B4 Trim data at the rising edge of the start trigger

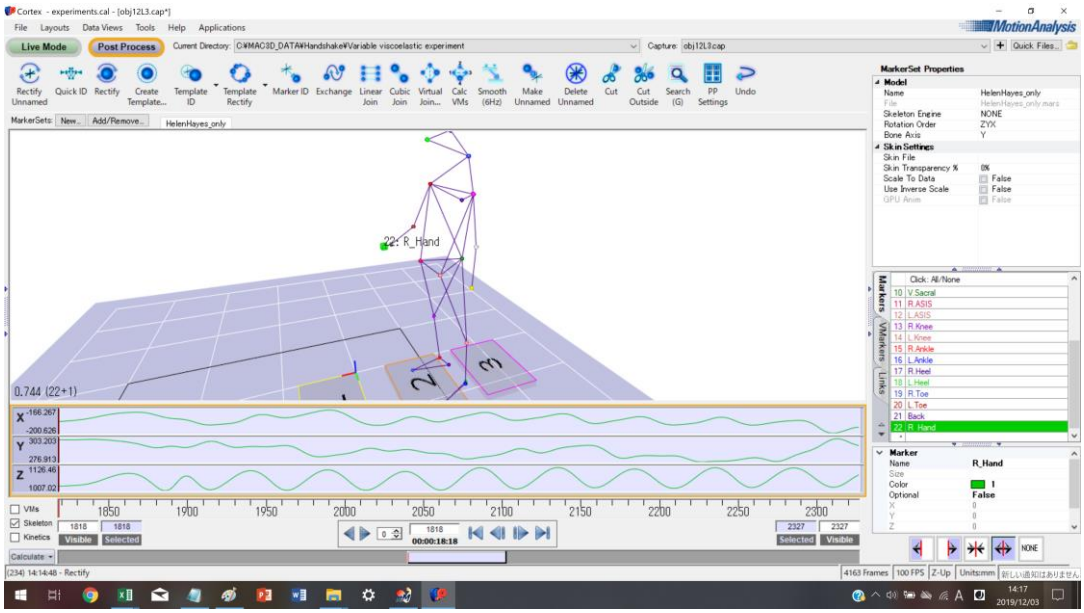

Fig. B5 Connect the missing data of each marker and apply filter

Appendix C: Loadcell

A load cell is a type of transducer, specifically a force transducer. It converts a force such as tension, compression, pressure, or torque into an electrical signal that can be measured and standardized. As the force applied to the load cell increases, the electrical signal changes proportionally. The most common types of load cell used are hydraulic, pneumatic, and strain gauge.

In this research, we used the strain gauge type of load cell for measuring the interaction force between two parties in a handshake. Strain gauge load cells are the kind most often found in industrial settings. It is ideal as it is highly accurate, versatile, and cost-effective. Structurally, a load cell has a metal body to which strain gauges have been secured. The body is usually made of aluminum, alloy steel, or stainless steel which makes it very sturdy but also minimally elastic. This elasticity gives rise to the term "spring element", referring to the body of the load cell. When force is exerted on the load cell, the spring element is slightly deformed, and unless overloaded, it always returns to its original shape. As the spring element deforms, the strain gauges also change shape. The resulting alteration to the resistance in the strain gauges can be measured as a voltage. The change in voltage is proportional to the amount of force applied to the cell, thus the amount of force can be calculated from the load cell's output. A strain gauge is constructed of very fine wire, or foil, set up in a grid pattern and attached to a flexible backing. When the shape of the strain gauge is altered, a change in its electrical resistance occurs. The wire or foil in the strain gauge is arranged in a way that, when force is applied in one direction, a linear change in resistance results. Tension force stretches a strain gauge, causing it to get thinner and longer, resulting in an increase in resistance. Compression force does the opposite. The strain gauge compresses, becomes thicker and shorter, and resistance decreases. The strain gauge is attached to a flexible backing enabling it to be easily applied to a load cell, mirroring the minute changes to be measured.

The load cell we used in this research is the product of Liniax Co., Ltd. The photo and size specifications are shown in Fig. C1 and Fig. C2 respectively. The measurable force and torque range was shown in Table C1. As the specifications indicate, the load cell is very small in size so that it can be installed in the interaction force measurement device. The load cell was connected to a signal amplifier, and the amplified signal was then sent into the A/D port of dSPACE, and the data was recorded. The input voltage data was then calculated to get the force and torque by a transformation matrix, which is shown in Fig. C3.

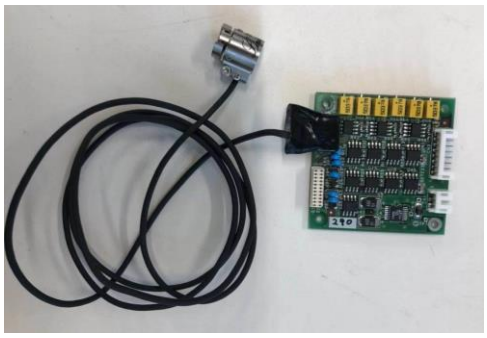

Fig. C1 The photo of the load cell

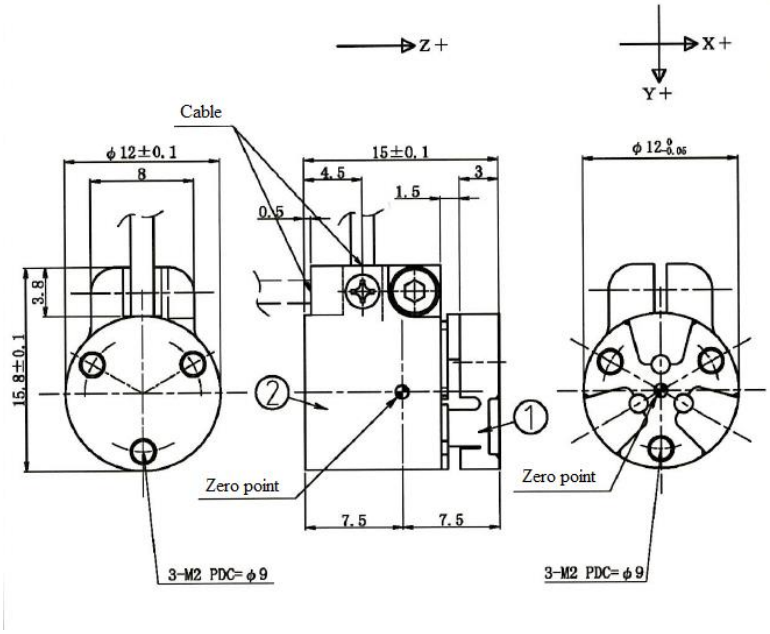

Fig. C2 Size of the load cell

Table C1 The measurable range of force and torque

Force	Measurable range (N)	Torque	Measurable range (Ncm)
Fx	0~25	Mx	0~30
Fy	0~25	My	0~30
Fz	0~50	Mz	0~30

$$\begin{bmatrix} Fx \\ Fy \\ Fz \\ Mx \\ My \\ Mz \end{bmatrix} = \begin{bmatrix} -16.025 & 15.036 & -11.291 & 2.851 & -3.036 & 12.166 \\ 4.851 & 5.555 & -11.461 & 17.125 & 17.028 & -11.397 \\ -13.424 & -13.066 & 11.617 & 14.454 & 15.191 & 11.757 \\ -4.604 & -4.180 & -5.247 & 0.569 & 0.318 & -5.219 \\ 3.686 & -2.886 & -2.400 & -5.727 & 5.831 & 1.348 \\ 4.665 & -5.045 & -3.780 & 4.219 & -4.795 & 4.769 \end{bmatrix} \times \begin{bmatrix} V11\ voltage \\ V12\ voltage \\ V21\ voltage \\ V22\ voltage \\ V31\ voltage \\ V32\ voltage \end{bmatrix}$$

Fig. C3 Transform matrix of the load cell

Appendix D: nMotion

For the skeletal muscle analysis, we used the software nMotion. Same as ordinary motion analysis software, nMotion can calculate kinematics and dynamics such as joint angles, joint moments, and joint power. Other musculoskeletal analysis such as muscle tension and muscle activity is also possible. In addition, since it has an anatomically natural biceps, tendon, and ligament model using its own virtual link, while other musculoskeletal analysis software calculates the tension of the Achilles tendon and the load on the ligament of the knee, nMotion can even analyze even the tendons and ligaments that are not used.

nMotion is still being developed and evolving. Inverse dynamics calculation, which was fast before, has been further accelerated. By improving the algorithm of the proprietary quadratic programming solver, the calculation speed is more than 10 times faster than the previous version, and the calculation that previously took several hours can be completed in just a few minutes. Until now, musculoskeletal analysis software, which has often been avoided because of the calculation time, however, nMotion changes the situation and can be used in various scenes such as sports, biomechanics, rehabilitation and so on.

For the skeletal muscle analysis, the first is to assign each marker in the motion capture data to the pre-restored skeletal model in nMotion, as shown in Fig. D1. In order to make the model as close to the subject as possible, sizes of the model can be adjusted according to the body features of the subject. In this research, the shoulder width of each subject was measured and the model was set accordingly, as shown in Fig. D2. Then the skeletal muscle model can be generated, as shown in Fig. D3. Finally, the kinetics and dynamics of each segment in the model can be calculated as shown in Fig. D4.

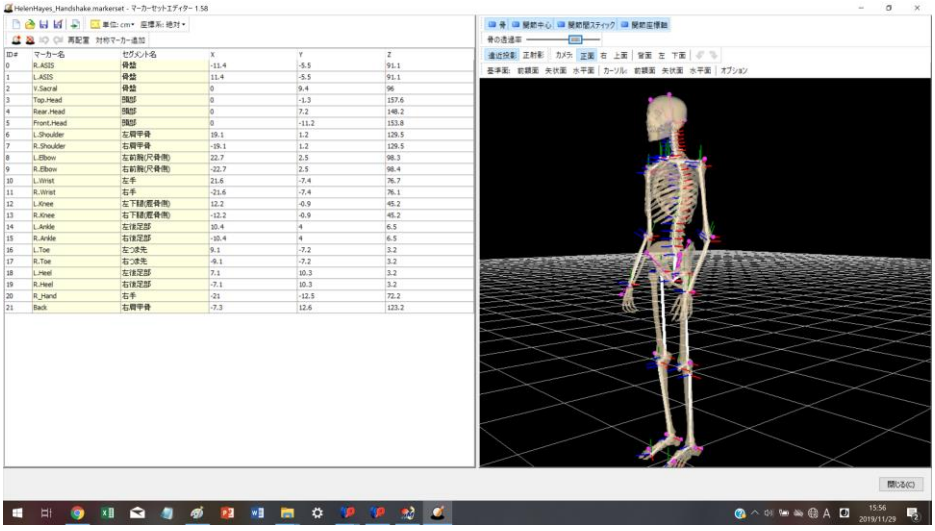

Fig. D1 Skeletal model in nMotion

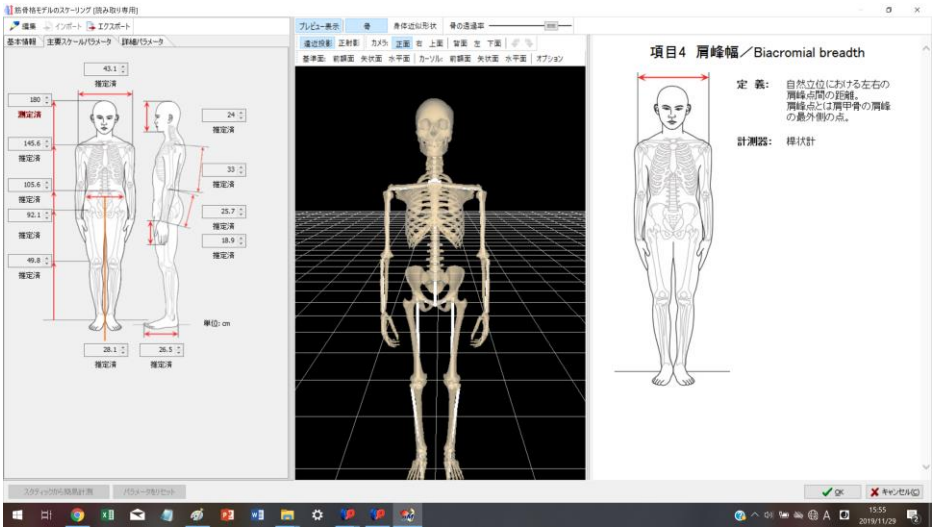

Fig. D2 Set the shoulder width of the subject to the model

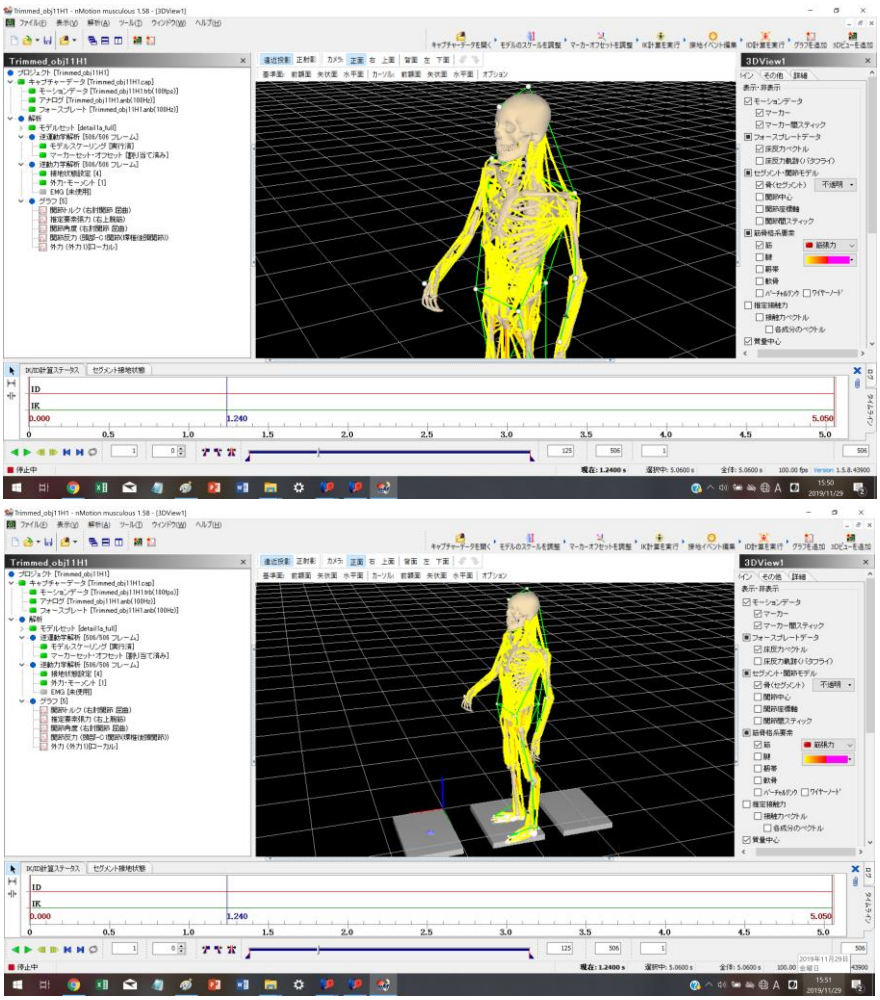

Fig. D3 The skeletal muscle model in nMotion

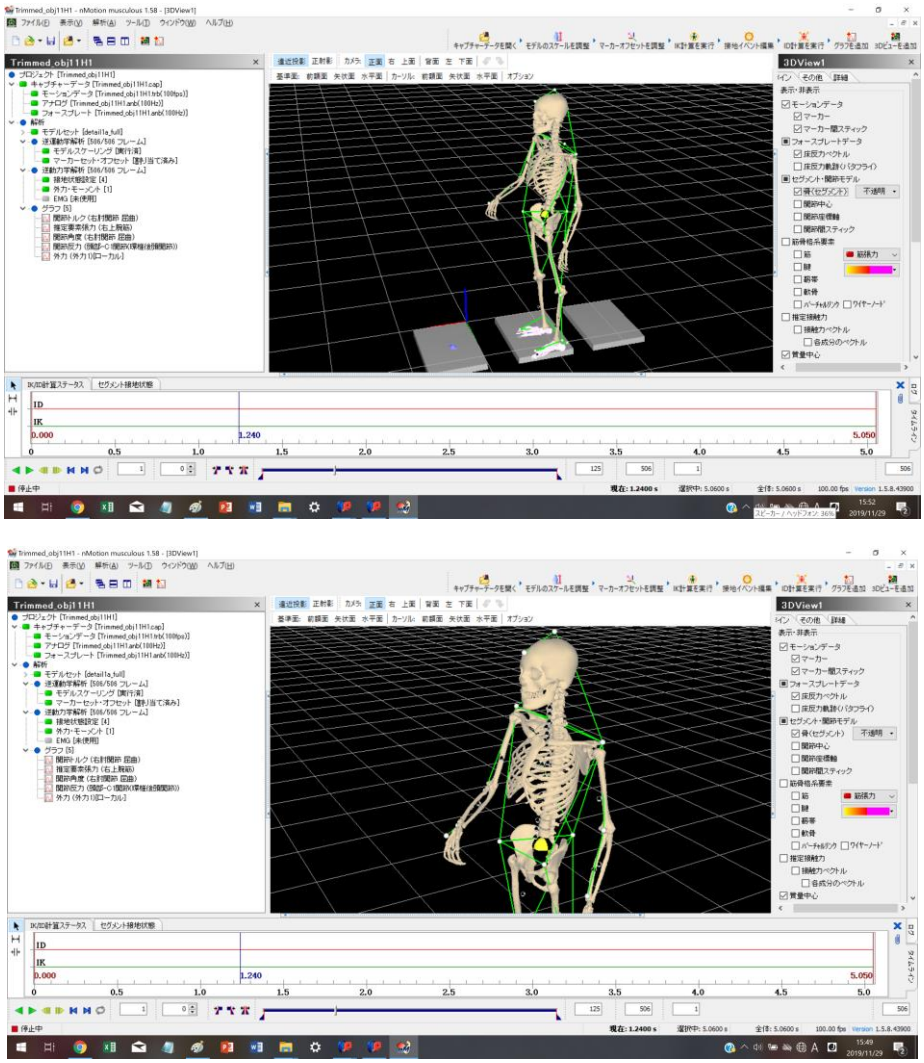

Fig. D4 Inverse kinetics and dynamics analysis of the model

Appendix E: Wireless EMG sensor

For the EMG analysis, we used the Delsys Trigno wireless biofeedback system. It is a high-performing device designed to make EMG signal detection reliable and easy. The system is capable of streaming data digitally into EMGworks, third-party software, or via analog outputs for integration with motion capture and other third-party data acquisition systems. Full triggering features further expand integration options for additional measurement technologies. The picture of the sensor was shown in Fig. E1. The sensor has built-in wi-fi modules to connect with the base station, which then sends signals to the computer for analysis, as shown in Fig. E2. Then specifications of the Trigno wireless sensor was shown in Fig. E3.

Fig. E1 Delsys Tringo wireless EMG sensor

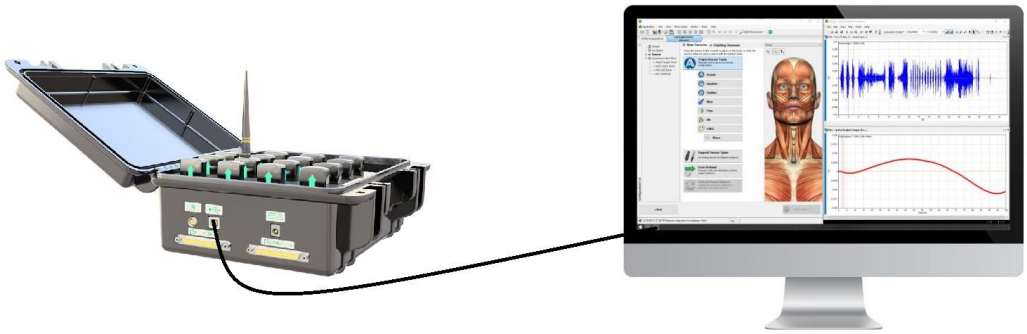

Fig. E2 Base station and analysis software

Sensor Channels
1x EMG, up to 6x IMU

Reference Type
Dual on-board stabilizing reference

Inter-Electrode Spacing
10 mm

Size (Body)
27 x 37 x 13 mm

Mass
14 g

Material
Medical Grade Polycarbonate

Operating Range
40 m in RF mode
Host Dependent/unlimited datalogger

Wireless Protocol
-2.400-2.483 GHz ISM Band,Proprietary RF Protocol
-BLE V4.2

EMG Bandwidths
10-850 Hz
20-450 Hz

EMG Sampling Rate (Max)
4370 sa/sec

Accelerometer Sampling Rate (Max)
963 sa/sec

Gyroscope Sampling Rate (Max)
741 sa/sec

Orientation Sampling Rate (Max)
222 sa/sec

Sensor Resolution
16 bits

EMG Baseline Noise (typical)
750 nV

EMG Input Range
11 mV / 22 mV rti

CMRR
<-80 dB

Battery Life
Up to 8 hours

Recharge Time (typical)
2.5 hours

Inter-Sensor Latency
< 1 sampling period

EMG Analog Output Delay
48 ms Fixed

ACC/Gyro Analog Output Delay
96 ms Fixed

Fig. E3 Specifications of the EMG sensor

Appendix F: ANN model for predicting a handshake

ANN

Artificial neural networks (ANN) is a computing system inspired by the biological neural networks that constitute animal brains. Such systems "learn" to perform tasks by considering examples, generally without being programmed with task-specific rules. For example, in image recognition, they might learn to identify images that contain cats by analyzing example images that have been manually labeled as "cat" or "no cat" and using the results to identify cats in other images. They do this without any prior knowledge of cats, for example, that they have fur, tails, whiskers and cat-like faces. Instead, they automatically generate identifying characteristics from the examples that they process. An ANN is based on a collection of connected units or nodes called artificial neurons, which loosely model the neurons in a biological brain. Each connection, like the synapses in a biological brain, can transmit a signal to other neurons. An artificial neuron that receives a signal then processes it and can signal neurons connected to it. The structure of a simple ANN was shown in Fig. F1

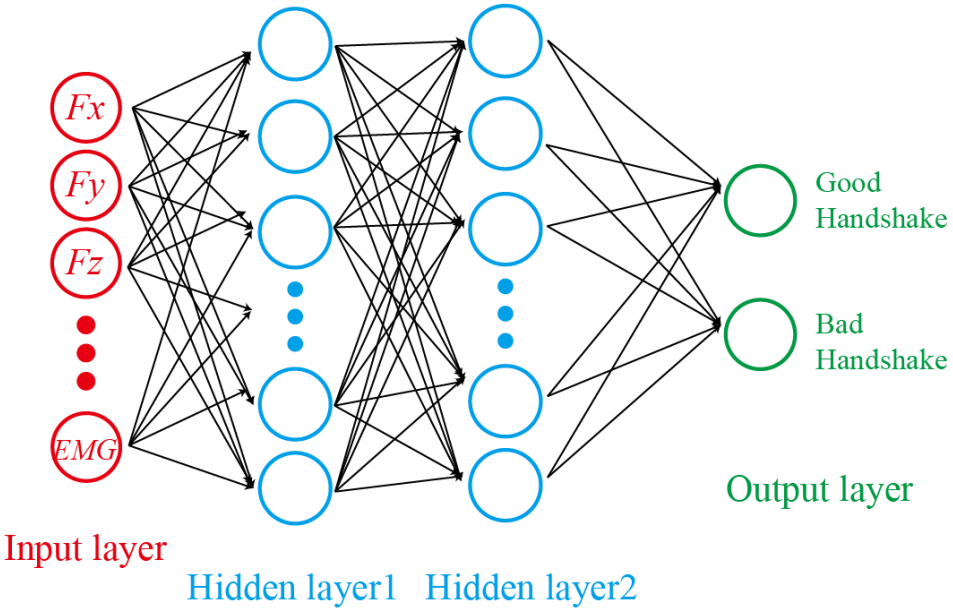

Fig. F1 The structure of ANN

In this experiment, an artificial neural network with 2 hidden layers was developed in python by the sklearn library. The source code of the ANN mode was shown below, and the dataset we used for training and testing the model was shown in Table F1.

```
# Importing the libraries
import numpy as np
import matplotlib.pyplot as plt
import pandas as pd

# Importing the dataset
dataset = pd.read_csv('Handshake properties.csv')
X = dataset.iloc[:, 3:13].values
y = dataset.iloc[:, 13].values

# Splitting the dataset into the Training set and Test set
from sklearn.model_selection import train_test_split
X_train, X_test, y_train, y_test = train_test_split(X, y, test_size = 0.2,
random_state = 0)

# Feature Scaling
from sklearn.preprocessing import StandardScaler
sc = StandardScaler()
X_train = sc.fit_transform(X_train)
X_test = sc.transform(X_test)

# Importing the Keras libraries and packages
import keras
from keras.models import Sequential
from keras.layers import Dense

# Initialising the ANN
classifier = Sequential()

# Adding the input layer and the first hidden layer
classifier.add(Dense(output_dim = 6, init = 'uniform', activation = 'relu',
input_dim = 11))

# Adding the second hidden layer
classifier.add(Dense(output_dim = 6, init = 'uniform', activation = 'relu'))

# Adding the output layer
classifier.add(Dense(output_dim = 1, init = 'uniform', activation = 'sigmoid'))

# Compiling the ANN
classifier.compile(optimizer = 'adam', loss = 'binary_crossentropy', metrics =
['accuracy'])
```

```
# Fitting the ANN to the Training set
classifier.fit(X_train, y_train, batch_size = 10, nb_epoch = 100)

# Predicting the Test set results
y_pred = classifier.predict(X_test)
y_pred = (y_pred > 0.5)

# Making the Confusion Matrix
from sklearn.metrics import confusion_matrix
cm = confusion_matrix(y_test, y_pred)
```

Table F1 Dataset for handshake prediction

No.	Condition	Ave. Fx(N)	Ave. Fy(N)	Ave. Fz(N)	Ave. grip(N)	Duration(s)	Angle range (rad)	Max speed(rad/s)	Max torque(Nm)	Ave stiff.(Nm/rad)	RMS bicep(μV)	RMS tricep(μV)
1	Firm	4.18	2.06	3.70	8.13	3.54	0.38	2.59	2.68	8.09	18.73	3.49
2	Firm	3.73	2.86	3.38	7.98	3.89	0.33	2.36	2.60	8.74	16.71	3.62
3	Firm	2.16	2.45	1.34	3.45	3.90	0.50	3.50	1.93	7.39	56.31	5.23
4	Firm	2.95	2.04	1.44	4.00	3.79	0.41	2.56	1.82	5.07	56.75	5.15
5	Firm	3.03	1.52	1.35	4.35	4.11	0.31	2.55	2.09	5.78	43.59	4.13
6	Firm	3.55	2.81	1.01	8.34	3.25	0.34	2.55	6.07	9.73	4.85	14.62
7	Firm	4.49	4.04	1.45	7.04	3.81	0.35	2.92	5.65	9.49	4.64	22.53
8	Firm	4.79	3.81	0.78	8.16	3.44	0.56	3.02	4.82	5.94	17.04	4.43
9	Firm	2.97	4.34	0.20	5.21	3.76	0.45	3.48	7.24	11.03	24.79	3.34
10	Firm	4.28	3.67	0.16	8.95	3.15	0.29	2.37	2.26	6.55	3.17	16.33
11	Firm	2.72	4.87	0.14	6.35	4.00	0.45	2.71	5.07	4.13	7.93	22.90
12	Firm	2.87	5.77	0.17	8.05	3.63	0.33	2.53	5.07	3.68	11.03	22.38
13	Firm	3.52	5.25	0.20	7.77	3.68	0.57	4.04	9.53	13.74	12.74	21.97
14	Firm	2.98	2.88	0.10	8.17	3.88	0.37	2.50	5.98	6.83	23.74	3.91
15	Firm	2.91	3.01	0.13	7.11	3.65	0.33	2.61	6.53	6.81	20.02	2.84
16	Firm	2.81	2.90	0.11	5.91	3.65	0.37	2.75	8.95	12.72	22.75	3.02
17	Firm	3.65	4.31	0.16	6.13	4.10	0.67	4.42	2.66	9.85	30.02	2.51
18	Firm	2.92	3.77	0.16	7.91	3.67	0.55	4.61	3.05	11.88	30.76	4.08
19	Firm	3.12	3.43	0.15	8.35	3.99	0.60	4.33	3.08	10.56	28.45	3.28
20	Firm	4.30	4.36	2.24	7.42	5.05	0.86	5.41	8.19	11.97	23.65	11.26
21	Firm	6.00	3.68	1.34	7.10	4.92	0.86	5.41	8.19	3.92	19.60	11.65
22	Firm	5.60	4.58	1.97	7.06	5.01	0.80	4.72	9.56	4.27	19.98	11.93
23	Firm	5.04	2.82	1.58	7.38	5.18	0.88	5.49	7.66	4.96	22.64	8.66
24	Firm	5.49	3.30	2.15	7.33	4.65	0.84	5.35	10.27	2.94	21.92	13.95
25	Weak	1.67	1.71	1.20	6.57	4.46	0.33	1.86	1.86	1.79	14.60	2.27
26	Weak	2.05	1.67	1.36	6.80	4.12	0.34	1.96	2.15	2.02	17.14	2.46
27	Weak	2.18	1.33	1.23	3.74	4.87	0.39	2.23	1.97	2.03	13.27	2.44
28	Weak	0.95	0.72	1.78	0.26	3.83	0.32	2.12	1.05	1.29	40.41	3.83
29	Weak	0.92	0.46	1.53	0.75	4.20	0.37	1.97	1.47	6.52	41.84	4.08
30	Weak	1.80	1.54	0.26	3.87	4.11	0.37	6.94	4.68	4.05	3.09	18.10
31	Weak	2.06	1.59	0.34	4.81	4.09	0.41	4.64	7.18	3.73	2.42	15.13
32	Weak	2.09	1.94	0.24	5.02	4.34	0.38	2.62	4.82	4.05	2.43	19.31
33	Weak	1.71	1.07	0.44	3.74	4.53	0.35	2.21	1.09	3.75	8.82	1.74
34	Weak	1.83	0.92	0.40	6.14	4.20	0.30	2.12	1.23	1.75	11.63	2.09
35	Weak	1.34	1.26	0.29	3.92	3.83	0.28	3.21	1.14	2.75	11.17	1.88
36	Weak	1.61	1.76	0.16	2.85	3.96	0.48	2.70	5.67	4.33	18.75	2.66
37	Weak	1.16	1.51	0.15	3.64	3.52	0.29	2.29	5.12	3.91	17.99	3.31
38	Weak	1.57	2.43	0.08	7.17	4.59	0.43	2.25	0.98	0.63	9.76	8.34
39	Weak	1.27	2.98	0.14	6.05	4.63	0.46	2.46	1.24	1.12	11.15	9.64
40	Weak	1.65	1.69	0.09	6.88	4.11	0.43	2.65	1.82	1.71	10.00	8.78
41	Weak	1.11	1.38	0.06	4.14	4.06	0.38	2.33	1.27	1.28	16.08	3.42
42	Weak	1.36	1.19	0.06	3.42	4.55	0.33	2.00	0.77	0.53	20.87	2.88
43	Weak	1.14	1.27	0.06	2.88	4.06	0.30	2.13	1.14	1.13	19.30	2.76
44	Weak	1.40	1.49	0.10	2.46	4.02	0.37	2.73	2.15	7.13	18.11	2.16
45	Weak	1.51	1.59	0.11	2.79	3.98	0.46	3.35	1.95	7.13	16.86	1.78
46	Weak	1.48	1.30	0.10	2.19	3.72	0.40	2.69	1.78	9.36	17.16	1.80
47	Weak	2.66	1.90	1.02	3.17	5.17	0.71	3.96	5.65	4.92	10.50	1.15
48	Weak	2.51	1.94	1.02	2.07	4.96	0.68	4.13	6.48	4.08	11.62	1.17
49	Weak	2.62	1.45	1.28	3.08	5.52	0.81	4.43	6.71	6.43	12.15	1.32
50	Weak	2.05	1.49	1.06	2.93	5.15	0.77	4.30	5.81	4.84	11.69	1.25
51	Weak	2.20	1.82	1.68	2.22	5.27	0.72	4.13	3.84	5.34	12.22	1.23

Appendix G: Motor driver

For the MR-brake control, we used the JW-143-2 motor driver which is a product of Okatech Co., Ltd. JW-143-2 is a compact, light-weight, high-output motor driver, which is suitable for current, speed, and position control. In this research, the current control mode was used for the accurate output torque control of the MR brake. A picture of the motor driver was shown in Fig. G1 and the specifications of the motor driver were shown in Table G1.

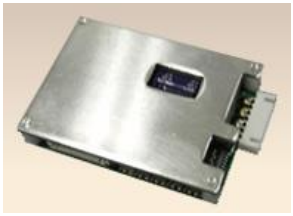

Fig. G1 JW-143-2 motor driver

Table G1 Specifications of the motor diver

No.	Item	Spec.
1	Rated output voltage	±24V
2	Rated output current	±5A
3	Max. output voltage	±30V
4	Max. output current	±10V
5	Max. output power	300W
6	Input voltage	9~35V
7	Input control voltage	0~5V
8	Size	71.5 ×52.6×13.0 mm
9	Weight	77g

Appendix H: Simulink model & Matlab source code

The feed-forward controller for the handshake manipulator in this research is implemented with a Simulink model, the complete model was shown in Fig. H1. It is mainly comprised of 3 units:

(1) The interaction force measurement data input unit.

(2) The air pressure calculation and output unit of each artificial muscle.

(3) The viscosity control unit.

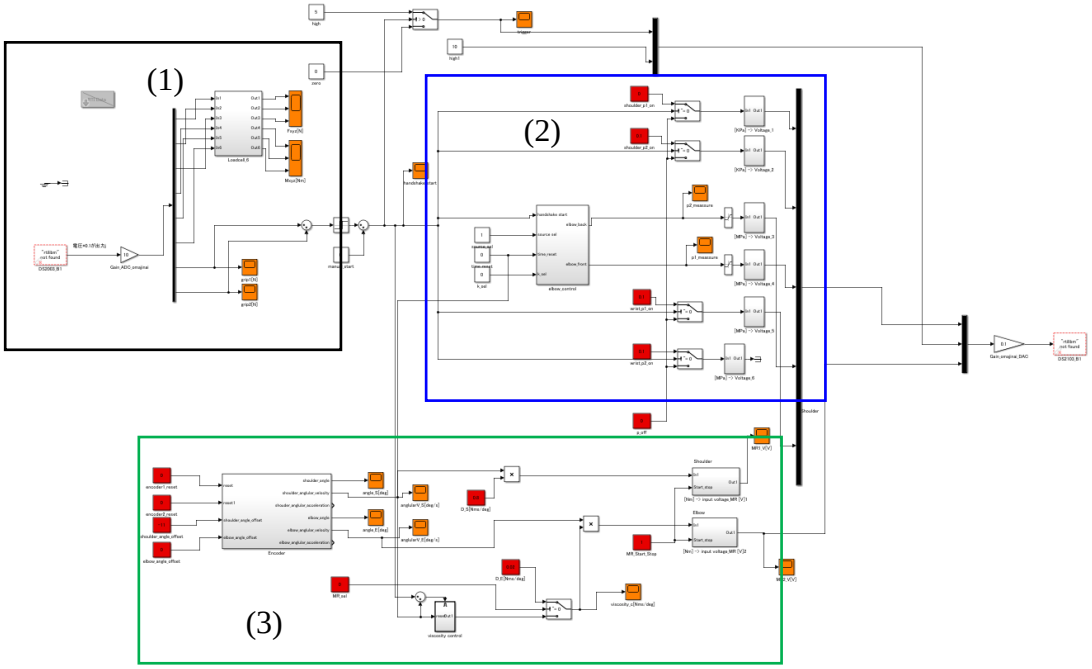

Fig. H1 The complete system of the feed-forward controller of the manipulator

The main control algorithm of the manipulator was implemented into the air pressure control of the elbow joint. The detailed deduction was explained in section 3.6, and the source code for the air pressure control was displayed below.

Source code:

```
function [G11,G21,G31,G12,G22,G32,P1,P2,P3] =
pressure_cal(KJ,thetaJ,tauJ)
% calculate the pressure to apply on the artificial muscle according
to the
% target stiffness KJ[Nm/deg], target angle thetaJ[deg] and target
torque tauJ
% xi(i=1,2) Displacement of the artificial muscle [m]
% xdi (i=1,2) Displacement of each section of the artificial muscle [m]


parameters;

[x1,x2]=angle_cal(thetaJ);

xd1=x1./N;
xd2=x2./N;
ld0=l0/N;


phai01=2.*alpha_af.*ld0^1.5.*(xd1.^0.5)./((alpha_af^2.*xd1.*ld0)+(l
d0-xd1).^2);
phai01_deg = phai01./pi.*180;

G11=2.*E.*(t_af./d0).*(ld0./d0).^2.*((sin(phai01)-phai01.*cos(phai0
1))./(phai01.^2));
G21=M.*tan(phai01)./(d0*n*b);
G31=2.*(ld0./d0).*(sin(phai01)./phai01)+((ld0./d0).^2).*((phai01-si
n(phai01).*cos(phai01))./(phai01.^2))+M.*d0.*pi.*tan(phai01)./(4*n*
b);

phai02=2.*alpha_af.*ld0^1.5.*(xd2.^0.5)./((alpha_af^2.*xd2.*ld0)+(l
d0-xd2).^2);
phai02_deg = phai02./pi.*180;

G12=2.*E.*(t_af./d0).*(ld0./d0).^2.*((sin(phai02)-phai02.*cos(phai0
2))./(phai02.^2));
G22=M.*tan(phai02)./(d0*n*b);
G32=2.*(ld0./d0).*(sin(phai02)./phai02)+((ld0./d0).^2).*((phai02-si
n(phai02).*cos(phai02))./(phai02.^2))+M.*d0.*pi.*tan(phai02)./(4*n*
b);
```

```
phai02=2*ld0*(alpha_af*ld0*xd2)^(0.5)/(alpha_af*(ld0-xd2)^2+xd2*ld0
);
G12=4*E*(t_af/d0)*(ld0/d0)^2*...
    ((sin(phai02)-phai02*cos(phai02))/(phai02^2));
G22=2*M*tan(phai02)/(d0*n*b);
G32=4*(ld0/d0)*(sin(phai02)/phai02)+2*((ld0/d0)^2)*...
    ((phai02-sin(phai02)*cos(phai02))/(phai02^2));
G42=M*d0*pi*tan(phai02)/(2*n*b);


P1=(G11.*G22+(KJ.*G21.*G22./(r1*r2*ka2))-G21.*G12);
P2=(G22.*G31+(r1./r2).*(ka1./ka2).*G21.*G32);
```

Appendix I

Participant consent form

Title of research: Variable viscoelasticity handshake manipulator for physical human-robot interaction using artificial muscle and MR brake

I _____ voluntarily agree to participate in this research study.

I understand that even if I agree to participate now, I can withdraw at any time or refuse to answer any question without any consequences of any kind.

I understand that I can withdraw permission to use data from my experiments within two weeks after the interview, in which case the material will be deleted.

I have had the purpose and nature of the study explained to me in writing and I have had the opportunity to ask questions about the study.

I understand that participation involves shaking hand with researchers, other participants and robot arm, answering questionnaires, and being recorded by motion capture devices and camera.

I understand that I will not benefit directly from participating in this research.

I agree to my experiments being video-recorded.

I understand that all information I provide for this study will be treated confidentially.

I understand that the photos and videos of my experiments be used in conference presentation and published papers.

I understand that if I inform the researcher that myself or someone else is at risk of harm, they may have to report this to the relevant authorities - they will discuss this with me first but may be required to report with or without my permission.

I understand that I am free to contact any of the people involved in the research to seek further clarification and information.

Names, degrees, affiliations and contact details of researchers (and academic supervisors when relevant).

Name of the research participant (printed)

_____

Signature of research participant Date

2017.7.1

Name of the researcher (printed)

Kejia Dai

I believe the participant is giving informed consent to participate in this study

Signature of researcher Date

Kejia Dai 2017.7.1